Directly induced neural stem cells

transplantation and prospects for stem cell-based therapy

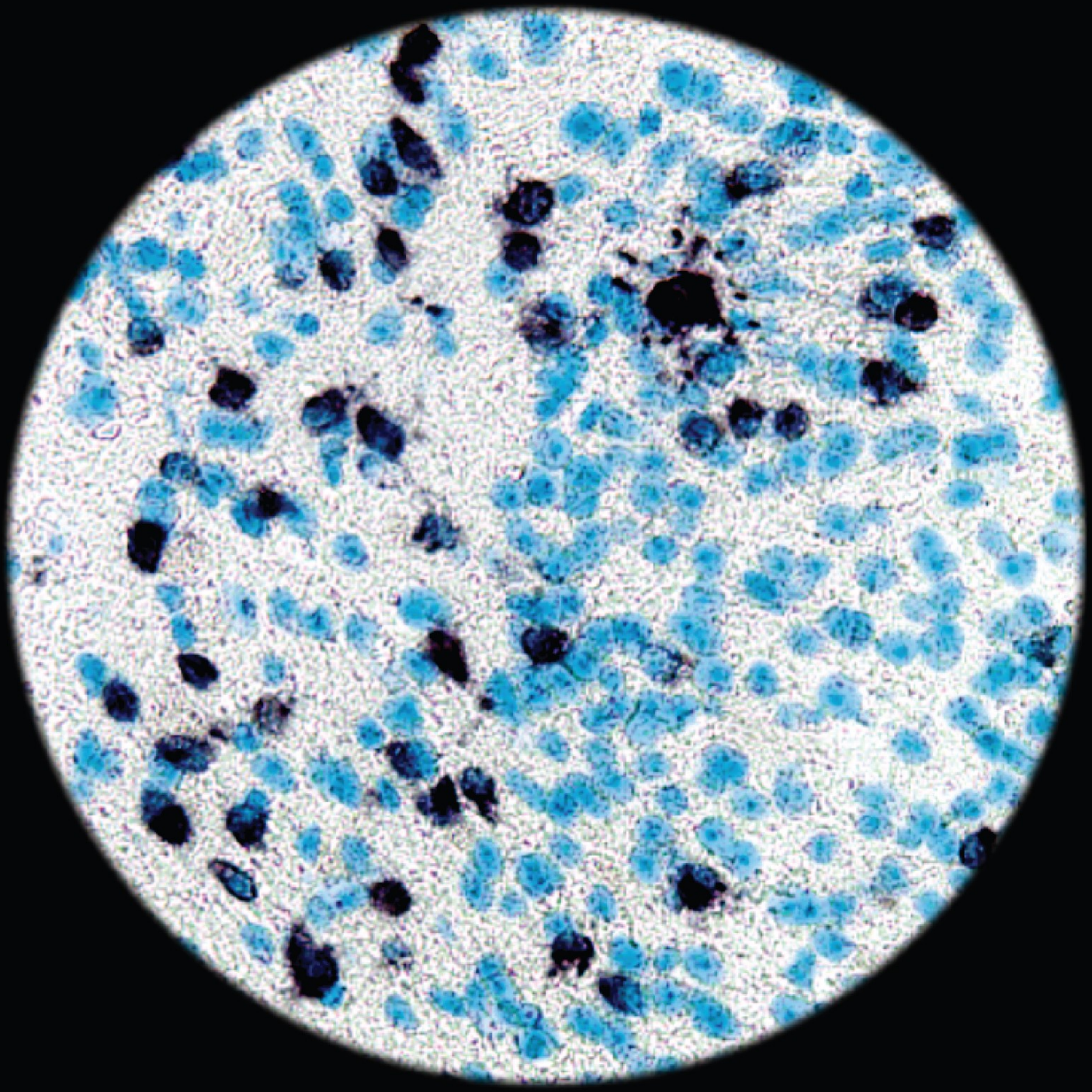

Nunzio Vicario

2017

Doctoral Dissertation

Directly induced Neural Stem Cells

transplantation and prospects for stem cell-based therapy

PhD Candidate: *Nunzio Vicario*

UNIVERSITY OF CATANIA, Catania (Italy)
Department of Biomedical and Biotechnological Sciences
International PhD Program in Neuroscience - XXX Cycle
Section of Physiology

UNIVERSITY OF CAMBRIDGE, Cambridge (UK)
Department of Clinical Neurosciences
Wellcome Trust-Medical Research Council Stem Cell Institute
Division of Stem Cell Neurobiology

Organization
University of Catania, Catania (IT).
Department of Biomedical and Biotechnological Sciences
Section of Physiology

Other Organization(s)
University of Cambridge, Cambridge (UK).
Department of Clinical Neuroscience
Wellcome Trust-Medical Research Council
Stem Cell Institute
Division of Stem Cell Neurobiology

Ph.D. Program
International Ph.D. Program
in Neuroscience
- XXX Cycle -

Document name
Doctoral dissertation

Author
Nunzio Vicario

Title
Directly induced Neural Stem Cells transplantation and prospects for stem cell-based therapy

Summary
Despite the remarkable beneficial effects of disease-modifying agents in relapsing-remitting multiple sclerosis (MS) patients, progressive forms of (P)MS still lack effective treatments. This stark contrast is partially dependent on the difficulties researchers have found in tackling the complex pathophysiology of this phase of disease, in which chronic inflammation within the central nervous system (CNS) is coupled by ongoing neurodegeneration and demyelination.
Cell transplantation is among the most promising therapeutic approaches in regenerative medicine, combining tissue trophic and immunomodulatory effects of the graft with its intrinsic potential for cell-replacement. These are all attributes that can be harnessed to treated patients with PMS.
As such, within this thesis, I have focused my attention on investigating how cellular therapies could be used to (i) prevent neuronal damage, (ii) modulate the chronic activation of the immune system and (iii) replace the damaged myelin in PMS.
Olfactory Ensheathing Cells (OECs) are a special population of glial cells known to exert neuroprotective mechanisms and capable of promoting neuroprotection. Using *in vitro* models of neuron-like cells, I have demonstrated that OECs exert their neuroprotective effect by reducing Cx43-mediated cell-to-cell and cell-to-extracellular environment communications. Despite this important finding, the immunomodulatory and remyelinating potential of OECs is still limited. As such, I decided to study a complementary stem cell approach that conjugates these attributes with ease in clinical applicability.
Induced Neural Stem Cells (iNSCs) are a source of autologous, stably expandable, tissue specific and easily accessible stem cells, which have the potential to differentiate into the three main neural lineages. Mouse iNSCs were characterized *in vitro* and i*n vivo* and their immunomodulatory potential was initially studied. This work uncovered a novel mechanism that underpins the potential of iNSCs to interact with the chronic CNS compartmentalised activation of the innate immune system. Specifically, I found that iNSCs are able to sense extracellular metabolites, which accumulate in the chronically inflamed CNS, and to ameliorate neuroinflammation via succinate-SUCNR1-dependend mechanisms. To characterize the potential for tissue replacement and remyelination of such a promising cell line, I have also analysed how iNSCs grafts differentiate in an experimental model of focal demyelination. I found that iNSCs are able to integrate and differentiate into remyelinating oligodendrocytes (OLs) in chronic demyelinated CNS. These data suggest that iNSCs are indeed an effective source of stem cell transplantation, being able to modulate inflammation and to effectively replace lost tissue in mouse models of PMS.
Altogether the evidences gathered in this thesis are important new steps in the field of cell transplantation, which will be pivotal in the march forward for future clinical applications in chronic demyelinating CNS disorders.

Key words
Stem Cells Transplantation, induced neural stem cells (iNSCs),
Demyelination, Remyelination, Multiple Sclerosis

Language
English

Number of Pages: 122
Number of Characters: 238,096

A mio padre.

Ci manchi.

“Due to illness and therapies some children have a weak immune system and they can’t receive vaccine. Vaccination has dropped […] and this represents a life threat to her and to thousands of children in this condition. I beg you, vaccinate your children.”
Nicola Pomaro
Dad of a 5-year-old girl

In memory of Albert Bruce Sabin
(Bialystok, 1906 – Washington, 1993)
Sabin developed the oral polio vaccine, which has played a key role in nearly eradicating the disease.
The Sabin’s vaccine was build off a weakened live virus. This method was arguably more effective in fully eradicating polio, instead of just preventing it. Most importantly, an oral vaccine was much easier to administer to kids than a big scary needle. For those reasons, the Sabin vaccine became the global standard for polio.
Sabin intentionally refused to patent his vaccine so that the low price would guarantee a more extensive spread of the treatment. From the development of his vaccine Sabin didn’t gain a single dollar, keeping on living with his salary as a Professor.

Cover
“Oligodendrocytes and neurons: the most spectacular and intimate cell-cell interactions in the nervous system”.
In situ hybridization for Myelin proteolipid protein (Plp) in mouse central nervous system.
Plp-mRNA positive cells: black; Nuclei: blue.

“A causa della malattia e delle cure alcuni bambini hanno un sistema immunitario debole e non possono essere vaccinati. La copertura vaccinale è scesa […] e questo rappresenta un pericolo mortale per mia figlia e le migliaia di bambini nella sua condizione. Vi prego, vaccinate i vostri figli.”
Nicola Pomaro,
Papà di una bimba di 5 anni

In memoria di Albert Bruce Sabin
(Bialystok, 1906 – Washington, 1993)
Sabin ha sviluppato il vaccino orale per la polio che ha avuto un ruolo chiave nell’eradicare quasi totalmente questa malattia.
Il vaccino di Sabin era fatto dal virus vitale indebolito. Questo metodo era probabilmente più efficace per eradicare totalmente la polio, piuttosto che prevenirla soltanto. In aggiunta, un vaccino orale era più semplice da somministrare ai bambini piuttosto che una puntura con un grande ago spaventoso. Per queste ragioni, il vaccino di Sabin divenne lo standard mondiale contro la polio.
Sabin rifiutò intenzionalmente di brevettare il suo vaccino cosicché il basso costo potesse garantire una larga diffusione del trattamento. Dallo sviluppo del suo vaccino Sabin non guadagno un dollaro, continuando a vivere con il suo stipendio da Professore.

Copertina
“Oligodendrociti e neuroni: l’interazione cellula-cellula più spettacolare e intima del sistema nervoso”.
Ibridazione in situ per Myelin proteolipid protein (Plp) nel sistema nervoso centrale murino.
Cellule Plp-mRNA positive: nero; Nuclei: blu.

I, the undersigned Nunzio Vicario,
Place of Birth: Catania (IT)
Date of Birth: 18th September 1989
Author of the PhD thesis entitled:
“Directly induced Neural Stem Cells transplantation and prospects for stem cell-based therapy”
Authorizes the consultation of the thesis.
It is not allowed to copy or to reproduce, in whole or in part, the data and the contents of the thesis.
The whole project or part of it have already been submitted to a publisher or are in press.

Il sottoscritto Nunzio Vicario,
Nato a: Catania (IT)
Data di nascita: 18 settembre 1989;
Autore della tesi di Dottorato di Ricerca dal titolo:
“Directly induced Neural Stem Cells transplantation and prospects for stem cell-based therapy”
Autorizza la consultazione della tesi.
E’ fatto divieto di copiare o di riprodurre, in tutto o in parte, i dati e i contenuti della tesi.
L’intera ricerca o parti sono già state sottoposte a un editore o sono in attesa di pubblicazione.

Catania,
21st August 2017 / 21 agosto 2017

Nunzio Vicario

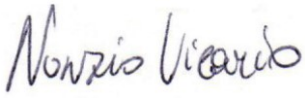

TABLE OF CONTENTS

SUMMARY

Despite the remarkable beneficial effects of disease-modifying agents in relapsing-remitting multiple sclerosis (MS) patients, progressive forms of (P)MS still lack effective treatments. This stark contrast is partially dependent on the difficulties researchers have found in tackling the complex pathophysiology of this phase of disease, in which chronic inflammation within the central nervous system (CNS) is coupled by ongoing neurodegeneration and demyelination.

Cell transplantation is among the most promising therapeutic approaches in regenerative medicine, combining tissue trophic and immunomodulatory effects of the graft with its intrinsic potential for cell-replacement. These are all attributes that can be harnessed to treated patients with PMS.

As such, within this thesis, I have focused my attention on investigating how cellular therapies could be used to (i) prevent neuronal damage, (ii) modulate the chronic activation of the immune system and (iii) replace the damaged myelin in PMS.

Olfactory Ensheathing Cells (OECs) are a special population of glial cells known to exert neuroprotective mechanisms and capable of promoting neuroprotection. Using *in vitro* models of neuron-like cells, I have demonstrated that OECs exert their neuroprotective effect by reducing Cx43-mediated cell-to-cell and cell-to-extracellular environment communications. Despite this important finding, the immunomodulatory and remyelinating potential of OECs is still limited. As such, I decided to study a complementary stem cell approach that conjugates these attributes with ease in clinical applicability.

Induced Neural Stem Cells (iNSCs) are a source of autologous, stably expandable, tissue specific and easily accessible stem cells, which have the potential to differentiate into the three main neural lineages. Mouse iNSCs were characterized *in vitro* and *in vivo* and their immunomodulatory potential

was initially studied. This work uncovered a novel mechanism that underpins the potential of iNSCs to interact with the chronic CNS compartmentalised activation of the innate immune system. Specifically, I found that iNSCs are able to sense extracellular metabolites, which accumulate in the chronically inflamed CNS, and to ameliorate neuroinflammation via succinate-SUCNR1-dependend mechanisms. To characterize the potential for tissue replacement and remyelination of such a promising cell line, I have also analysed how iNSCs grafts differentiate in an experimental model of focal demyelination. I found that iNSCs are able to integrate and differentiate into remyelinating oligodendrocytes (OLs) in chronic demyelinated CNS. These data suggest that iNSCs are indeed an effective source of stem cell transplantation, being able to modulate inflammation and to effectively replace lost tissue in mouse models of PMS.

Altogether the evidences gathered in this thesis are important new steps in the field of cell transplantation, which will be pivotal in the march forward for future clinical applications in chronic demyelinating CNS disorders.

INTRODUCTION

Epidemiology of Multiple Sclerosis (MS)

Multiple sclerosis (MS) is an inflammatory autoimmune disorder of the central nervous system (CNS) and one of the most common causes of neurological disability in young adults. Most people are diagnosed between the ages of 20 and 50, although MS can occur in young children and significantly older adults (Compston and Coles, 2008). MS is a typical disease of the female sex, with recent longitudinal studies suggesting a significant increase in incidence of MS in women, causing a change in the female to male ratio to more than 3:1 (Orton et al., 2006).

The global distribution of MS shows increasing prevalence with more distance (north or south) form the equator. However, prevalence rates may still significantly differ among groups living in the same geographic area. Studies indicate that immigrants who move later in life, conserve the risk of the original geographic area, and the change in risk level may not appear until the next generation. Instead, those who move in early childhood tend to take on the new risk themselves.

These evidences suggest an interplay between environmental and genetic factors in the pathogenesis of MS.

MS has a familial recurrence rate of 3% risk in first-degree relatives (siblings, 5%; parents, 2%; and children, 2%) and of 1% risk in second-degree and third degree relatives, suggesting genetic factors in determining familiar clustering and susceptibility.

However, many environmental factors have been reported as linked to MS triggering. Later ages infections has been reported as helpers in trigging MS supporting the so-called hygiene hypothesis, whereby individuals not exposed to infections in childhood, make aberrant responses to infections in adulthood (Martyn et al., 1993). Similarly, active smoking seems to play a role

with a 1.8 ratio for men and 1.4 ratio for women with MS versus healthy individuals (Hedstrom et al., 2011). On the contrary, vitamin D has shown protective effects in large epidemiologic studies. Healthy controls have higher serum levels of 25(OH)D3 and 1,25(OH)2D3 (the active form of vitamin D) than relapsing remitting (RR) MS patients. Moreover, RR-MS patients present lower serum levels of vitamin D during relapses compared to the levels during remissions. The molecular mechanisms underpinning those evidences are still to be fully elucidated, but it has been demonstrated that 1,25(OH)2D3 supports the induction of CD4+ factor forkhead box P3 (FOXP3+) regulatory T cells by the rendering of tolerogenic dendritic cells (Penna et al., 2005).

Clinical forms of MS

The initial phase of MS is usually characterized by a relapsing remitting phase, in which discrete episodes of acute neurological deficits or worsening of a given neurological function (i.e. relapse), are followed by a complete or partial recovery (i.e. remission) (Lublin and Reingold, 1996). The spontaneous recovery observed in the early stages of RR-MS is relieved by a later progressive course of the disease, called secondary progressive (SP) MS, in which failure of endogenous regenerative process occurs (Compston and Coles, 2008). Both types can be either active or inactive and may develop with or without a clear clinical progression (Lublin et al., 2014).

We now have several therapies to stop relapses and induce recovery in RR-MS patients. However, still around 65% of people with RR-MS will go into SP-MS with a chronic worsening of disability within 15 years after being diagnosed.

Of note, some patients develop a progressive course of disease from the onset (primary progressive) while others present only a clinically isolated syndrome (CIS). CIS, which was not included in the initial clinical descriptions, is now recognised as the initial clinical presentation of a disease

that displays the characteristics of an inflammatory demyelinating disorder that has yet to fulfil the MS diagnosis criteria (Miller et al., 2005a, b).

Pathophysiology of MS

The major early driver of tissue damage in MS lesions is the migration of autoreactive lymphocytes from the periphery, which cross the blood-brain barrier to invade the CNS. Accumulation of T and B lymphocytes, plasma cells and activated mononuclear phagocytes triggers the secretion of pro-inflammatory cytokines, amplifying the immune response through recruitment of naïve microglia (Compston and Coles, 2008).

Demyelination observed in MS patients is typically the completion of a direct insult to the oligodendrocytes (OLs) (Ferguson et al., 1997; Trapp et al., 1998). In physiological conditions, OLs accomplish wrap segments of axons and produce myelin. Neurons, taking advantages from this intimate contact with OLs, are able to rapidly conduct stimuli via *saltatory conduction* of action potentials that propagate throughout the so-called *nodes of Ranvier*. In demyelinating conditions, the disruption of these structures impairs the conductivity but also affects axonal tropism, leading to neurodegeneration as a chronic condition. While axonal loss and neurodegeneration coexist with demyelination in the progressive stage of the disease, compensatory mechanisms are initiated to try to overcome the chronic damage. Among these, oligodendrocyte precursors cells (OPCs) recruiting is important as these cells can migrate into demyelinated area and differentiate into mature myelinating OLs (Chandran et al., 2008). However, these mechanisms seem largely inadequate, and remyelination is less successful after cycles of demyelination and remyelination, probably because of exhausting the capacity of tissue repair.

Cell therapies for PMS

The progressive course and failure of endogenous regenerative processes of repair are the rationale for cell therapy-based approaches in PMS (Ben-Hur, 2011; Franklin, 2002). Cellular approaches for PMS have great advantages compared to conventional biologics or drugs due to their intrinsic potential to replace damaged cells, to attenuate the autoimmune response in a non-systemic manner, and also to stimulate endogenous regenerative processes; features summarised as *therapeutic plasticity* (Ben-Hur, 2011). This is a milestone of stem cell therapy promise, and described as the combination of abilities of cells to provide bystander effects and neurotrophic support, to exert CNS-confined immunomodulation and to replace damaged cells.

Olfactory ensheathing cells (OECs), a special glial cell population sharing properties with both Schwann cells (SC) and the astrocytes (Franklin and Barnett, 1997; Wewetzer et al., 2002), are able to secrete high level of growth factors, such as nerve growth factor (NGF), basic fibroblast growth factor (bFGF), brain derived neurotrophic factor (BDNF) and glial derived neurotrophic factor (GDNF), exerting remarkable neuroprotective and neuroregenerative functions (Boruch et al., 2001; Lipson et al., 2003; Mackay-Sim and Chuah, 2000). Several reports demonstrate that transplantation of OECs could provide a remarkable improvement in recovery of functions in experimental models of CNS-injury (Li et al., 1997; Li et al., 2003; Lu et al., 2002; Nash et al., 2002). However, poor evidences support the immunomodulatory potential of OECs and their regenerative properties are although modest. These characteristics and the SC-like remyelinating features of OECs grafts, prompted us to develop a stem cell-based approach for immunomodulation, regeneration and neuroprotection (Franklin and Barnett, 1997).

Neural Stem Cells (NSCs) are multipotent stem cells of the brain, which have shown remarkable abilities to reduce necrosis, secondary cell loss and glial

scar formation in experimental models of CNS diseases (Keyoung et al., 2001; Teng et al., 2002). These effects have been attributed to the generation of a permissive environment for axonal regeneration, the secretion of neurotrophic factors and induction of matrix metalloproteinases that allow neurite outgrowth (Kumagai et al., 2009; Lu et al., 2003; Zhang et al., 2007). The neurotrophins increase and the immunomodulatory functions are coupled with the promotion of endogenous regenerative mechanisms, facilitating endogenous oligodendrocytes precursor cells maturation into mature remyelinating oligodendrocytes and enhancing neurogenesis and axonal growth (Ben-Shaanan et al., 2008; Einstein et al., 2009; Pluchino et al., 2003).

Among the crucial effects mediated by grafted cells, immunomodulation is one of the mechanisms by which transplanted NSCs can ameliorate mice with experimental autoimmune encephalomyelitis (EAE), a widely used experimental model of MS. It has been demonstrated that a reduction of brain inflammation, acute and chronic injury and demyelination leads to an overall improvement of the clinical conditions of EAE mice (Pluchino et al., 2003; Pluchino et al., 2005).

In this scenario, NSCs possess the potential advantages to be able to self-renew and largely expandable, the plasticity of multipotent stem cells and the ability to differentiate towards the main neuronal lineages, neurons, astrocytes and oligodendrocytes, thus allowing cell replacement in the CNS and improving endogenous spontaneous regeneration (Ben-Hur, 2011; Keyoung et al., 2001; Nunes et al., 2003).

Recent advances in the generation of multipotent and stably expandable induced neural stem cells (iNSCs) are exciting. In fact, the direct reprogramming of mouse and human somatic cells into iNSCs yields homogenous patient-specific NSCs in a relatively rapid manner. It only requires one step that is completed within around 4 weeks *in vitro* and yields

iNSCs that are expandable for at least 30 passages. Also, iNSC are safer than iPSCs, making them an outmost attractive tool for autologous cell therapies (Meyer et al., 2015; Thier et al., 2012).

AIMS OF THIS THESIS

The general objective of this thesis was to investigate how cellular therapies could be used to prevent neuronal damage, modulate the chronic activation of the immune system and replace the damaged myelin in CNS disorders.

More specifically, the main aims were:

I. Characterize the mechanisms underpinning the action of OECs in experimental *in vitro* models of neurodegeneration to investigate potential candidates that mediate neuroprotective effects;

II. Study the immunomodulatory and therapeutic mechanisms of mouse iNSCs in the EAE experimental model of MS;

III. Promote endogenous- and exogenous-mediated remyelination using mouse iNSCs in the lysophosphatidylcholine (LPC) induced focal demyelination model of MS.

RESULTS

Inhibition of Cx43 mediates protective effects on hypoxic/ reoxygenated human neuroblastoma cells

Nunzio Vicario [a], Giovanna Calabrese [a], Agata Zappalà [a], Carmela Parenti [b], Stefano Forte [c], Adriana Carol Eleonora Graziano [a], Luca Vanella [b], Rosalia Pellitteri [d], Venera Cardile [a], Rosalba Parenti [a, *].

[a] *Department of Biomedical and Biotechnological Sciences, Physiology Section, University of Catania. 95125 - Catania, Italy.*
[b] *Department of Drug Sciences, University of Catania. 95125 - Catania, Italy.*
[c] *IOM Ricerca, 95029 - Viagrande, Italy.*
[d] *Institute Neurological Sciences, National Research Council. 95126 - Catania, Italy.*

Journal of Cellular and Molecular Medicine
Received: October 28, 2016; Accepted: February 28, 2017

Abstract

Olfactory Ensheathing Cells (OECs), a special population of glial cells, are able to synthesise several trophic factors exerting a neuroprotective action and promoting growth and functional recovery in both *in vitro* and *in vivo* models. In the present work, we investigated the neuroprotective effects of OEC-conditioned medium (OEC-CM) on two different human neuron-like cell lines, SH-SY5Y and SK-N-SH (neuroblastoma cell lines), under normoxic and hypoxic conditions. In addition, we also focused our attention on the role of connexins (Cxs) in the neuroprotective processes. Our results confirmed OEC-CM mediated neuroprotection as shown by cell adherence, proliferation and cellular viability analyses. Reduced connexin 43 (Cx43) levels in OEC-CM compared to unconditioned cells in hypoxic conditions prompted us to investigate the role of Cx43-Gap junctions (GJs) and Cx43- hemichannels (HCs) in hypoxic/reoxygenation injury using carbenoxolone (non-selective GJ inhibitor), ioxynil octanoato (selective Cx43-GJ inhibitor) and Gap19 (selective Cx43-HC inhibitor). We found that Cx43-GJ and Cx43-HC inhibitors are able to protect SH-SY5Y and allow to these cultures to overcome the injury. Our findings support the hypothesis that both OEC-CM and the inhibition of Cx43-GJs and Cx43-HCs offer a neuroprotective effect by reducing Cx43-mediated cell-to-cell and cell-to-extracellular environment communications.

Keywords

Olfactory glia, Growth Factors, Neuroprotection, Gap Junctions, Connexin 43

*Correspondence to: Rosalba PARENTI, Ph.D.
E-mail: parenti@unict.it

Doi: 10.1111/jcmm.13177

Introduction

The olfactory system is a specific area of the central nervous system (CNS) capable of supporting neurogenesis throughout the life of mammals by forming new olfactory receptor neurons (ORNs) [1–3]. These neurons are then able to spread axons from the peripheral nervous system of the olfactory epithelium into the CNS environment of the olfactory bulb [4]. The capacity of ORNs to stimulate neurogenesis in the adult olfactory system may be due to both the neural stem cells present in the olfactory epithelium and the glial cells known as Olfactory Ensheathing Cells (OECs) [5, 6]. OECs, originally described by Golgi and Blanes [7–9] at the end of the 19th century, are a special glial cell population sharing properties with both Schwann cells and the astrocytes [10, 11]. Similarly to Schwann cells, OECs express some characteristic markers such as the low affinity neurotrophin receptor (p75NTR) and adhesion molecules such as laminin, L1 and NCAM; likewise to astrocytes they express the S-100 protein and the glial fibrillary acidic protein (GFAP), a member of the intermediate filament family that offers support to glial cells [12, 13]. Furthermore, OECs are able to secrete high level of growth factors, such as nerve growth factor (NGF), basic fibroblast growth factor (bFGF), brain derived neurotrophic factor (BDNF), glial derived neurotrophic factor (GDNF), ciliary neurotrophic factor (CNTF), neurotrophins NT4, NT5 and neuregulins, which exhibit important functions as neuronal supporting elements [14–19].

Gap junctions (GJs) are specialized intercellular channels that directly connect cytoplasms of adjacent cells, enabling direct exchanges of small molecules (less than 1200 Da). GJs are composed by two docked hemichannels (HCs), also named connexons, one on each cell. HCs are hexamers of homotypic or heterotypic connexins (Cxs), which are the transmembrane proteins encoded by a multigene family of approximately 20 members in mammals [20–25] that form respectively homotypic or heterotypic GJs.

Besides constituting ‘GJs plaques’ that allow GJ intercellular communication (GJIC), Cxs also constitute free HCs throughout the plasma membrane, allowing exchange of a number of autocrine and paracrine signalling molecules between the cytoplasm and the extracellular environments [26–28]. GJs, as well as HCs, play a crucial role in a wide range of cellular activities, including cell signalling, differentiation, growth, pro-apoptotic signalling, either as anti-apoptotic gates or pathogenic pores depending on conditions and cell type [29–32]. GJs and free HCs are extensively distributed in different tissues and organs [33] in which different cell type usually expresses specific Cxs profile involved in the selective permeability of channels formed, according to the metabolic or functional

needs [34–38]. Also in the CNS, GJs and HCs are extensively distributed among neurons and glial cells [39–41], where, contributing to GJIC and cell-extracellular communication, they provide specific exchange pathways under resting conditions, and also play a context-dependent role in contradictory cell survival or cell death phenomena [42]. In recent years, much attention has been paid to the exploitation of neuroprotective effects in combatting the progression and chronicity of neurodegeneration. In particular, evidence shows altered Cxs expression and functions under pathological conditions, suggesting a central role of glial GJs and HCs in the development of various neurodegenerative diseases [21, 43–46]. Conversely, the therapeutic potential of OECs is attracting considerable interest owing to their exceptional ability to promote functional recovery of the damaged CNS [3, 47–50]. However, the molecular mechanisms underlying this protective function are not yet known. The aim of this study was firstly to investigate the neuroprotective effects of OEC conditioned medium (OEC-CM) on two different neuroblastoma cell lines (SH-SY5Y and SK-N-SH) exposed to hypoxic/reoxygenation (H/R) injury. Towards this goal we explored the relationship between OEC-CM and Cxs, HCs and GJs following H/R injury in cultures grown with and without OEC-CM. We found that: (1) OEC-CM offers a neuroprotective effect to the SH-SY5Y and SK-N-SH cells exposed to H/R injury; (2) injured SH-SY5Y and SK-N-SH cells show higher Cx43 levels compared to normoxic cultures; and (3) H/R cultures grown in the presence of GJ and/or HC chemical inhibitors, such as carbenoxolone (CBX, non-selective GJIC inhibitor) [51], ioxynil octanoato (IO, Cx43 homotypic GJ inhibitor) [52], and Gap19 (Cx43 homotypic HC inhibitor) [53], show higher viability compared to control cultures. Our results, showing the neuroprotective effects of OEC-CM likely afforded by inhibition of Cx43 GJ/HC signalling pathways, suggest potential new therapeutic tools against neurodegenerative diseases.

Materials and Methods

Primary Olfactory Ensheathing Cells cultures

Primary OECs were isolated from post-natal day 0 (P0) CD1 mice olfactory bulbs. Experiments were performed in compliance with current guidelines for animal care and in accordance with the European Community Council Directive (86/609/EEC). All efforts were made to minimize animal suffering and to use the fewest animals possible.

Ten P0 pups were decapitated, the entire brain was exposed and bulbs removed and dissected out in cold (+4 °C) Leibowitz L-15 medium (Sigma). Subsequently, collected olfactory bulbs were digested twice in fresh minimum essential medium-H (MEM-H; Sigma) containing 0.03% collagenase (Sigma) and 0.25% trypsin (Sigma) for 15 min at 37 °C. Suspension was mechanically triturated and filtrated through a 80 μm nylon filter and centrifuged at 600 g for 10 min. Cells were suspended with fresh complete Dulbecco's modified

Eagle's medium (DMEM, Sigma) supplemented with 10% fetal bovine serum (FBS, Sigma), 2 mM L-glutamine (Sigma), penicillin (50 U/ml, Sigma), and streptomycin (50 mg/ml, Sigma) and plated in 25 cm^2 flasks. Cytosine arabinoside (Sigma) at final concentration of $1x10^{-5}$ M was added 24 hours (hrs) after plating to reduce the number of dividing fibroblasts. After 2 passages purity of OECs was verified by using immunofluorescence with p75 and S-100 (data not shown). Media were replaced twice a week for 3 passages and then cultures were used to collect the conditioned medium. OEC-CM was removed from the cultures and filtered through a membrane filter (0.22 µm pore diameter) to remove cells and debris.

Neuroblastoma cell lines cultures

The human neuroblastoma cell lines, SH-SY5Y and SK-N-SH, were purchased from ATCC (Rockville, MD, USA) and grown as previously described [56]. Briefly, cells were incubated at 37 °C in a humidified 5% CO_2/95% air atmosphere and maintained in DMEM/F12 (Sigma) supplemented with 10% FBS (Sigma), 2 mM L-glutamine (Sigma), penicillin (50 U/ml, Sigma), and streptomycin (50 mg/ml, Sigma). The medium was replaced twice a week.

H/R injury and OEC-CM treatment

Cells at a density of $2.5x10^4$ cells/cm^2 were seeded on appropriate supports for analysis 16 hrs before performing the experiments (time 0). The following experimental culture groups were established: untreated control groups (CTRL Normoxia) and hypoxic groups (CTRL Hypoxia) at 0, 3, 8 and 24 hrs. Each group was grown in normal culture conditions for 16 hrs, after which they were subjected to hypoxia (1% O_2) for 3 hrs, followed by reoxygenation to 24 hrs. All cultures were grown with DMEM-F12 (89%), FBS (10%) and P/S (1%). For OEC-CM treatment, at time 0, media conditioning (25%, 50% and 100%) obtained from OECs cultured for 24, 48 and 72 hrs were applied in the same experimental culture groups. To verify the status of hypoxia, the expression of hypoxia-inducible factor 1-alpha (HIF1A), a specific transcription factor of the hypoxic response, was analysed by immunofluorescence (data not shown).

Immunofluorescence

Immunofluorescence analysis on SH-SY5Y cells was performed as previously described [54]. Briefly, after fixation with 4% Paraformaldehyde (PFA), cells were permeabilized in 0.2% Triton X100, blocked by incubation with 10% normal goat serum (NGS, Gibco) for 1 hr at room temperature (RT) and incubated overnight at 4 °C with the following primary antibodies: rabbit anti-p75 (1:500, Chemicon), mouse anti-S-100 (1:100; Sigma), rabbit anti-HIF1A (1:200; Sigma), mouse anti-Cx43 (1:150, Cell Signaling) and rabbit β-tubulin (1:200, Cell Signaling).

After washing, slides were incubated with the appropriate secondary antibodies: fluorescence isothiocyanate (FITC) labelled anti-rabbit antibody (1:200, Chemicon) and Cy3 labelled anti-mouse antibody (Chemicon, 1:1000) for 1 hr at RT. Nuclei were stained with DAPI (1:1000) for 5 min. Finally, slides were mounted in fluorescent mounting medium Permafluor (Thermo Scientific) and digital images were acquired using a Leica DM IRB fluorescence microscope and with Leica TCS SP8 confocal microscope. Nonspecific staining of cells was observed in control incubations in which the primary antibodies were omitted.

Western blot analysis

Cell pellets were homogenized in lysis buffer (Tris-HCl pH 7.4, 1% Triton X100, NaCl 150 mmol/L and EDTA 1 mmol/L) supplemented with a cocktail of protease inhibitors (1:100, Sigma). For Western blot quantification, 50 µg of protein were electrophoresed on 12% SDS-PAGE gels and transferred to nitrocellulose membranes. After blocking with 5% non-fat milk powder in Tris-buffered saline with 0.05%

Tween-20 (TBST), membranes were incubated overnight at 4 °C with the following primary antibodies: rabbit caspase-3 cleaved (1:1000, Cell Signaling), mouse anti-Cx47 (1:200, Invitrogen), mouse anti-Cx43 (1:1,000, Cell Signaling), rabbit anti-Cx40 (1:200, Invitrogen), mouse anti-Cx36 (1:200, Invitrogen), mouse anti-Cx32 (1:500, Novex), rabbit anti-Cx30 (1:200, Invitrogen) and rabbit β-tubulin (1:1,000, Cell Signaling). After 3 washes in TBST, the membranes were incubated with anti-mouse (1:20,000, Jackson) and anti-rabbit HRP-conjugated (1:50,000, Jackson) secondary antibodies for 1 hr at RT. Proteins bands were visualized with premixed ready-to-use chemiluminescent HRP detection reagent (Millipore) according to the manufacturer's instructions and captured with an Uvitec Cambridge Imaging System. The density of each band was quantified using ImageJ analysis software and normalized to β-tubulin levels measured in the same membranes.

Monitoring cell adherence and proliferation

Cell adherence and proliferation was monitored in real-time using the xCELLigence system E-Plate. Different cell numbers were tested, with the *optimum* cell density to found to be $2.5x10^4$ cells/cm^2 (data not shown). Experiments were performed at different time points and with various percentages of media derived from OEC cultures mixed with fresh medium, with 100% of fresh medium employed as a control. The impedance value of each well was monitored by the xCELLigence system for a time of 24 hrs and expressed as a cell index (CI) value. Data for cell adherence were normalized at 16 hrs after plating. Normalized CI, representing a quantitative measure of cell number, was calculated by dividing CI at the time point into the CI at the normalization time point (time 0). The Rate of Cell Growth (RCG) was determined by calculating the slope of the line between starting point and ending point.

Cellular viability

Cells were trypsinized and adjusted to a concentration of $2.5x10^4$ cells/cm^2 seeded in 96-well plates (Costar) and incubated for 16 hrs with basal growth medium. Then the medium was replaced with basal growth medium in control cultures and with 50% basal growth medium mixed 1:1 with OEC-CM. Normoxic cultures were placed in both normal-oxygen and in 1% O_2 conditions. Cellular viability was evaluated at time 0, 3, 8 and 24 hrs after 2.5 hrs of incubation with a solution of 3-(4,5-dimethylthiazol-2-yl)-2,5-diphenyltetrazolium bromide (MTT; Sigma Aldrich, Italy) 5 mg/ml. Media were gently removed, MTT solvent (DMSO, Sigma) was added, and cells were agitated on an orbital shaker for 5 min at RT. The absorbance was measured using a Varioskan Flash spectrophotometer (Thermo Scientific) at 550 nm. Results were expressed as the percentage MTT reduction of control cells. The experiment was performed 3 times with 6 replicates per condition each time. Data are shown via standard box-and-whiskers plots in which the central-line represents the median, the upper- and lower-bounds of the boxes are min and max value and points represent all values expressed as percentage of control, assumed as 100%.

Statistical analysis

n way-Anova has been performed in order to determine the existences of interaction between *n* independent variables (time and treatment for two way ANOVA and time, treatment and oxygen levels for three way Anova) on a continuous dependent variable. Tukey honest significant difference (HSD) has been used as post-hoc test when ANOVA test indicated statistically significant differences to identify specific changes in time points or treatment conditions. Statistical calculation has been performed using R software (R Foundation for Statistical Computing). Values are represented in graphs as mean ± standard error of the mean (SEM). All calculation was performed using GraphPad Prism v7 software.

Results

OEC-CM exerts a protective effect in an *in vitro* H/R injury model

To induce hypoxia/reoxygenation (H/R) injury, $2.5x10^4$ cells/cm^2 were plated in growth medium and incubated in a controlled humidified atmosphere at 37 °C with constant 5% CO_2 level. Sixteen hours after plating (time 0) hypoxic cultures were exposed to 3 hrs of hypoxia (1% O_2) and then reoxygenated to 24 hrs. In OEC-CM supplemented cell cultures the conditioned media was added at time 0 (Fig. 1A).

To investigate the potential protective effects of OEC-CM on cell cultures after H/R injury, we supplemented growth medium with three different percentage of conditioned medium, 25%, 50% and 100%, collected from primary OECs cultures at different conditioning times (24, 48 and 72 hrs) (Fig. 1A). Our results showed that in normoxic conditions there was a significant reduction of normalized cell index (CI) in all cell cultures grown in 100% OEC-CM (Fig. 1B–D), as result of reduced cell confluence and cell number. A similar result, although less marked than previous, was observed when the cells were cultured with 50% OEC-CM collected after 72 hrs (Fig. 1D). This was probably linked to the lower level of serum and nutrients compared to the fresh medium. Cell cultures grown with 25% and 50% OEC-CM, collected after 24 hrs and 48 hrs (Fig. 1A and B), did not show any significant difference compared to cells grown in 100% growth medium (CTRL) (Fig. 1A–C). Cells exposed to H/R injury, treated with 25%, 50% and 100% OEC-CM collected at any time-points, showed a significant increase of normalized CI compared to CTRL (Fig. 1E–G). Our findings also indicated that OEC-CM, used at concentrations of 50% and 100%, exerted a higher protective effect on cells compared to 25% OEC-CM and CTRL (Fig. 1E–G). To further analyse, the effects of OEC-CM on cell cultures, we evaluated the rate of cell growth (RCG) in both normoxic and H/R injured cultures (Fig. 1H–K). Our results demonstrated that in normoxic conditions, cell lines supplemented with 25% OEC-CM, collected from OECs after 24, 48 and 72 hrs, did not show significant reduction of the RCG. The same effect was observed when cells were grown in 50% OEC-CM collected after 24 or 48 hrs. In contrast, cultures grown in 50% OEC-CM, collected after 72 hrs and in 100% of OEC-CM (all conditioning times), showed a significant decrease of RCG (Fig. 1H and J). Interestingly, all conditioned media used at 25%, 50% and 100% on H/R injured cultures showed a significant increase of RCG compared to control cultures (Fig. 1I and K). Taken together, these findings suggested that, in both normoxic and H/R injured cultures, the cells grown in 48 hrs OEC-CM mixed 1:1 in maintenance medium, showed a higher protective effect and supported a better RCG. For this reason all further studies

have been performed by using 50% OEC-CM collected after 48 hrs. These findings confirmed that OECs, affecting the media composition, were able to exert neuroprotective actions and to increase cell survival and cell proliferation after injury.

OEC-CM improves cell viability in H/R cultures

In order to investigate the effect of H/R condition on cell viability, we exposed hypoxic cell cultures to 1% O_2 levels for 3 hrs and reoxygenation up to 24 hrs. Cell cultures viability was evaluated at different time-points after injury (Fig. 2A). Our results demonstrated that cells immediately after H/R injury and after 5 hrs of reoxygenation had significantly lower cell viability (MTT test). Furthermore, we established that the addition of OEC-CM to the H/R injured cultures significantly improved cell viability compared to untreated cells. Otherwise cells cultured in presence of OEC-CM for 24 hrs in normoxic conditions did not show any significant difference compared to control (Fig. 2A).

Further, we evaluated the levels of cleaved caspase-3, a marker of apoptosis, in normoxic and H/R cultures with and without OEC-CM. We found that cleaved caspase-3 levels were significantly higher in hypoxic cultures, at all reoxygenation times, compared to normoxic cultures (Fig. 2B). Cells grown with OEC-CM, in normoxia and exposed to H/R, did not show significant differences of cleaved caspase-3 levels compared to unconditioned cultures (Fig. 2C).

Expression levels of different Cxs in neuroblastoma cell lines under normoxic and hypoxic conditions

To identify whether SH-SY5Y cells, cultured in presence or in absence of OEC-CM in normoxic and H/R conditions, expressed some specific Cxs (including Cx47, Cx43, Cx40, Cx36, Cx32, and Cx30), we performed Western blot analyses. Our data indicated that cells grown in all experimental conditions showed no or a very low expression of Cx47, Cx32, Cx40 and Cx30 (Fig. 3A). The cultures, maintained under normoxic conditions, showed basal expression levels for Cx36 and Cx43 that were reduced in presence of OEC-CM. H/R injured cultures showed an intensely increased Cx43 levels and OEC-CM was able to reduce this overexpression to normoxic levels (Fig. 3A). To better evaluate levels and localization of Cx43 in SH-SY5Y cells we performed Western blots and immunofluorescence analysis at different time-points. These experiments confirmed high levels of this marker from the end of the injury (3 hrs) in untreated SH-SY5Y cells (Figs. 3B and 4A, B). The expression levels appeared to increase markedly after 8 hrs and then

clearly decrease at 24 hrs (Fig. 3B) in both intracellular and extracellular compartments (Fig. 4B). However, our data showed that H/R cultures, in absence of OEC-CM, had higher levels of Cx43 at each analysed time-point compared to the cultures in normoxia with and without OEC-CM. On the contrary, in injured cultures, in the presence of OEC-CM the expression levels of Cx43 seemed unaffected along the different time-points (Figs. 3A and B, 4B) compared to the cultures in normoxia with and without OEC-CM. Moreover, H/R cultures exposed to OEC-CM exhibited an evident reduction of Cx43 expression when compared to the unconditioned injured cultures (Figs. 3B and 4B). To further confirm the increased Cx43 expression levels in hypoxic condition we performed Western blots analysis on SK-N-SH at 24 hrs (Fig. 3C). These experiments confirmed that also in this cell line the Cx43 levels were up-regulated in H/R injured cultures while did not show any significant differences in OEC-CM cultures compared to control cultures.

Gap junction and/or hemichannel chemical inhibitors protect SH-SY5Y cells from H/R injury

To analyse whether the neuroprotective effect on SH-SY5Y cells exposed to H/R injury was related to GJ and/or HC functions of Cx43 we performed MTT-viability test after adding GJ and/or HC inhibitors. We used CBX, a non-selective GJIC inhibitor, IO to selectively target Cx43 homotypic GJs, and Gap19 to selectively inhibit Cx43 homotypic HCs. Results obtained from the titration of GJ and/or HC inhibitors (data not shown) suggested that the best inhibitor concentrations were 10 μM in culture medium. Our results demonstrated that H/R injured cultures treated with both GJ and HC chemical inhibitors significantly increase the cell viability over time compared to the control cultures exposed to H/R injury (Fig. 5).

Discussion

The strengthening of some endogenous neuroprotective mechanisms as a mean by which to prevent and/or slow down the outcome of the various forms of neurodegenerative disorders has recently emerged as one of the most popular topics in applied neurobiology. It has been described that OECs exhibit the ability to promote regeneration in the damaged CNS, thus they could be involved as possible mediators of repair in neurological diseases [12, 14]. As a source of different trophic factors, OECs have attracted an increasing interest as tool for regenerative medicine with applications that include spinal cord injury [55, 56] or axonal growth [57, 58] with a view towards new therapeutic approaches. It has been also demonstrated *in vitro* that the addition of OEC-CM to the neuroblastoma SH-SY5Y and SK-N-SH cells exposed to the neurotoxin 6-hydroxydopamine (6-OHDA) provides neuroprotective properties [59].

In this work we showed that OEC-CM exerts a concentration and time-dependent protective effect on SH-SY5Y and SK-N-SH cells subjected to H/R injury. Our aim was to investigate the molecular mechanism underlying this effect. A number of evidence revealed that, in the CNS, intercellular communication among neurons and glial cells via GJs and/or HCs could be critical in the spread of protective and/or deleterious signals. Cxs are dynamically expressed during injury and stress conditions and, for each condition and context, up- or down-regulation of such proteins likely influencing gate properties of GJs and free HCs, may influence cell survival or cell death [21, 43–46]. In particular, several independent studies have pointed out that onset and progression of homeostatic imbalances observed during neurodegeneration could be associated with an enhanced HC activity in the CNS [60–66]. Here we demonstrated *in vitro* that SH-SY5Y and SK-N-SH cells grown in normoxia displayed no or low expression of Cx47, Cx43, Cx40, Cx36, Cx32 and Cx30 with or without the addition of OEC-CM. When cells are cultured under hypoxic conditions, the Cx43 exhibited an increased expression whereas, the addition of OEC-CM to the growth medium, restored the basal expression observed in normoxia.

These evidence suggest that, while Cx43 may be involved in hypoxic response, the protective effect of OEC-CM may be exerted through the modulation of this specific Cxs. Cx43 is the principal astrocytic GJ protein in the CNS where it contributes to the formation of the functional syncytium, implicated in maintaining the homeostasis of the extracellular milieu of neurons [67, 68]. Many studies support the potential therapeutic effects of Cx43-GJ blockade on neuronal survival in various models of injury including stroke, epilepsy, ischemia, optic nerve damage and spinal cord injury, with GJ communication and HC

opening leading to increased secondary damage via the inflammatory response [69–71]. To investigate the possible interplay between OEC-CM and Cx43 in protection after H/R injury, the effects of Cx43 chemical inhibition has been assessed. When H/R stress is induced in SH-SY5Y cells, both Cx43-GJ and Cx43-HC chemical inhibition significantly increased the cell viability over time compared to control cultures. The functional modulation of Cx43 provides additional support on its involvement in OEC-CM mediated neuroprotection, likely exerted through the prevention of the spread of injury signals. One appealing hypothesis is that OEC-CM works by influencing Cx43 expression in the SH-SY5Y cells via paracrine factors likely involved in the physiological role of OECs within the CNS. It is noteworthy that several studies have demonstrated a role of Cx proteins in the regulation of tissue homeostasis occurring independently of their channel activities, in the context of cell growth, adhesion, migration, apoptosis and signalling [72]. While further investigations are needed to unveil the molecular details of such neuroprotection, these data point to the possibility that the proposed model may be useful in the context of therapeutic applications after brain injury. The involvement of Cxs in maintaining the delicate balance of CNS cells, via GJs and/or HCs, may indeed stimulate the development of new modulators for Cxs-based channels as novel therapeutic agents for the cure of nervous disorders [73–76].

Acknowledgements

The authors would like to thank Dr Jayden A. Smith, (University of Cambridge, UK), for critically review this work.

Conflicts of Interest

The authors confirm that there are no conflicts of interest.

Author contributions

N.V. and R.Pa. designed the research study; N.V., G.C. and R.Pe. performed experiments; N.V. and S.F. collected and analysed data; C.P. and L.V. provided some reagents and instruments; A.G., A.Z., C.P. and V.C. gave technical support and conceptual advice; N.V., G.C. and R.Pa. wrote the manuscript.

References

1. Farbman AI. Olfactory neurogenesis: genetic or environmental controls. Trends Neurosci. 1990; 13: 362–5.
2. Graziadei PP, Graziadei GA. Neurogenesis and neuron regeneration in the olfactory system of mammals. I. Morphological aspects of differentiation and structural organization of the olfactory sensory neurons. J Neurocytol. 1979; 8: 1–18.
3. Bartolomei JC, Greer CA. Olfactory ensheathing cells: bridging the gap in spinal cord injury. Neurosurgery. 2000; 47: 1057–69.
4. Chung RS, Woodhouse A, Fung S, et al. Olfactory ensheathing cells promote neurite sprouting of injured axons in vitro by direct cellular contact and secretion of soluble factors. Cell Mol Life Sci. 2004; 61: 1238–45.
5. Doucette R. Glial influences on axonal growth in the primary olfactory system. Glia. 1990; 3: 433–49.
6. Raisman G. Specialized neuroglial arrangement may explain the capacity of vomeronasal axons to reinnervate central neurons. Neuroscience. 1985; 14: 237–54.
7. Ramon-Cueto A, Avila J. Olfactory ensheathing glia: properties and function. Brain Res Bull. 1998; 46: 175–87.
8. Golgi C. Sulla fina anatomia dei bulbi olfattorii. Rivista Sperimentale di Freniatria. 1875; 1: 403–25.
9. Blanes T. Sobre algunos puntos dudosos de la estructura del bulbo olfatorio. Revista Trimestral Micrografica. 1898; 3: 99–127.
10. Wewetzer K, Verdù E, Angelov DN, et al. Olfactory ensheathing glia and Schwann cells: two of a kind? Cell Tissue Res. 2002; 309: 337–45.
11. Franklin RJM, Barnett SC. Do olfactory glia have advantages over Schwann cells for CNS repair? J Neurosci Res. 1997; 50: 665–72.
12. Pellitteri R, Spatuzza M, Russo A, et al. Olfactory ensheathing cells exert a trophic effect on the hypothalamic neurons in vitro. Neurosci Lett. 2007; 417: 24–9.
13. Franceschini IA, Barnett SC. Low-affinity NGF-receptor and E-N-CAM expression define two types of olfactory nerve ensheathing cells that share a common lineage. Dev Biol. 1996; 173: 327–43.
14. Franklin RJM, Barnett SC. Olfactory ensheathing cells and CNS regeneration – the sweet smell of success? Neuron. 2000; 28: 1–4.
15. Lipson AC, Widenfalk J, Lindqvist E, et al. Neurotrophic properties of olfactory ensheathing glia. Exp Neurol. 2003; 180: 167–71.
16. Mackay-Sim A, Chuah MI. Neurotrophic factors in the primary olfactory pathway. Prog Neurobiol. 2000; 62: 527–59.
17. Woodhall E, West AK, Chuah MI. Cultured olfactory ensheathing cells express nerve growth factor, brain-derived neurotrophic factor, glia cell line-derived neurotrophic factor and their receptors. Brain Res Mol Brain Res. 2001; 88: 203–13.
18. Wewetzer K, Grothe C, Claus P. In vitro expression and regulation of ciliary neurotrophic factor and its α receptor subunit in neonatal rat olfactory ensheathing cells. Neurosci Lett. 2001; 306: 165–8.
19. Boruch AV, Conners JJ, Pipitone M, et al. Neurotrophic and migratory properties of an olfactory ensheathing cell line. Glia. 2001; 33: 225–9.
20. Simon AM, Goodenough DA. Diverse functions of vertebrate gap junctions. Trends Cell Biol. 1998; 8: 477–82.
21. Nakase T, Naus CC. Gap junctions and neurological disorders of the central nervous system. Biochim Biophys Acta. 2004; 1662: 149–58.
22. Söhl G, Willecke K. Gap junctions and the connexin protein family. Cardiovasc Res. 2004; 62: 228–32.
23. Nagy JI, Rash JE. Connexins and gap junctions of astrocytes and oligodendrocytes in the CNS. Brain Res Brain Res Rev. 2000; 32: 29–44.
24. Mugnaini E. Cell junctions of astrocytes, ependyma, and related cells in the mammalian central nervous system, with emphasis on the hypothesis of a generalized functional syncytium of supporting cells. In: Federoff S, Vernadakis A, editors. Development, morphology, and regional specialization of astrocytes, vol. I, Orlando, FL: Academic Press; 1986. pp. 329–71.
25. Parenti R, Campisi A, Vanella A, et al. Immunocytochemical and RT-PCR analysis of connexin 36 in cultures of mammalian glial cells. Arch Ital Biol. 2002; 140: 101–8.
26. Goodenough DA, Paul DL. Beyond the gap: functions of unpaired connexon channels. Nat Rev Mol Cell Biol. 2003; 4: 285–94.
27. Evans WH, De Vuyst E, Leybaert L. The gap junction cellular internet: connexin hemichannels enter the signalling limelight. Biochem J. 2006; 397: 1–14.
28. Spray DC, Ye ZC, Ransom BR. Functional connexin “hemichannels”: a critical appraisal. Glia. 2006; 54: 758–73.
29. Plotkin LI, Manolagas SC, Bellido T. Transduction of cell survival signals by connexin-43 hemichannels. J Biol Chem. 2002; 277: 8648–57.

30. Hur KC, Shim JE, Johnson RG. A potential role for Cx43-hemichannels in staurosporin-induced apoptosis. Cell Commun Adhes. 2003; 10: 271–7.
31. Kalvelyte A, Imbrasaite A, Bukauskiene A, et al. Connexins and apoptotic transformation. Biochem Pharmacol. 2003; 66: 1661–72.
32. Krysko DV, Leybaert L, Vandenabeele P, et al. Gap junctions and the propagation of cell survival and cell death signals. Apoptosis. 2005; 10: 459–69.
33. Bruzzone R, White TW, Paul DL. Connections with connexins: the molecular basis of direct intercellular signaling. Eur J Biochem. 1996; 238: 1–27.
34. Bevans CG, Kordel M, Rhee SK, et al. Isoform composition of connexin channels determines selectivity among second messengers and uncharged molecules. J Biol Chem. 1998; 273: 2808–16.
35. Bruzzone R, White TW, Paul DL. Expression of chimeric connexins reveals new properties of the formation and gating behavior of gap junction channels. J Cell Sci. 1994; 107: 955–67.
36. Cottrell GT, Burt JM. Functional consequences of heterogeneous gap junction channel formation and its influence in health and disease. Biochim Biophys Acta. 2005; 1711: 126-41.
37. Johnstone S, Isakson B, Locke D. Biological and biophysical properties of vascular connexin channels. Int Rev Cell Mol Biol. 2009; 278: 69–118.
38. Veenstra RD. Size and selectivity of gap junction channels formed from different connexins. J Bioenerg Biomembr. 1996; 28: 327–37.
39. Dermietzel R, Farooq M, Kessler JA, et al. Oligodendrocytes express gap junction proteins connexin32 and connexin45. Glia. 1997; 20: 101–14.
40. Kamasawa N, Sik A, Morita M, et al. Connexin-47 and connexin-32 in gap junctions of oligodendrocyte somata, myelin sheaths, paranodal loops and Schmidt-Lanterman incisures: implications for ionic homeostasis and potassium siphoning. Neuroscience. 2005; 136: 65–86.
41. Nagy JI, Rash JE. Astrocyte and oligodendrocyte connexins of the glial syncytium in relation to astrocyte anatomical domains and spatial buffering. Cell Commun Adhes. 2003; 10: 401–6.
42. Barnett SC, Riddell JS. Olfactory ensheathing cells (OECs) and the treatment of CNS injury: advantages and possible caveats. J Anat. 2004; 204: 57–67.
43. Parenti R, Cicirata F, Zappalà A, et al. Dynamic expression of Cx47 in mouse brain development and in the cuprizone model of myelin plasticity. Glia. 2010; 58(13): 1594–609.
44. Orellana JA, Avendaño BC, Montero TD. Role of connexins and pannexins in ischemic stroke. Curr Med Chem. 2014; 21: 2165–82.
45. Xie H, Cui Y, Deng F, et al. Connexin: a potential novel target for protecting the central nervous system? Neural Regen Res. 2015; 10: 659–66.
46. Li X, Zhao H, Tan X, et al. Inhibition of connexin43 improves functional recovery after ischemic brain injury in neonatal rats. Glia. 2015; 63: 1553–67.
47. Bennett MV, Contreras JE, Bukauskas FF, et al. New roles for astrocytes: gap junction hemichannels have something to communicate. Trends Neurosci. 2003; 26: 610–7.
48. Franssen EH, de Bree FM, Verhaagen J. Olfactory ensheathing glia: their contribution to primary olfactory nervous system regeneration and their regenerative potential following transplantation into the injured spinal cord. Brain Res Rev. 2007; 56: 236–58.
49. Raisman G. Olfactory ensheathing cells – anothermiracle cure for spinal cord injury? Nat Rev Neurosci. 2001; 2: 369–75.
50. Ramon-Cueto A, Corsero MI, Santos-Benito FF, et al. Functional recovery of paraplegic rats and motor axon regeneration in their spinal cords by olfactory ensheathing cells. Neuron. 2000; 25: 425–35.
51. Rozental R, Srinivas M, Spray DC. How to close a gap junction channel. Efficacies and potencies of uncoupling agents. Methods Mol Biol. 2001; 154: 447–76.
52. Leithe E, Kjenseth A, Bruun J, et al. Inhibition of connexin 43 gap junction channels by the endocrine disruptor ioxynil. Toxicol Appl Pharmacol. 2010; 247(1): 10–7.
53. Wang N, De Vuyst E, Ponsaerts R, et al. Selective inhibition of Cx43 hemichannels by Gap19 and its impact on myocardial ischemia/reperfusion injury. Basic Res Cardiol. 2013; 108(1): 309.
54. Maugeri G, D'Amico AG, Rasà DM, et al. Expression profile of Wilms Tumor 1 (WT1) isoforms in undifferentiated and all-trans retinoic acid differentiated neuroblastoma cells. Genes Cancer. 2016; 7(1–2): 47–58.
55. Lindsay SL, Riddell JS, Barnett SC. Olfactory mucosa for transplant mediated repair: a complex tissue for a complex injury? Glia. 2010; 58: 125–34.
56. Raisman G, Li Y. Repair of neural pathways by olfactory ensheathing cells. Nat Rev Neurosci. 2007; 8: 312–9.
57. Chehrehasa F, Windus LC, Ekberg JA, et al. Olfactory glia enhance neonatal axon regeneration. Mol Cell Neurosci. 2010; 45: 277–88.
58. Su Z, He C. Olfactory ensheathing cells: biology in neural development and regeneration. Prog Neurobiol. 2010; 92: 517–32.

59. Pellitteri R, Cova L, Zaccheo D, et al. Phenotypic modulation and neuroprotective effects of olfactory ensheathing cells: a promising tool for cell therapy. Stem Cell Rev. 2016; 12: 224–34.
60. Takeuchi H, Jin S, Wang J, et al. Tumor necrosis factor-alpha induces neurotoxicity via glutamate release from hemichannels of activated microglia in an autocrine manner. J Biol Chem. 2006; 281: 21362–8.
61. Thompson RJ, Jackson MF, Olah ME, et al. Activation of pannexin-1 hemichannels augments aberrant bursting in the hippocampus. Science. 2008; 322: 1555–9.
62. Karpuk N, Burkovetskaya M, Fritz T, et al. Neuroinflammation leads to region-dependent alterations in astrocyte gap junction communication and hemichannel activity. J Neurosci. 2011; 31: 414–25.
63. Orellana JA, Froger N, Ezan P, et al. ATP and glutamate released via astroglial connexin 43 hemichannels mediate neuronal death through activation of pannexin 1 hemichannels. J Neurochem. 2011a; 118: 826–40.
64. Orellana JA, Shoji KF, Abudara V, et al. Amyloid β-induced death in neurons involves glial and neuronal hemichannels. J Neurosci. 2011b; 31: 4962–77.
65. Gulbransen BD, Bashashati M, Hirota SA, et al. Activation of neuronal P2X7 receptor-pannexin-1 mediates death of enteric neurons during colitis. Nat Med. 2012; 18: 600–4.
66. Burkovetskaya M, Karpuk N, Xiong J, et al. Evidence for aberrant astrocyte hemichannel activity in Juvenile Neuronal Ceroid Lipofuscinosis (JNCL). PLoS ONE. 2014; 9: e95023.
67. Rouach N, Koulakoff A, Giaume C. Neurons set the tone of gap junctional communication in astrocytic networks. Neurochem Int. 2004; 45(2–3): 265–72.
68. Chew SS, Johnson CS, Green CR, et al. Role of connexion 43 in central nervous system injury. Exp Neurol. 2010; 225(2): 250–61.
69. Orellana JA, Hernández DE, Ezan P, et al. Hypoxia in high glucose followed by reoxygenation in normal glucose reduces the viability of cortical astrocytes through increased permeability of connexin 43 hemichannels. Glia. 2010; 58: 329–43.
70. O'Carroll SJ, Becker DL, Davidson JO, et al. The use of connexin-based therapeutic approaches to target inflammatory diseases. Methods Mol Biol. 2013; 1037: 519–46.
71. Bennett MV, Garré JM, Orellana JA, et al. Connexin and pannexin hemichannels in inflammatory responses of glia and neurons. Brain Res. 2012; 1487: 3–15.
72. Zhou JZ, Jiang JX. Gap junction and hemichannel-independent actions of connexins on cell and tissue functions–an update. FEBS Lett. 2014; 588(8): 1186–92.
73. Yoon JJ, Green CR, O'Carroll SJ, et al. Dose-dependent protective effect of connexin43 mimetic peptide against neurodegeneration in an ex vivo model of epileptiform lesion. Epilepsy Res. 2010; 92: 153–62.
74. Schulz R, Görge PM, Görbe A, et al. Connexin 43 is an emerging therapeutic target in ischemia/reperfusion injury, cardioprotection and neuroprotection. Pharmacol Ther. 2015; 153: 90–106.
75. Davidson JO, Green CR, Bennet L, et al. Battle of the hemichannels–Connexins and pannexins in ischemic brain injury. Int J Dev Neurosci. 2015; 45: 66–74.
76. Davidson JO, Green CR, Nicholson LF, et al. Connexin hemichannel blockade is neuroprotective after, but not during, global cerebral ischemia in near-term fetal sheep. Exp Neurol. 2013; 248: 301–8.

Figure 1

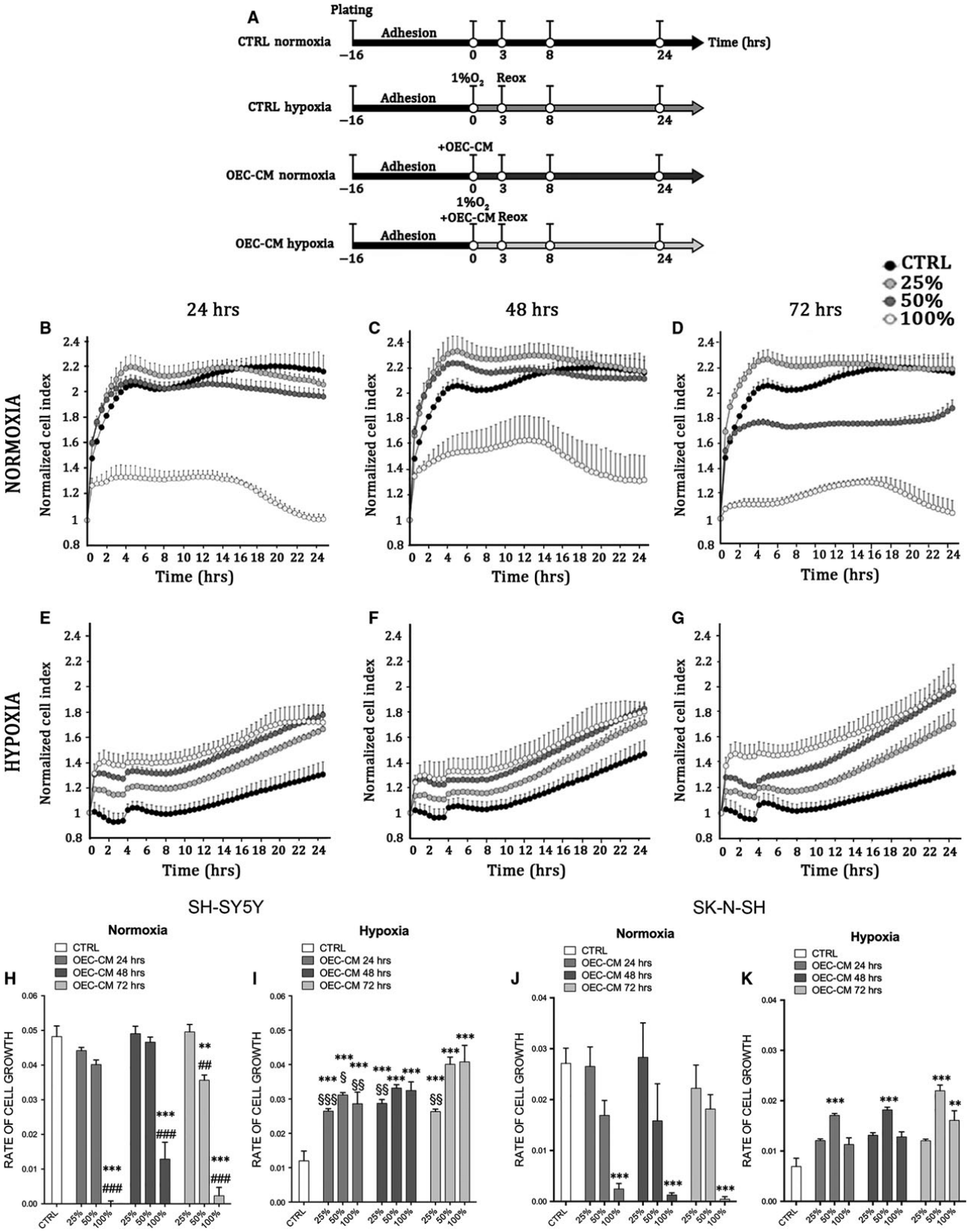
A
Plating
CTRL normoxia
Adhesion
Time (hrs)
−16
0
3
8
24
CTRL hypoxia
1%O2
Reox
OEC-CM normoxia
+OEC-CM
OEC-CM hypoxia
CTRL
25%
50%
100%
24 hrs
48 hrs
72 hrs
NORMOXIA
HYPOXIA
Normalized cell index
Time (hrs)
SH-SY5Y
SK-N-SH
Normoxia
Hypoxia
OEC-CM 24 hrs
OEC-CM 48 hrs
OEC-CM 72 hrs
RATE OF CELL GROWTH

Fig. 1 OEC-CM exhibits neuroprotective effects on the human neuroblastoma cell lines. (**A**) Experimental plan. (**B–G**) xCELLigence system E-Plate analysis of cell viability on SH-SY5Y cell cultures. Each dot represents the cell index (CI) mean (± SEM) of three independent analyses and CI was revealed every 30 min on the same cultures. (**H–K**) Rate of Cell Growth (slope of the line between time 0 and time 24) in normoxic and hypoxic SH-SY5Y (**H, I**) and SK-N-SH (**J, K**) cell cultures exposed to different conditioning-time and percentage of OEC-CM. **P < 0.01 versus CTRL. ***P < 0.001 versus CTRL. ##P < 0.01 versus corresponding OEC-CM 25%. ###P < 0.001 versus corresponding OEC-CM 25%. §P < 0.05 versus OEC-CM 72 hr 100%. §§P < 0.01 versus OEC-CM 72 hr 100%. §§§P < 0.001 versus OEC-CM 72 hr 100%. (mANOVAs and Tukey honest significant difference (HSD) post hoc test).

Figure 2

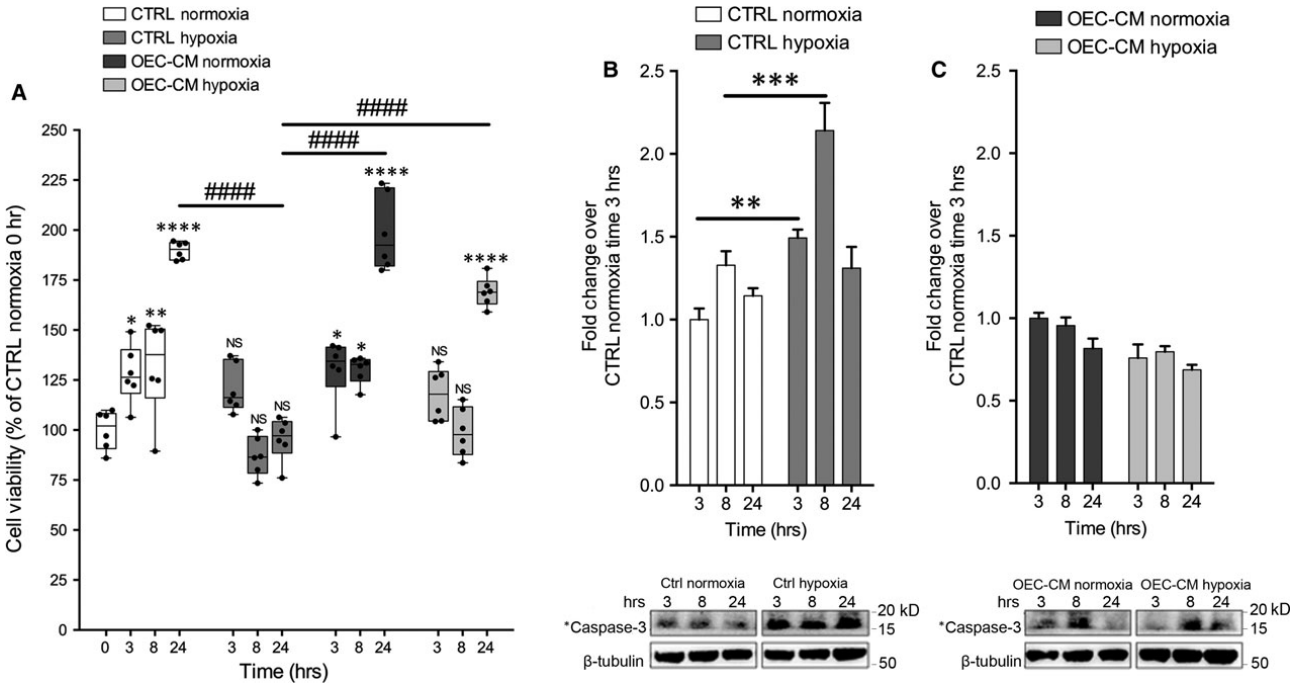

Fig. 2 OEC-CM increased SH-SY5Y cell viability and reduced H/R injury mediated damage. (**A**) MTT-viability tests performed at 0, 3, 8 and 24 hrs. Values of spectrophotometric determination at 550 nm are reported as percentage of cultures at time 0, considered as 100%. Data are shown via standard box-and-whiskers plots in which the central-line represents the median, the upper- and lower bounds of the boxes are min and max value and dots represent all value expressed as percentage of control. NS not significant, *P < 0.05, **P < 0.01 and ***P < 0.001 versus CTRL Normoxia time 0. ####P < 0.0001 (mANOVAs and Tukey honest significant difference (HSD) post hoc test). (**B**) Western blot analysis of Cleaved Caspase-3 levels on SH-SY5Y in control and H/R injured cultures. Proteins levels are plotted as fold change over 3 hrs after treatment in control culture considered as 1. **P < 0.01, ***P < 0.001 (mANOVAs and Tukey honest significant difference (HSD) post hoc test). (**C**) Western blot analysis of Cleaved Caspase-3 levels on SH-SY5Y in OEC-CM conditioned cultures in normoxic and in H/R injured cultures. Proteins levels are plotted as fold change over 3 hrs after treatment in OEC-CM normoxic cultures considered as 1.

Figure 3

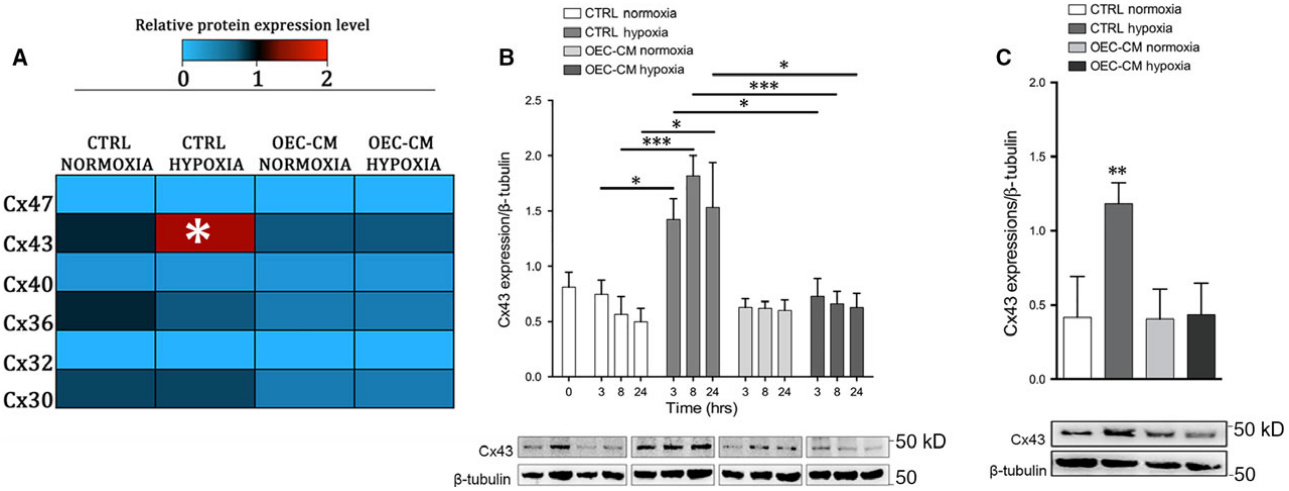

Fig. 3 Cxs profile of SH-SY5Y and SK-N-SH cell lines. (**A**) Heatmap of Cx47, Cx43, Cx40, Cx36, Cx32 and Cx30 protein expression levels on SH-SY5Y cell line at 24 hrs. Western blots were digitally analysed by integrating the density of each protein band and its corresponding ß-Tubulin band intensity. Colour key shown for each protein reveals the colour code used to visualise the relative protein expression level, light blue colours correspond to low relative protein expression levels, while red colour correspond to high relative protein expression levels. Average protein expression levels from duplicate cultures were assessed at 24 hrs post-H/R injury. *P < 0.05 versus CTRL Normoxia. (mANOVAs and Tukey honest significant difference (HSD) post hoc test). (**B**) Western blot analysis of Cx43 in lysates of SH-SY5Y normoxic and H/R cultures. Data show the ratio between intensity of Cx43 bands divided by relative ß-Tubulin bands intensity quantified using ImageJ software. Blot shown is representative of three independent experiments. *P < 0,05, ***P < 0.001. (mANOVAs and Tukey honest significant difference (HSD) post hoc test). (**C**) Western blot analysis of Cx43 in lysates of SK-N-SH normoxic and H/R cultures. Data show the ratio between intensity of Cx43 bands divided by relative ß-Tubulin bands intensity quantified using ImageJ software. Blot shown is representative of three independent experiments. **P < 0.01. (mANOVAs and Tukey honest significant difference (HSD) post hoc test).

Figure 4

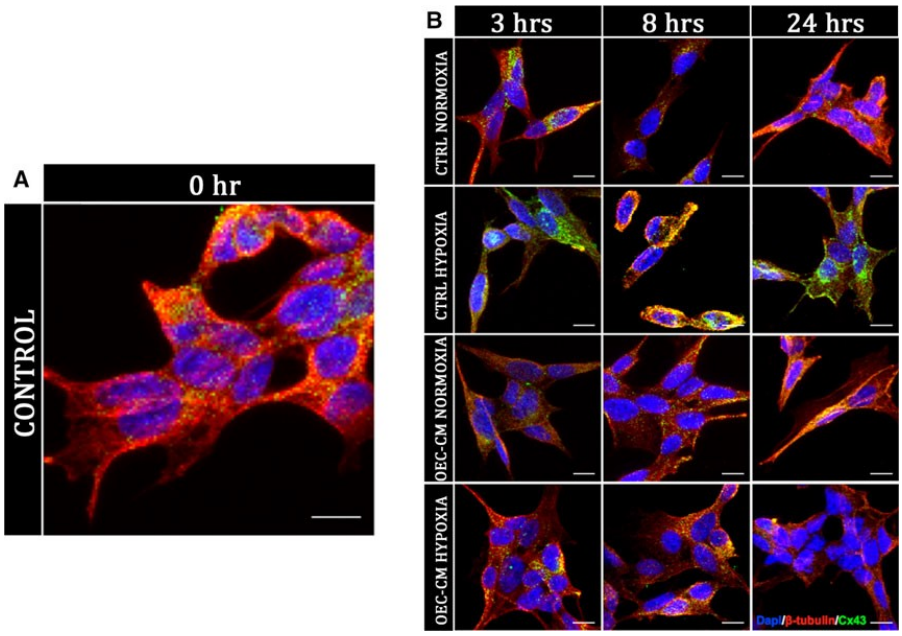

Fig. 4 Cx43 immunofluorescence analysis in SH-SY5Y cell cultures. Cx43 localization analysis by immunofluorescence on unconditioned control cultures (**A**) and on OEC-CM treated cultures in normoxic condition and H/R injured cultures (**B**). Scale bar: 10 μm.

Figure 5

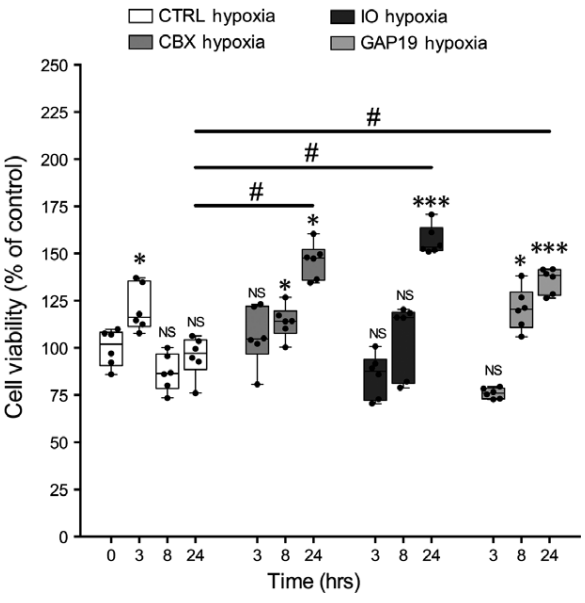

Fig. 5 MTT-viability tests on SH-SY5Y exposed to H/R injury treated with a non-selective GJIC inhibitor (CBX), selective inhibitor of homotypic Cx43-GJs (IO) and, selective inhibitor of homotypic Cx43-HCs (GAP19). MTT-viability tests performed at 0, 3, 8 and 24 hrs. Values of spectrophotometric determination at 550 nm are reported as percentage of cultures at time 0, considered as 100%. Data are shown via standard box-and-whiskers plots in which the central-line represents the median, the upper and lower bounds of the box are min and max value and dots represent all value. NS not significant, *P < 0.05 and ***P < 0.001 versus CTRL Normoxia time 0. #P < 0.05. (mANOVAs and Tukey honest significant difference (HSD) post hoc test).

Neural stem cells respond to extracellular succinate via SUCNR1/GPR91 to ameliorate chronic neuroinflammation

Luca Peruzzotti-Jametti[1], Joshua D. Bernstock[1,2], **Nunzio Vicario**[1], Ana S H Costa[3], Chee-Keong Kwok[4], Tommaso Leonardi[1], Lee M. Booty[5], Iacopo Bicci[1], Beatrice Balzarotti[1], Giulio Volpe[1], Giulia Mallucci[1], Giulia Manferrari[1], Nunzio Iraci[1,7], Alice Braga[1], John M. Hallenbeck[2], Michael P. Murphy[5], Frank Edenhofer[4,6]*, Christian Frezza[3]* and Stefano Pluchino[1]*

[1]Department of Clinical Neurosciences - Division of Stem Cell Neurobiology, Wellcome Trust-Medical Research Council Stem Cell Institute and NIHR Biomedical Research Centre, University of Cambridge, UK;
[2]Stroke Branch, National Institute of Neurological Disorders and Stroke, National Institutes of Health (NINDS/NIH), Bethesda, MD, USA;
[3]MRC Cancer Unit, University of Cambridge, Hutchison/MRC Research Centre, University of Cambridge, UK;
[4]Institute of Anatomy and Cell Biology, University Wurzburg, Germany;
[5]MRC Mitochondrial Biology Unit, Hills Road, University of Cambridge, UK;
[6]Institute of Molecular Biology & CMBI, Genomics, Stem Cell Biology & Regenerative Medicine, Leopold-Franzens-University Innsbruck, Austria;
[7]Department of Biomedical and Biotechnological Sciences (BIOMETEC), University of Catania, Via S. Sofia 97, Catania 95125, Italy.
*These authors contributed equally to this work.

1st round revision: Cell Stem Cell

Correspondence:

Stefano Pluchino: spp24@cam.ac.uk; Luca Peruzzotti-Jametti: lp429@cam.ac.uk; Frank Edenhofer: Frank.Edenhofer@uibk.ac.at; or Christian Frezza: CF366@MRC-CU.cam.ac.uk

Running title: SUCNR1 and anti-inflammatory neural stem cells

Summary

Neural stem cell (NSC) transplantation induces recovery in animal models of central nervous system (CNS) diseases, in part by modulating adaptive and innate immune responses. Since metabolism governs the phenotype and function of immune cells, we investigated whether NSCs have the ability to regulate the immunometabolic components underpinning neuroinflammation.

Here we identify a new mechanism by which transplanted somatic and directly-induced NSCs counteract CNS-compartmentalised chronic inflammation in mice. NSC transplantation reduces the immunometabolite succinate in the cerebrospinal fluid, while decreasing the burden of mononuclear phagocyte (MP) infiltration and secondary CNS damage. Mechanistically, the antiinflammatory activity of NSCs arises in response to succinate released by inflammatory MPs, which activates succinate receptor 1 (SUCNR1)/GPR91 on NSCs, thus initiating prostaglandin E2 secretion and extracellular succinate scavenging. Our work uncovers a succinate-SUCNR1 axis in NSCs that clarifies how stem cells respond to inflammatory metabolic signals to inhibit the activation of type-1 MPs in the chronically inflamed brain.

Keywords

Neural stem cells (NSCs), induced neural stem cells (iNSCs), stem cells, immunometabolism, macrophages, succinate, SUCNR1/GPR91, experimental autoimmune encephalomyelitis (EAE), multiple sclerosis (MS), regenerative neuroimmunology.

Graphical Abstract

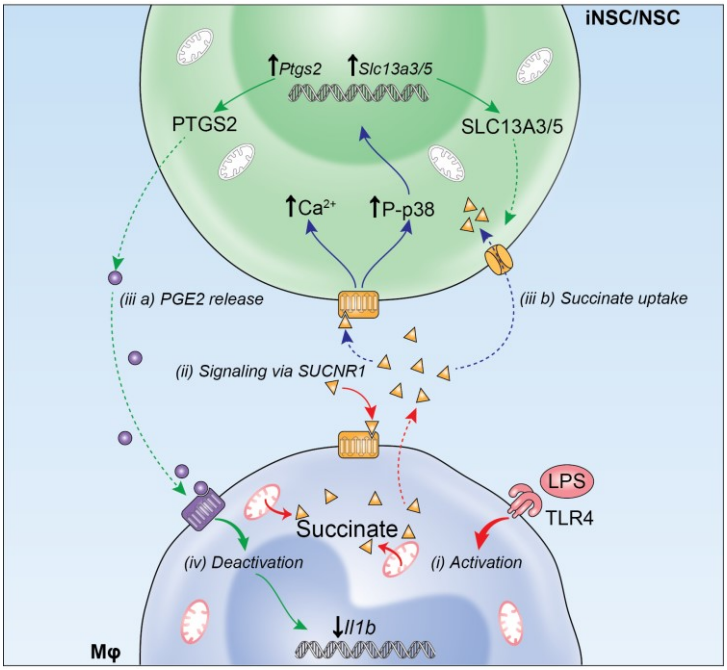

Highlights

• The transplantation of iNSCs or NSCs is functionally equivalent in ameliorating chronic neuroinflammation;

• iNSCs/NSCs reduce extracellular succinate in the CSF of EAE mice after transplantation and reset the metabolism of type-1 MPs to an anti-inflammatory phenotype in co-cultures;

• Succinate activates SUCNR1/GPR91 on NSCs to initiate the secretion of PGE2 and the scavenging of extracellular succinate;

• Sucnr1 loss-of-function NSCs show reduced anti-inflammatory activities *in vitro* and *in vivo* after transplantation.

Introduction

Advances in stem cell biology have raised hopes that diseases of the central nervous system (CNS) may be ameliorated by non-hematopoietic stem cell medicines (Martino and Pluchino, 2006). We have provided compelling evidence that the transplantation of somatic neural stem cells (NSCs) improves the clinico-pathological features of animal models of inflammatory CNS disorders. Beyond the structural replacement of injured CNS cells, our work has shown that transplanted NSCs engage in complex stem cell graft-to-host communication programs, overall leading to trophic support and modulation of adaptive and innate immune responses (Bacigaluppi et al., 2009; Bacigaluppi et al., 2016; Pluchino and Cossetti, 2013; Pluchino et al., 2009b; Pluchino et al., 2005). Specifically, NSCs transplants reduce the burden of inflammation at site of injury (Pluchino et al., 2009a; Pluchino et al., 2005), decrease the number of type-1 inflammatory mononuclear phagocytes (MPs) (Cusimano et al., 2012), and promote the healing of the injured CNS via yet poorly characterised mechanisms.

However, the clinical translation of experimental NSC therapies is still limited by the sources from which human NSCs (hNSCs) are derived (Anderson et al., 2017), the intrinsic immunogenicity of allogeneic hNSC lines (Ramos-Zuniga et al., 2012; Rice et al., 2013), and the stability of the so called ‘intended clinical cell lot’ (Anderson et al., 2017; Wright et al., 2006). Autologous and stably expandable directly-induced NSCs (iNSCs) from patients’ dermal fibroblasts are emerging as a valid alternative to NSCs therapies (Lu et al., 2013; Meyer et al., 2015; Thier et al., 2012). The efficacy of reprogrammed NSCs in treating inflammatory CNS disorders has not yet been tested. In progressive forms of multiple sclerosis (MS), chronic CNS inflammation is sustained by widespread activation of MPs that include both CNS resident microglia and blood-derived macrophages (Mallucci et

al., 2015). MPs are found in grey matter lesions, close to degenerating neurites and neuronal cell bodies (Peterson et al., 2001), and in white matter lesions, where the external rim of activated microglia is associated with chronic tissue damage (Bramow et al., 2010; Prineas et al., 2001). Areas of normal appearing white matter are also characterised by MP accumulation, which leads to the formation of microglial nodules that drive disease pathology irrespective of concomitant T cell activation (Moll et al., 2011). The detrimental role of chronic MP driven inflammation in progressive MS is also supported by evidence in animal disease models where its overall burden correlates with impaired neuronal function (Planche et al., 2017), brain atrophy (Tambalo et al., 2015), and reduced regenerative responses (Jiang et al., 2014). Activation of MPs by pro-inflammatory stimuli causes a metabolic switch towards glycolysis and reduced oxidative phosphorylation (OXPHOS) (Kelly and O'Neill, 2015). Recent evidence suggests that, within this metabolic rewiring, type-1 inflammatory MPs accumulate succinate, with important pathophysiological implications (Tannahill et al., 2013). Intracellular succinate inhibits the activity of prolyl hydroxylases enzymes (PHDs), thereby stabilising hypoxia responsive element (HIF)-1α and inducing the transcription of interleukin (IL)-1β (Tannahill et al., 2013). Furthermore, oxidation of succinate by succinate dehydrogenase (SDH) repurposes mitochondria from ATP synthesis to ROS production, as additional pro-inflammatory signal (Mills et al., 2016). Type-1 inflammatory MPs also release succinate extracellularly and up-regulate its cognate succinate receptor 1 (SUCNR1), a G protein–coupled receptor (also known as GPR91), which functions as autocrine and paracrine sensor to enhance IL-1β production (Littlewood-Evans et al., 2016).

As such, succinate is being proposed as key immune modulatory metabolite, and MP metabolism is emerging as an important therapeutic target in acute and chronic inflammatory diseases (Tannahill et al., 2015). Given the established immune modulatory properties of NSCs (Pluchino and Cossetti, 2013), we hypothesised that NSCs may exert their therapeutic effects in chronic neuroinflammation by modulating MP metabolism towards reduction of secondary CNS damage.

In this work, we investigated the molecular mechanisms that underpin the capacity of somatic and directly-induced NSCs to counteract the metabolic changes of type-1 inflammatory MPs both *in vivo* and *in vitro*. We show that transplanted iNSCs and NSCs are functionally equivalent in ameliorating chronic neuroinflammation in mice with experimental autoimmune encephalomyelitis (EAE). Furthermore, transplanted iNSCs/NSCs reduce the numbers of type-1 inflammatory MPs in the brain and in the spinal

cord, as well as the levels of the immunometabolite succinate in the cerebrospinal fluid (CSF). iNSCs/NSCs also decrease extracellular succinate released by type-1 inflammatory MPs to reprogram their metabolism towards OXPHOS *in vitro*. Mechanistically, we find that succinate secreted by type-1 MPs elicits in iNSCs/NSCs a signalling cascade downstream SUCNR1, which enables their anti-inflammatory activity. This succinate-licensed anti-inflammatory function of iNSCs/NSCs is mediated by the secretion of prostaglandin (PG) E2, as well as by considerable scavenging of extracellular succinate. Loss of Sucnr1 function in NSCs leads to significantly reduced anti-inflammatory activities *in vitro* and *in vivo* after transplantation in EAE. Our work uncovers an unexpected succinate-SUCNR1 axis in NSCs that clarifies how stem cells respond to inflammatory metabolic signals to inhibit the activation of type-1 MPs in the chronically inflamed brain.

Results

NSC transplantation ameliorates chronic neuroinflammation and is coupled with reduction of the immunometabolite succinate in the cerebrospinal fluid.

We first assessed the effects of the intracerebroventricular (icv) transplantation at peak of disease (PD) of iNSCs or NSCs, in mice with MOG35-55-induced chronic EAE. Prior to transplantation, iNSCs and NSCs were expanded, characterised (**Figure S1**), and labelled with farnesylated (f)GFP *in vitro*. At 30 days post transplantation (dpt), iNSC and NSC transplants survived, distributed and integrated within the EAE brain and spinal cord (**Figure S2**). Only a minority of retrieved fGFP+ (iNSCs: 2.1 ± 0.9%; NSCs: 1.7 ± 0.1%) cells were proliferating (**Figure 1A**), or expressing neuronal (**Figure 1B**), astroglial (**Figure 1C**) or oligodendroglial (**Figure 1D**) lineage markers (**Figure S2**). The majority (~ 75%) of iNSCs surviving to transplantation were found instead not to be expressing any of the neural lineage markers tested, and localising around perivascular areas close to F4/80+ endogenous MPs (**Figure 1E**), as previously observed in somatic NSCs grafts (Cusimano et al., 2012; Pluchino et al., 2003). The transplantation of iNSCs induced a significant and long lasting (up to 90 dpt) amelioration of EAE scores, which started from 15-20 dpt onwards (**Figure 1F** and **Figure S3**). Functional recovery was also confirmed by computer-assisted automated gait analysis (**Figure S4**). Overall, icv-transplanted iNSCs were safe, and led to behavioural and pathological recovery.

We then analysed the expression levels of the main pro- and anti-inflammatory genes in the whole CNS. iNSC- and NSC-transplanted EAE mice both exhibited significantly reduced levels of interleukin 1 beta (Il1b) in the brain and spinal cord, and increased levels of mannose receptor C type 1 (Mrc1) in the spinal cord, both at 10 dpt (**Figure 1G**). The transplantation of iNSCs or NSCs also significantly reduced the immunoreactivity for the MP marker F4/80, with no significant effects on CD3 (T cells) and CD20 (B cells) immunoreactivity, both in the brain and in the spinal cord (**Figure 1H**). F4/80+ MPs from iNSCs-/NSCs-transplanted EAE mice also exhibited a decrease in the expression of the type-1 inflammatory MP marker inducible nitric oxide synthase (iNOS) (**Figure 1I** and **J**). Finally, iNSC- and NSC-transplanted EAE mice accumulated significantly reduced axonal loss (**Figure 1K**) and demyelination (**Figure 1L**) in the spinal cord.

Given the established importance of metabolism in regulating the phenotype and function of MPs, we investigated whether NSC transplants affected the neuroinflammatory metabolic microenvironment. To this end, we performed an untargeted metabolic profiling of polar metabolites by liquid chromatography coupled to mass spectrometry (LC-MS) of

matched CSF and plasma samples (**Data S1**). EAE mice showed a significant increase of several CSF (but not plasma) metabolites, among which succinate and histidine both peaked at 45 days postimmunization (dpi; corresponding to 30 dpt). While we did not detect any significant metabolite changes in plasma between stem cell-treated and control EAE mice (**Figure 1M** and **Data S1**), we found that the transplantation of iNSCs or NSCs led to a significant drop in CSF succinate at 30 dpt (**Figure 1M** and **Data S1**).
These results suggest that the transplantation of iNSCs/NSCs directly into the CNS exerts a local anti-inflammatory and tissue protective effect that is coupled with a reduction of the immunometabolite succinate in the CSF only.

NSCs reduce succinate levels and reprogram the metabolism of type-1 inflammatory Mφ *in vitro*

We then investigated the molecular mechanisms through which iNSCs/NSCs display antiinflammatory activities on type-1 MPs, using an *in vitro* system. Naïve bone marrow derived macrophages (Mφ) were polarized into a type-1 inflammatory phenotype with LPS ($M\varphi^{LPS}$), as described (Tannahill et al., 2013). $M\varphi^{LPS}$ were then co-cultured with iNSCs ($M\varphi^{LPS}$-iNSCs) or NSCs ($M\varphi^{LPS}$-NSCs) in a trans-well system that avoids cell-to-cell contacts (**Figure 2A**). Unpolarised Mφ were used as controls.
Microarray gene expression profiling showed significant transcriptional changes in MφLPS with 7,401 genes affected (vs. Mφ, adjusted p value< 0.1, **Figure 2B**, **Data S2**), and 51 genes differentially expressed in $M\varphi^{LPS}$-iNSCs or $M\varphi^{LPS}$-NSCs (vs. $M\varphi^{LPS}$, adjusted p value< 0.1, **Figure 2B-C**, **Data S2**). This latter set of genes was enriched in biological processes related to positive regulation of leukocyte activation (GO: 0002696), myeloid leukocyte differentiation (GO: 0002761) and immune system processes (GO: 0002376). Independent qRT-PCR validation of selected Mφ pro-inflammatory genes confirmed significant down-regulation of the expression levels of Il12b, Il15, Il15ra and Cd69, as well as the classical inflammatory genes Nos2, tumor necrosis factor (Tnf) and Il1b in $M\varphi^{LPS}$-iNSCs and $M\varphi^{LPS}$-NSCs (vs. $M\varphi^{LPS}$, **Figure 2D**). This effect was coupled with the concomitant up-regulation of the expression levels of genes associated with an antiinflammatory Mφ phenotype, such as uronyl-2-sulfotransferase (Ust) and bone marrow stromal cell antigen 1 (Bst1) (Al-Shabany et al., 2016; Martinez et al., 2015), as well as arginase 1 (Arg1) and Mrc1 (vs. $M\varphi^{LPS}$, **Figure 2E**). When iNSCs/NSCs were co-cultured with LPS-activated mouse BV2 microglial cells as before, significant reduction of the expression levels of the pro-inflammatory genes Nos2 and Il1b was also observed (**Figure**

2F).

To link gene expression profiles with functional metabolic states, we assessed the basal oxygen consumption rate (OCR) and extracellular acidification rate (ECAR) of $M\varphi^{LPS}$, as readouts of their TCA cycle and glycolytic activities, respectively. We found a significant reduction of OCR and a significant increase of ECAR in $M\varphi^{LPS}$ (vs. Mφ). Instead, $M\varphi^{LPS}$-iNSCs and $M\varphi^{LPS}$-NSCs underwent significant restoration of both OCR and ECAR values (vs. $M\varphi^{LPS}$, **Figure 2G**), as observed in Mφ switching to an anti-inflammatory phenotype (O'Neill and Pearce, 2016).

In an effort to clarify the metabolic determinants of these anti-inflammatory effects, we performed an untargeted LC-MS analysis of the extracellular and intracellular small molecule metabolite content of $M\varphi^{LPS}$. As expected, LPS stimulation profoundly changed the extracellular and intracellular metabolic milieu of Mφ ($M\varphi^{LPS}$) (vs. Mφ; **Data S3**). In co-cultures, $M\varphi^{LPS}$-iNSCs and $M\varphi^{LPS}$-NSCs both showed significant reduction of extracellular glutamate, GABA and succinate (vs. $M\varphi^{LPS}$, **Figure 2H** and **Data S3**). Furthermore, $M\varphi^{LPS}$-iNSCs and $M\varphi^{LPS}$-NSCs also displayed a significant reduction of intracellular succinate and itaconate (vs. $M\varphi^{LPS}$, **Figure 2H** and **Data S3**).

Consistent with the reduction of succinate levels, we found that $M\varphi^{LPS}$-iNSCs and $M\varphi^{LPS}$-NSCs exhibited significantly reduced levels of HIF-1α, of the upstream protein pyruvate kinase isozyme M2 (PKM2) (Palsson-McDermott et al., 2015) (**Figure 2I**), as well as of IL-1β (vs. $M\varphi^{LPS}$, **Figure 2J**).

Altogether these *in vitro* data provide evidence that iNSCs/NSCs reduce the accumulation of both intracellular and extracellular succinate in co-cultures with type-1 inflammatory MPs, reprogramming them towards an anti-inflammatory phenotype.

Succinate signals via SUCNR1/GPR91 in mouse and human NSCs

Given the importance of succinate as immunometabolic signal, we investigated whether succinate released by type-1 pro-inflammatory MPs could regulate the activity of surrounding cells *in situ*, including that of transplanted stem cells.

We found that transplanted iNSCs, detected in proximity to perivascular F4/80+ MPs, expressed SUCNR1 *in vivo* in the CNS (**Figure 3A**). SUCNR1 was also expressed at protein level on both iNSCs and NSCs *in vitro* (**Figure 3B**).

To further assess whether SUCNR1 in iNSCs/NSCs was functionally activated by succinate, we investigated its downstream signalling cascade *in vitro*.

When exposed to succinate (**Figure 3C**) (Rubic et al., 2008), iNSCs/NSCs triggered a

rapid release of intracellular calcium stores (**Figure 3D**), followed by a significant up-regulation of the Phospho-p38 mitogen-activated protein kinase (MAPK) (**Figure 3E**), indicative of its activation. We confirmed the expression of SUCNR1 and SUCNR1 also in human foetal NSCs (hNSCs) and human iNSCs (hiNSCs) (**Figure 3F** and **G**). As in mouse iNSCs, succinate-dependent p38 signalling was evoked in hiNSCs, but not in hiNSCs pre-treated with the selective SUCNR1 inhibitor 4c (**Figure 3H**).

Thus, we show that mouse and human iNSCs and NSCs express functional SUCNR1, which induces a signalling pathway downstream of its stimulation with the immunometabolite succinate.

SUCNR1 stimulation initiates the secretion of prostaglandin E2 by NSCs

To clarify the functional consequences of SUCNR1 signalling in NSCs, we generated NSCs from mice lacking Sucnr1 ($Sucnr1^{-/-}$ NSCs) (**Figure S5**) (Rubic et al., 2008), and performed a gene expression profiling microarray following treatment with succinate (**Data S4**).

We found that Prostaglandin-Endoperoxide Synthase 2 (Ptgs2), the key enzyme in PG biosynthesis encoding the inducible PTGS2, was the most up-regulated gene in succinatestimulated NSCs (log2 fold change 1.05), but not in succinate-stumulated $Sucnr1^{-/-}$ NSCs (log2 fold change -0.43) (**Figure 4A**). We validated these results on Ptgs2 by qRT-PCR, confirming that its expression levels were significantly up-regulated (2.1-2.7 fold change) in succinate-stumulated iNSCs and NSCs, whereas they were not in succinate-treated $Sucnr1^{-/-}$ NSCs (**Figure 4B**).

Given the role of PGE2 as regulator of the immunosuppressive effects of mesenchymal stem cells (MSCs) (Vasandan et al., 2016; Yanez et al., 2010), we tested its accumulation in tissue culture media from iNSCs, NSCs and $Sucnr1^{-/-}$ NSCs after stumulation with succinate. iNSCs and NSCs, but not $Sucnr1^{-/-}$ NSCs, showed significant (>2.5-fold) increase of their basal release of PGE2, as early as 30 min after succinate. This succinate-induced effect was abolished by pretreatment with the irreversible PTGS2 blocker SC-58125 (**Figure 4C**). As in mouse iNSCs, exposure of hiNSCs to succinate elicited a significant increase of PGE2 concentrations in tissue culture media, while again pre-treatment with either SC-58125 or 4c prevented its release (**Figure 4D**).

To further extend the relevance of these findings to co-cultures between NSCs and $M\varphi^{LPS}$, we analysed the levels of PGE2 in tissue culture media. We found that $M\varphi^{LPS}$-NSCs accumulated higher levels of PGE2 compared to $M\varphi^{LPS}$, while pre-treatment of co-cultured

NSCs with SC-58125 significantly reduced PGE2 levels (**Figure 4E**). SC-58125 pre-treatment of NSCs was also coupled with a significant increase of Il1b expression in $M\varphi^{LPS}$ (**Figure 4F**), and with a reduction of OCR values indicative of a pro-inflammatory phenotype (**Figure 4G**). However, we noticed that NSCs pre-treated with SC-58125 retained some residual anti-inflammatory effects on $M\varphi^{LPS}$, compared to Sucnr1$^{-/-}$ NSCs (**Figure 4F**). On the contrary, Sucnr1 loss of function in NSCs completely abolished their anti-inflammatory effects on $M\varphi^{LPS}$ (**Figure 4F** and **G**).

We also show that the observed PGE2-dependent anti-inflammatory ability of NSCs is conserved and relevant for human NSCs.

As such, hiNSCs induced a significant reduction of Il1b expression in $M\varphi^{LPS}$ in co-cultures (**Figure 4H**); which was coupled with a significant restoration of OCR values (**Figure 4I**), and increased PGE2 levels in tissue culture media (**Figure 4J**). These effects were completely suppressed by pre-treatment of hiNSCs with the selective SUCNR1 inhibitor 4c (**Figure 4H-J**). Thus, the activation of SUCNR1 signalling pathway in mouse and human NSCs triggers the release of PGE2 leading to anti-inflammatory effects on type-1 MPs.

However, inhibition experiments targeting either PTGS2 or SUCNR1 anticipate that additional SUCNR1-dependent - PGE2-independent - mechanisms are likely to play a key role in the antiinflammatory effects of NSCs.

SUCNR1 stimulation triggers the uptake of succinate by NSCs

Gene expression arrays of succinate-stimulated NSCs revealed that, besides Ptgs2, NaCT/Slc13a5 was among the most up-regulated genes in WT NSCs (log2 fold change 0.49), but not in Sucnr1$^{-/-}$ NSCs (log2 fold change -0.12). SCL13A5 is a dicarboxylate co-transporter, known to be involved in succinate transport (Srisawang et al., 2007). Given the consistent depletion of succinate found both *in vivo* in the CSF of iNSC- or NSC-transplanted EAE mice, and *in vitro* in cocultures with $M\varphi^{LPS}$, we hypothesised that iNSCs/NSCs would activate SCL13A5 to scavenge succinate. We found that the expression of SLC13A5, as well as of the high affinity dicarboxylate cotransporter SLC13A3, were significantly increased in iNSCs and NSCs, but not in Sucnr1$^{-/-}$ NSCs, upon succinate stimulation (**Figure 5A**). Similarly, hiNSCs exposed to succinate up-regulated the protein expression levels of both these SLC13 co-transporters *in vitro* (**Figure 5B**).

We next investigated the role of these co-transporters by measuring succinate uptake in iNSCs and NSCs. We found that both iNSCs and NSCs significantly accumulated [14C]-

labelled succinate (**Figure 5C**), while reducing the amount of extracellular [14C]-succinate in tissue culture media (**Figure 5D**). Sucnr1$^{-/-}$ NSCs neither accumulated [14C]-succinate intracellularly nor did they deplete it extracellularly (**Figure 5C** and **D**). Interestingly, Sucnr1$^{-/-}$ NSCs, which we have shown to have no effects on Il1b expression in Mφ^{LPS} (**Figure 4F**), failed to reduce the extracellular succinate levels in co-cultures with Mφ^{LPS} (**Figure 5E**). As further proof of the importance of succinate depletion in modulating the phenotype of type-1 pro-inflammatory MPs, we show that treatment with active recombinant (r)SDH complex subunit A is able to significantly reduce the expression of Il1b in Mφ^{LPS} (**Figure S6**).

Thus, SUCNR1 signalling in NSCs prompts the uptake of the immunometabolite succinate, thereby depleting the available extracellular pool sustaining the autocrine and paracrine activation of type-1 MPs.

Transplantation of Sucnr1 loss-of-function NSCs shows impaired ability to ameliorate chronic neuroinflammation *in vivo*

To confirm the role of the succinate-SUCNR1 axis in mediating the response of NSC grafts to succinate *in vivo*, we assessed the effects of the icv transplantation of Sucnr1$^{-/-}$ NSCs in mice with chronic EAE.

At 30 dpt, the transplantation of Sucnr1$^{-/-}$ NSCs induced only a slight recovery of EAE behavioural deficits, vs. control EAE mice (EAE score - Sucnr1$^{-/-}$ NSCs: 2.9 ± 0.2; PBS: 3.6 ± 0.4), which was significantly less pronounced (50% of the effect) than that observed in EAE mice transplanted with NSCs (EAE score - NSCs: 2.1 ± 0.3) (**Figure 6A**). *Ex vivo* metabolomics of matched CSF and plasma samples showed lack of succinate depletion in the CSF from EAE mice transplanted with Sucnr1$^{-/-}$ NSCs (**Figure 6B**). Post-mortem tissue pathology confirmed the reduced anti-inflammatory (**Figure 6C**) and tissue protective effects (**Figure 6D** and **E**) of Sucnr1$^{-/-}$ NSC grafts.

These data confirm the requirement of functional SUCNR1 signalling pathway in the regulation of the anti-inflammatory and neuroprotective effects of NSC transplants *in vivo*.

Discussion

There is an unmet clinical need to develop cellular and molecular approaches to target core drivers of the pathophysiology of chronic neuroinflammatory conditions that include progressive forms of MS (Volpe et al., 2016). In principle, stem cells possess a therapeutic potential that is distinct from that of small molecules and biologics and extend far beyond

the classical regenerative medicine arena. Part drug and part device, stem cells could work as biological disease modifying agents (DMAs) that sense diverse signals, migrate to specific sites in the body, integrate inputs to make decisions, and execute complex response behaviours, in the context of a specific tissue microenvironment (Fischbach et al., 2013). All these attributes could be harnessed to treat several disease processes, including the persistent MP-driven inflammation and tissue degeneration that occur in progressive MS.

Here we used accessible, autologous and stably expandable directly-induced NSCs (iNSCs) (Thier et al., 2012), as well as somatic NSCs, to investigate the effects of stem cell transplantation in a mouse model of chronic neuroinflammation, which mimics the inflammatory cascade observed in progressive MS.

We found that the transplantation of iNSCs into the CSF circulation of EAE mice promotes equivalent outcomes to those previously observed in mice transplanted with somatic NSCs (Pluchino et al., 2003). Transplanted iNSCs or NSCs induced significant clinical amelioration, as well as reduced axonal and myelin damage, which were coupled with a reduction of type-1 MP infiltrates in the brain and spinal cord. Of note, transplanted stem cells widely distributed in the CNS of EAE mice and preferentially localised in perivascular areas of inflammation, which suggested some yet unknown mechanisms of intercellular coupling.

We then investigated the underlying immunological mechanisms driving the beneficial effects of NSCs on MPs during chronic neuroinflammation. Untargeted small molecule analysis of matched CSF and plasma samples revealed profound metabolic changes in the CSF of EAE mice, with differences between the early and the delayed phases of disease.

Leucine+isoleucine, uric acid, allantoin, carnitine and ornithine were all significantly increased in the EAE CSF at the peak of disease. Our findings are consistent with published evidence showing that leucine, as well as uric acid and its by-product allantoin, are all increased in the CSF of subjects with MS (Amorini et al., 2009; Hooper et al., 1998; Monaco et al., 1979). While increased CSF carnitine has not been reported in MS, important increases have been described in non-MS inflammatory conditions of the CNS, such as encephalitis (Wikoff et al., 2008) and meningitis (Shinawi et al., 1998).

Conversely, histidine and succinate showed a delayed (i.e. 45 dpi) increase in the EAE CSF. While high CSF levels of histidine have been previously linked with conditions where neurodegeneration prevails (Molina et al., 1998), succinate is becoming a valuable *in vivo*

biomarker of metabolic distress and inflammatory activity (Littlewood-Evans et al., 2016; Mills and O'Neill, 2014). Importantly, we found that succinate was significantly decreased in the CSF of iNSC-/NSC-transplanted mice. The reduction of CSF succinate following iNSC or NSC transplantation was of interest and might have a prominent role in interfering with chronic neuroinflammation.

Succinate released from type-1 inflammatory MPs is a key inflammatory signal, which interacts with its specific G protein-coupled receptor SUCNR1. SUCNR1 acts as an early detector of metabolic stress in several physiological and pathological conditions, including renin-induced hypertension, ischemia/reperfusion injury, inflammation, platelet aggregation and retinal angiogenesis (de Castro Fonseca et al., 2016; Gilissen et al., 2016). Notably, we found that the expression of SUCNR1 is required for the therapeutic effects of transplanted NSCs *in vivo*. Succinate-mediated activation of SUCNR1 on rodent and human iNSCs and NSCs, activates calcium signalling and MAPK phosphorylation *in vitro*, thus eliciting the acquisition of a concerted anti-inflammatory phenotype in NSCs.

On the one hand, SUCNR1 activated the secretion of PGE2, a well-established pleiotropic immune modulator, whose function targets multiple cell types within the inflamed microenvironment, including MPs (Kota et al., 2017; Vasandan et al., 2016). On the other hand, succinate-SUCNR1 signalling in iNSCs and NSCs led to the up-regulation of two members of the SLC13 family of co-transporters (i.e SLC13A3 and SLC13A5). As such, iNSCs and NSCs effectively scavenged extracellular succinate as part of their response to increased substrate availability (Srisawang et al., 2007).

This novel mechanism of intercellular coupling fits well with the available literature showing that, within specific microenvironments, cells compete for available nutrients, affecting each other’s function and fate (Pearce and Pearce, 2013).

We anticipate that SUCNR1-mediated scavenging of succinate by iNSCs and NSCs, plays a crucial role in reducing the availability of a key metabolic signal in inflammatory contexts where the interactions between transplanted stem cells and host immune cells become complementary (Pluchino and Cossetti, 2013). More generally, our findings are in line with the provocative, yet still emerging, concept of NSCs as ancestral guardians of the brain (Martino and Pluchino, 2007). As such, chronic inflammatory processes affecting the CNS would activate SUCNR1 on neural cells, which in turn trigger the release of paracrine anti-inflammatory molecules and the scavenging of a key metabolic signal of inflammation. Additional studies will be needed to further characterise the function of the succinate-SUCNR1 axis in neuro-immune interactions, and provide additional insights on the critical

role of cellular metabolism in determining the functional properties of neural stem/progenitor cells during brain development or repair after injuries (Knobloch and Jessberger, 2017).

In conclusion, we show here that NSCs sense the extracellular succinate that accumulates in the chronically inflamed CNS to ameliorate neuroinflammation via succinate-SUCNR1-dependent mechanisms.

Our work identifies a novel anti-inflammatory mechanism that underpins the regenerative potential of somatic and directly-induced NSCs, thus paving the way for a new era of personalised stem cell medicines for chronic inflammatory and degenerative neurological diseases.

Author Contributions

Conceptualization, L.P.J., C.F. and SP; Methodology, J.D.B., F.E. and S.P.; Formal Analysis, L.P.J., J.D.B., N.V., A.S.H.C., T.L., C.F. and S.P.; Investigation, L.P.J., J.D.B., N.V., I.B., A.S.H.C., B.B., G.Mal., G.Man., G.V., N.I. and L.M.B.; Resources, M.P.M., J.H., F.E., C.F. and S.P.; Data Curation, L.P.J., J.D.B. and N.V.; Writing – Original Draft, L.P.J., J.D.B., N.V., C.F. and S.P.; Writing – Review & Editing, L.P.J., J.D.B., N.V., M.P.M., J.H., F.E., C.F. and S.P.; Supervision, M.P.M., J.H., F.E., C.F. and S.P.; Project Administration, L.P.J., J.D.B., N.V., C.F. and S.P.; Funding Acquisition, L.P.J. and S.P.

Acknowledgments

The authors thank P. Chinnery, F. Dazzi, D. Franciotta, J. Jones, A. Tolkovsky and L. Vallier for critically discussing the article. The authors wish to acknowledge M. Donegà, G. Pluchino, J. Smith, G. Tannahil and K. Saeb-Parsy for their technical contributions and critical insights throughout the execution of the study; A. Elkalhoun and W. Wu of the NIH/NHGRI IRP Microarray Core Facility for their assistance with the transcriptomic/microarray studies. The authors also thank J. M. Carballido (Novartis, Switzerland) for providing the C57BL/6 Sucnr1-/- mice, A. L. Vescovi (Milano, Italy) for providing the RNA and protein extracts from human foetal NSCs (hNSCs) and S. De (Advinus Therapeutics Ltd. TATA Enterprise, India) for providing the compound 4c used in this study.

This work was funded by the Italian Multiple Sclerosis Association (AISM, grant 2010/R/31 and grant 2014/PMS/4 to SP), the United States Department of Defense (DoD) Congressionally Directed Medical Research Programs (CDMRP) (grant MS140019 to SP),

the Italian Ministry of Health (GR08-7 to SP), the European Research Council (ERC) under the ERC-2010-StG grant agreement n° 260511-SEM_SEM, the Medical Research Council, the Engineering and Physical Sciences Research Council, and the Biotechnology and Biological Sciences Research Council UK Regenerative Medicine Platform Hub “Acellular Approaches for Therapeutic Delivery” (MR/K026682/1 to SP), the Evelyn Trust (RG 69865 to SP), the Bascule Charitable Trust (RG 75149 to SP) and a core support grant from the Wellcome Trust and Medical Research Council to the Wellcome Trust – MRC Cambridge Stem Cell Institute. LPJ was supported by a research training fellowship from the Wellcome Trust (RRZA/057 RG79423). JDB was supported by a NIHOxCam training fellowship. Work in FE lab was supported by grants from the ERA-Net E-rare research programme and the Austrian Science Fund (FWF). CKK was supported by a stipend of the German Excellence Initiative to the Graduate School of Life Sciences, University of Würzburg. JMH was supported by the Intramural Research Program (IRP) of NINDS/NIH. Work in MPM's lab was supported by grants from the Medical Research Council UK (MC_U105663142) and by a Wellcome Trust Investigator award (110159/Z/15/Z).

Accession number

The microarray data have been deposited in ArrayExpress with the accession numbers E-MTAB-5579 and E-MTAB-5586.

References

Al-Shabany, A.J., Moody, A.J., Foey, A.D., and Billington, R.A. (2016). Intracellular NAD+ levels are associated with LPS-induced TNF-alpha release in pro-inflammatory macrophages. Biosci Rep 36, e00301.

Amorini, A.M., Petzold, A., Tavazzi, B., Eikelenboom, J., Keir, G., Belli, A., Giovannoni, G., Di Pietro, V., Polman, C., D'Urso, S., et al. (2009). Increase of uric acid and purine compounds in biological fluids of multiple sclerosis patients. Clin Biochem 42, 1001-1006.

Anderson, A.J., Piltti, K.M., Hooshmand, M.J., Nishi, R.A., and Cummings, B.J. (2017). Preclinical Efficacy Failure of Human CNS-Derived Stem Cells for Use in the Pathway Study of Cervical Spinal Cord Injury. Stem Cell Reports 8, 249-263.

Bacigaluppi, M., Pluchino, S., Peruzzotti-Jametti, L., Kilic, E., Kilic, U., Salani, G., Brambilla, E., West, M.J., Comi, G., Martino, G., et al. (2009). Delayed post-ischaemic neuroprotection following systemic neural stem cell transplantation involves multiple mechanisms. Brain 132, 2239-2251.

Bacigaluppi, M., Russo, G.L., Peruzzotti-Jametti, L., Rossi, S., Sandrone, S., Butti, E., De Ceglia, R., Bergamaschi, A., Motta, C., Gallizioli, M., et al. (2016). Neural Stem Cell Transplantation Induces Stroke Recovery by Upregulating Glutamate Transporter GLT-1 in Astrocytes. J Neurosci 36, 10529-10544.

Bramow, S., Frischer, J.M., Lassmann, H., Koch-Henriksen, N., Lucchinetti, C.F., Sorensen, P.S., and Laursen, H. (2010). Demyelination versus remyelination in progressive multiple sclerosis. Brain 133, 2983-2998.

Cusimano, M., Biziato, D., Brambilla, E., Donega, M., Alfaro-Cervello, C., Snider, S., Salani, G., Pucci, F., Comi, G., Garcia-Verdugo, J.M., et al. (2012). Transplanted neural stem/precursor cells instruct phagocytes and reduce secondary tissue damage in the injured spinal cord. Brain : a journal of neurology 135, 447-460.

de Castro Fonseca, M., Aguiar, C.J., da Rocha Franco, J.A., Gingold, R.N., and Leite, M.F. (2016). GPR91: expanding the frontiers of Krebs cycle intermediates. Cell Commun Signal 14, 3.

Fischbach, M.A., Bluestone, J.A., and Lim, W.A. (2013). Cell-based therapeutics: the next pillar of medicine. Science translational medicine 5, 179ps177.

Gilissen, J., Jouret, F., Pirotte, B., and Hanson, J. (2016). Insight into SUCNR1 (GPR91) structure and function. Pharmacology & therapeutics 159, 56-65.

Hooper, D.C., Spitsin, S., Kean, R.B., Champion, J.M., Dickson, G.M., Chaudhry, I., and Koprowski, H. (1998). Uric acid, a natural scavenger of peroxynitrite, in experimental allergic encephalomyelitis and multiple sclerosis. Proc Natl Acad Sci U S A 95, 675-680.

Jiang, Z., Jiang, J.X., and Zhang, G.X. (2014). Macrophages: a double-edged sword in experimental autoimmune encephalomyelitis. Immunol Lett 160, 17-22.

Kelly, B., and O'Neill, L.A. (2015). Metabolic reprogramming in macrophages and dendritic cells in innate immunity. Cell research 25, 771-784.

Knobloch, M., and Jessberger, S. (2017). Metabolism and neurogenesis. Curr Opin Neurobiol 42, 45-52.

Kota, D.J., Prabhakara, K.S., Toledano-Furman, N., Bhattarai, D., Chen, Q., DiCarlo, B., Smith, P., Triolo, F., Wenzel, P.L., Cox, C.S., Jr., et al. (2017). Prostaglandin E2 Indicates Therapeutic Efficacy Of Mesenchymal Stem Cells In Experimental Traumatic Brain Injury. Stem Cells.

Littlewood-Evans, A., Sarret, S., Apfel, V., Loesle, P., Dawson, J., Zhang, J., Muller, A., Tigani, B., Kneuer, R., Patel, S., et al. (2016). GPR91 senses extracellular succinate released from inflammatory macrophages and exacerbates rheumatoid arthritis. J Exp Med 213, 1655-1662.

Lu, J., Liu, H., Huang, C.T., Chen, H., Du, Z., Liu, Y., Sherafat, M.A., and Zhang, S.C. (2013). Generation of integration-free and region-specific neural progenitors from primate fibroblasts. Cell reports 3, 1580-1591.

Mallucci, G., Peruzzotti-Jametti, L., Bernstock, J.D., and Pluchino, S. (2015). The role of immune cells, glia and neurons in white and gray matter pathology in multiple sclerosis. Prog Neurobiol 127-128, 1-22.

Martinez, P., Denys, A., Delos, M., Sikora, A.S., Carpentier, M., Julien, S., Pestel, J., and Allain, F. (2015). Macrophage polarization alters the expression and sulfation pattern of glycosaminoglycans. Glycobiology 25, 502-513.

Martino, G., and Pluchino, S. (2006). The therapeutic potential of neural stem cells. Nat Rev Neurosci 7, 395-406.

Martino, G., and Pluchino, S. (2007). Neural stem cells: guardians of the brain. Nat Cell Biol 9, 1031-1034.

Meyer, S., Worsdorfer, P., Gunther, K., Thier, M., and Edenhofer, F. (2015). Derivation of Adult Human Fibroblasts and their Direct Conversion into Expandable Neural Progenitor Cells. Journal of visualized experiments : JoVE, e52831.

Mills, E., and O'Neill, L.A. (2014). Succinate: a metabolic signal in inflammation. Trends in cell biology 24, 313-320.

Mills, E.L., Kelly, B., Logan, A., Costa, A.S., Varma, M., Bryant, C.E., Tourlomousis, P., Dabritz, J.H., Gottlieb, E., Latorre, I., et al. (2016). Succinate Dehydrogenase Supports Metabolic Repurposing of Mitochondria to Drive Inflammatory Macrophages. Cell 167, 457-470 e413.

Molina, J.A., Jimenez-Jimenez, F.J., Vargas, C., Gomez, P., de Bustos, F., Orti-Pareja, M., Tallon-Barranco, A., Benito-Leon, J., Arenas, J., and Enriquez-de-Salamanca, R. (1998). Cerebrospinal fluid levels of non-

neurotransmitter amino acids in patients with Alzheimer's disease. J Neural Transm (Vienna) 105, 279-286.
Moll, N.M., Rietsch, A.M., Thomas, S., Ransohoff, A.J., Lee, J.C., Fox, R., Chang, A., Ransohoff, R.M., and Fisher, E. (2011). Multiple sclerosis normal-appearing white matter: pathology-imaging correlations. Ann Neurol 70, 764-773.
Monaco, F., Fumero, S., Mondino, A., and Mutani, R. (1979). Plasma and cerebrospinal fluid tryptophan in multiple sclerosis and degenerative diseases. J Neurol Neurosurg Psychiatry 42, 640-641.
O'Neill, L.A., and Pearce, E.J. (2016). Immunometabolism governs dendritic cell and macrophage function. J Exp Med 213, 15-23.
Palsson-McDermott, E.M., Curtis, A.M., Goel, G., Lauterbach, M.A., Sheedy, F.J., Gleeson, L.E., van den Bosch, M.W., Quinn, S.R., Domingo-Fernandez, R., Johnston, D.G., et al. (2015). Pyruvate kinase M2 regulates Hif-1alpha activity and IL-1beta induction and is a critical determinant of the warburg effect in LPS-activated macrophages. Cell metabolism 21, 65-80.
Pearce, E.L., and Pearce, E.J. (2013). Metabolic pathways in immune cell activation and quiescence. Immunity 38, 633-643.
Peterson, J.W., Bo, L., Mork, S., Chang, A., and Trapp, B.D. (2001). Transected neurites, apoptotic neurons, and reduced inflammation in cortical multiple sclerosis lesions. Ann Neurol 50, 389-400.
Planche, V., Panatier, A., Hiba, B., Ducourneau, E.G., Raffard, G., Dubourdieu, N., Maitre, M., Leste-Lasserre, T., Brochet, B., Dousset, V., et al. (2017). Selective dentate gyrus disruption causes memory impairment at the early stage of experimental multiple sclerosis. Brain Behav Immun 60, 240-254.
Pluchino, S., and Cossetti, C. (2013). How stem cells speak with host immune cells in inflammatory brain diseases. Glia 61, 1379-1401.
Pluchino, S., Gritti, A., Blezer, E., Amadio, S., Brambilla, E., Borsellino, G., Cossetti, C., Del Carro, U., Comi, G., t Hart, B., et al. (2009a). Human neural stem cells ameliorate autoimmune encephalomyelitis in non-human primates. Ann Neurol 66, 343-354.
Pluchino, S., Quattrini, A., Brambilla, E., Gritti, A., Salani, G., Dina, G., Galli, R., Del Carro, U., Amadio, S., Bergami, A., et al. (2003). Injection of adult neurospheres induces recovery in a chronic model of multiple sclerosis. Nature 422, 688-694.
Pluchino, S., Zanotti, L., Brambilla, E., Rovere-Querini, P., Capobianco, A., Alfaro-Cervello, C., Salani, G., Cossetti, C., Borsellino, G., Battistini, L., et al. (2009b). Immune regulatory neural stem/precursor cells protect from central nervous system autoimmunity by restraining dendritic cell function. PLoS One 4, e5959.
Pluchino, S., Zanotti, L., Rossi, B., Brambilla, E., Ottoboni, L., Salani, G., Martinello, M., Cattalini, A., Bergami, A., Furlan, R., et al. (2005). Neurosphere-derived multipotent precursors promote neuroprotection by an immunomodulatory mechanism. Nature 436, 266-271.
Prineas, J.W., Kwon, E.E., Cho, E.S., Sharer, L.R., Barnett, M.H., Oleszak, E.L., Hoffman, B., and Morgan, B.P. (2001). Immunopathology of secondary-progressive multiple sclerosis. Ann Neurol 50, 646-657.
Ramos-Zuniga, R., Gonzalez-Perez, O., Macias-Ornelas, A., Capilla-Gonzalez, V., and Quinones-Hinojosa, A. (2012). Ethical implications in the use of embryonic and adult neural stem cells. Stem Cells Int 2012, 470949.
Rice, C.M., Kemp, K., Wilkins, A., and Scolding, N.J. (2013). Cell therapy for multiple sclerosis: an evolving concept with implications for other neurodegenerative diseases. Lancet 382, 1204-1213.
Rubic, T., Lametschwandtner, G., Jost, S., Hinteregger, S., Kund, J., Carballido-Perrig, N., Schwarzler, C., Junt, T., Voshol, H., Meingassner, J.G., et al. (2008). Triggering the succinate receptor GPR91 on dendritic cells enhances immunity. Nat Immunol 9, 1261-1269.
Shinawi, M., Gruener, N., and Lerner, A. (1998). CSF levels of carnitine in children with meningitis, neurologic disorders, acute gastroenteritis, and seizure. Neurology 50, 1869-1871.
Srisawang, P., Chatsudthipong, A., and Chatsudthipong, V. (2007). Modulation of succinate transport in Hep G2 cell line by PKC. Biochim Biophys Acta 1768, 1378-1388.
Tambalo, S., Peruzzotti-Jametti, L., Rigolio, R., Fiorini, S., Bontempi, P., Mallucci, G., Balzarotti, B., Marmiroli, P., Sbarbati, A., Cavaletti, G., et al. (2015). Functional Magnetic Resonance Imaging of Rats with Experimental Autoimmune Encephalomyelitis Reveals Brain Cortex Remodeling. J Neurosci 35, 10088-10100.
Tannahill, G.M., Curtis, A.M., Adamik, J., Palsson-McDermott, E.M., McGettrick, A.F., Goel, G., Frezza, C., Bernard, N.J., Kelly, B., Foley, N.H., et al. (2013). Succinate is an inflammatory signal that induces IL-1beta through HIF-1alpha. Nature 496, 238-242.
Tannahill, G.M., Iraci, N., Gaude, E., Frezza, C., and Pluchino, S. (2015). Metabolic reprograming of mononuclear phagocytes in progressive multiple sclerosis. Front Immunol 6, 106.
Thier, M., Worsdorfer, P., Lakes, Y.B., Gorris, R., Herms, S., Opitz, T., Seiferling, D., Quandel, T., Hoffmann, P., Nothen, M.M., et al. (2012). Direct conversion of fibroblasts into stably expandable neural stem cells. Cell stem cell 10, 473-479.
Vasandan, A.B., Jahnavi, S., Shashank, C., Prasad, P., Kumar, A., and Prasanna, S.J. (2016). Human Mesenchymal stem cells program macrophage plasticity by altering their metabolic status via a PGE2-dependent mechanism. Scientific reports 6, 38308.

Volpe, G., Bernstock, J.D., Peruzzotti-Jametti, L., and Pluchino, S. (2016). Modulation of host immune responses following non-hematopoietic stem cell transplantation: Translational implications in progressive multiple sclerosis. J Neuroimmunol.
Wikoff, W.R., Pendyala, G., Siuzdak, G., and Fox, H.S. (2008). Metabolomic analysis of the cerebrospinal fluid reveals changes in phospholipase expression in the CNS of SIV-infected macaques. J Clin Invest 118, 2661-2669.
Wright, L.S., Prowse, K.R., Wallace, K., Linskens, M.H., and Svendsen, C.N. (2006). Human progenitor cells isolated from the developing cortex undergo decreased neurogenesis and eventual senescence following expansion in vitro. Exp Cell Res 312, 2107-2120.
Yanez, R., Oviedo, A., Aldea, M., Bueren, J.A., and Lamana, M.L. (2010). Prostaglandin E2 plays a key role in the immunosuppressive properties of adipose and bone marrow tissue-derived mesenchymal stromal cells. Exp Cell Res 316, 3109-3123.

Figure 1

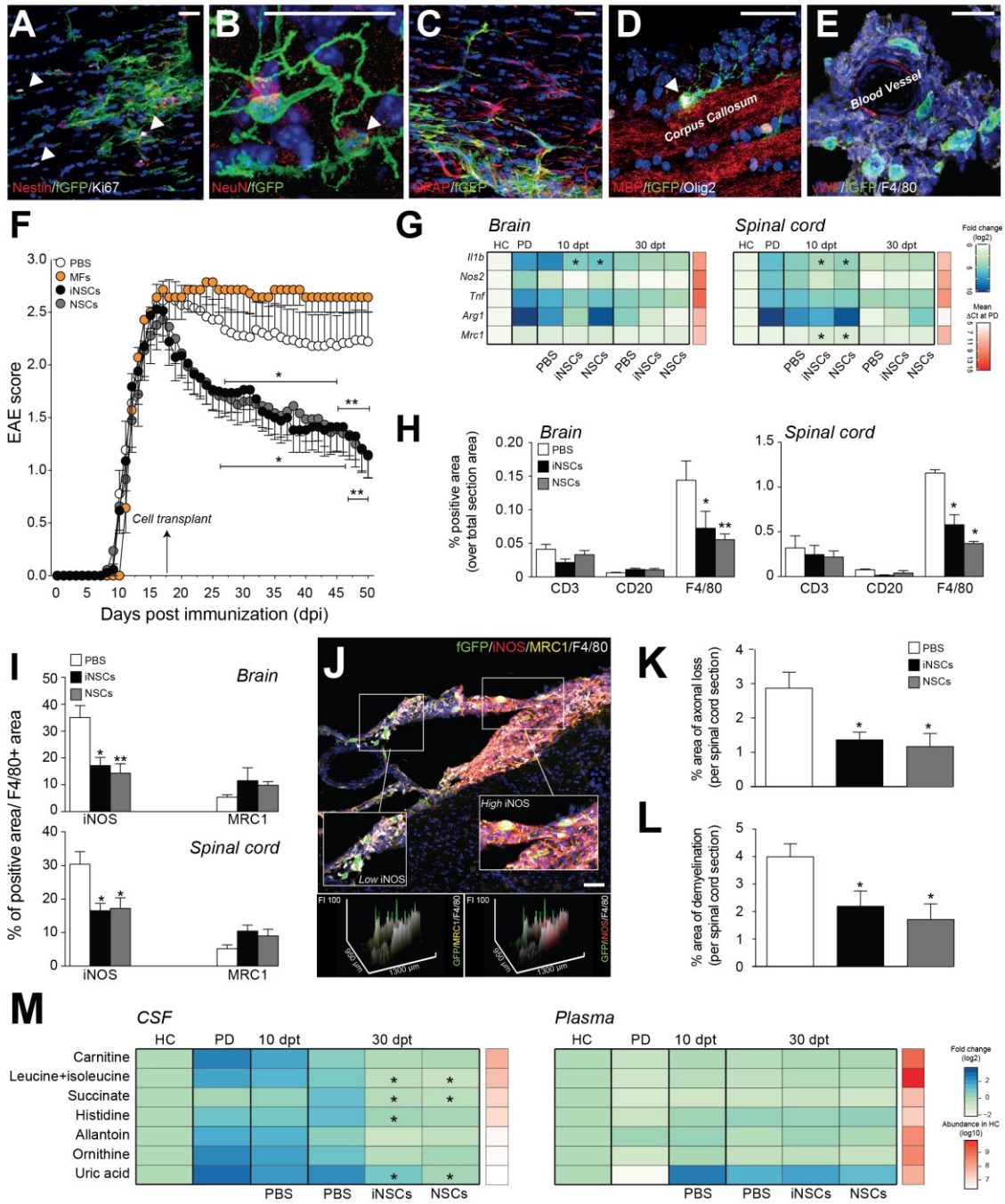

Peruzzotti-Jametti et al. Figure 1

Figure 1. NSCs transplantation ameliorates chronic neuroinflammation and reduces succinate levels in the CSF of EAE mice.

(A-D) Representative images of fGFP+ iNSCs at 30 dpt expressing the proliferation marker Ki67 (A, arrowheads) and the neural marker Nestin (A), the mature neuronal marker NeuN (B, arrowhead), the astroglial lineage marker GFAP (C) or the oligodendroglial lineage marker Olig2 (D, arrowhead).

(E) Confocal microscopy image of a perivascular area with several fGFP+ iNSCs in juxtaposition with fGFP-/F4/80+ MPs. Nuclei in A-E are stained with DAPI (blue).

(F) Behavioural outcome of iNSCs/NSCs-transplanted EAE mice. Data are mean EAE score (± SEM) from n≥ 7 mice/group over n= 2 independent experiments. EAE mice injected icv with Mouse Fibroblasts (MFs) or PBS were used as controls.
(G) Heat map of the expression levels (qRT-PCR) of pro- and anti-inflammatory genes. Data are mean fold change (log2) vs. HC from n≥ 3 mice/group. Relative abundance (ΔCT) at PD is shown.
(H) Quantification of the area stained for CD3, CD20 and F4/80.
(I) Quantification of the proportion of F4/80+ cells expressing the type-1 inflammatory MPs marker iNOS, or the anti-inflammatory MPs marker MRC1. Data in H and I are mean % of positive-stained area/total section area and % of positive-stained area/F4/80+ area (± SEM), respectively. Data are from n≥ 5 mice/group over n= 2 independent experiments.
(J) Representative confocal microscopy image and comparative histograms of a perivascular area with several fGFP+ iNSCs in juxtaposition to F4/80+ MPs. Low iNOS and prevalent MRC1 expression is detected in F4/80+ MPs close to fGFP+ iNSCs (inset on the left), while high iNOS expression is observed in the remaining MP infiltrate (inset on the right). Nuclei are stained with DAPI.
(K-L) Quantification of spinal cord damage in iNSCs/NSCs-transplanted EAE mice. Data are mean % of Bielschowsky negative-stained axonal loss (K) or Luxol fast blue (LFB) negative-stained demyelinated (L) areas/spinal cord section (± SEM) from n≥ 5 mice/group over n= 2 independent experiments.
(M) Heat map of the levels of CSF metabolites significantly changed during EAE (vs. HC). Corresponding levels in matched plasma samples are also shown. Data are mean fold change (log2), vs. HC from n≥ 3 mice/group. Relative abundance (log10) in HC is shown. Scale bars: 25 μm (A-E), 50 μm (J).
*p≤ 0.05, **p≤ 0.01, vs. PBS; dpt: days post transplantation, PD: peak of disease, HC: healthy controls, FI: Fluorescence Intensity.
See also **Figure S1-4** and **Data S1**.

Figure 2

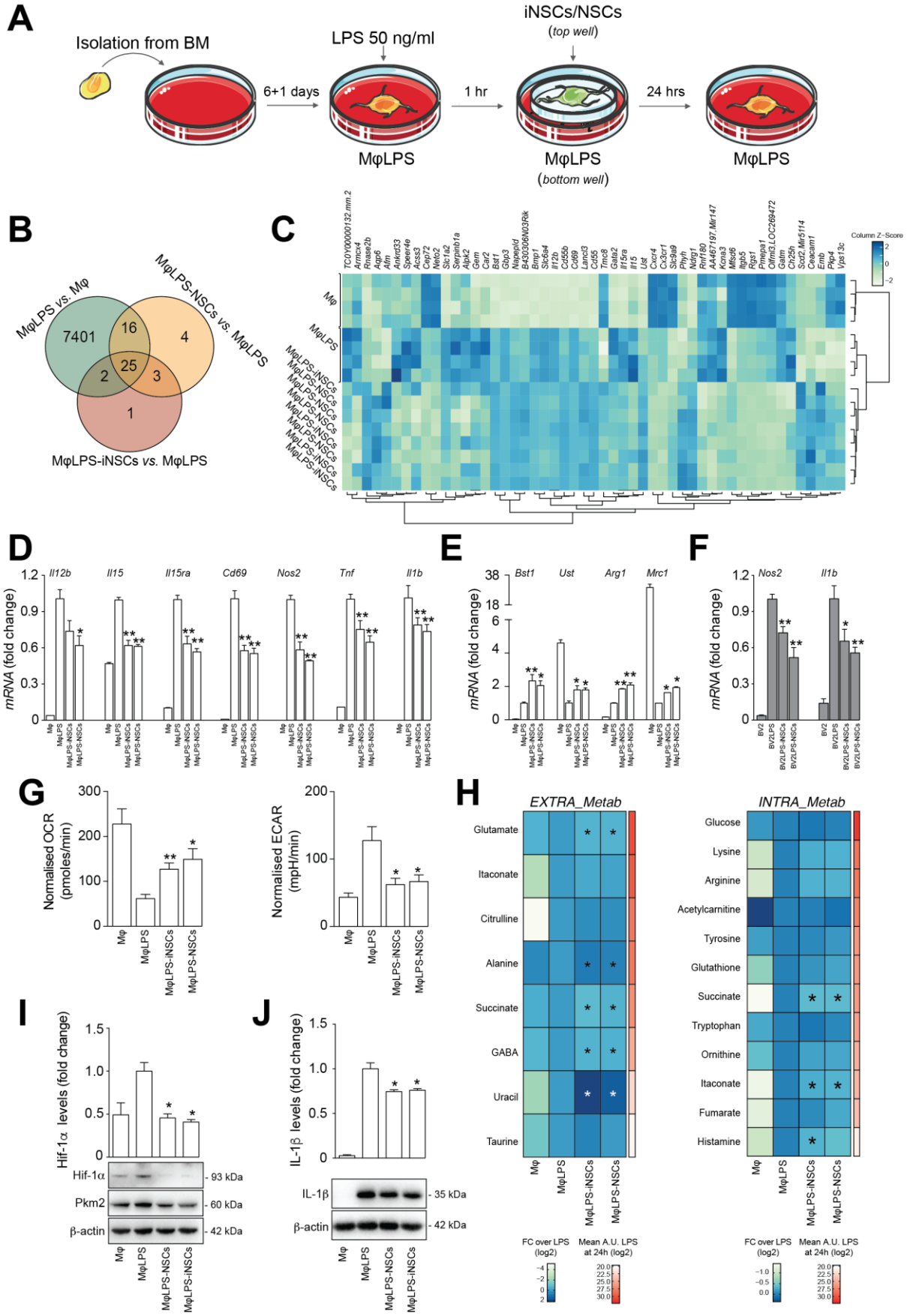

Peruzzotti-Jametti et al. Figure 2

Figure 2. NSCs reduce succinate levels and reprogram the metabolism of type 1 pro-inflammatory Mφ towards oxidative phosphorylation *in vitro*

(A) Experimental setup for *in vitro* $M\varphi^{LPS}$ co-cultures with iNSCs/NSCs.

(B-C) Gene expression microarrays of $M\varphi^{LPS}$-iNSCs/NSCs. (B) Venn diagram of differentially expressed genes (adjusted p value < 0.1). (C) Heatmap of genes differentially expressed (adjusted p value < 0.1) in $M\varphi^{LPS}$-iNSCs or $M\varphi^{LPS}$-NSCs.

(D-E) qRT-PCR independent validation of differentially expressed inflammatory genes as in C. (D) Expression of genes related to type-1 inflammatory (E) and anti-inflammatory Mφ phenoptypes relative to Actb. Data are mean fold change (± SEM) vs. $M\varphi^{LPS}$ from n≥ 3 independent replicates per condition.

(F) qRT-PCR of $BV2^{LPS}$-iNSCs/NSCs (± SEM) from n≥ 3 independent experiments per condition. BV2 and $BV2^{LPS}$ are shown as controls.

(G) Extracellular flux (XF) assay of the Oxygen Consumption rate (OCR) and Extracellular Acidification Rate (ECAR) in $M\varphi^{LPS}$-iNSCs/NSCs. Data were normalized on total protein content and are expressed as mean values (± SEM) from n≥ 3 independent experiments per condition.

(H) Heatmap of the levels of significantly changed extracellular (EXTRA_Metab) and intracellular (INTRA_Metab) metabolites in $M\varphi^{LPS}$ vs. Mφ at 25 hrs. Data are mean fold change (log2) vs. $M\varphi^{LPS}$ from n≥ 2 independent experiments per condition. Relative abundance (log10) of metabolites in $M\varphi^{LPS}$ (at 25 hrs) is shown.

(I and J) Hif-1α, PKM2 and IL-1β expression levels relative to β-actin. Data are mean fold change vs. $M\varphi^{LPS}$ (± SEM) from n≥ 3 independent experiments per condition.

*p≤ 0.05, **p≤ 0.01 vs. $M\varphi^{LPS}$.

See also **Data S2-3**.

Figure 3

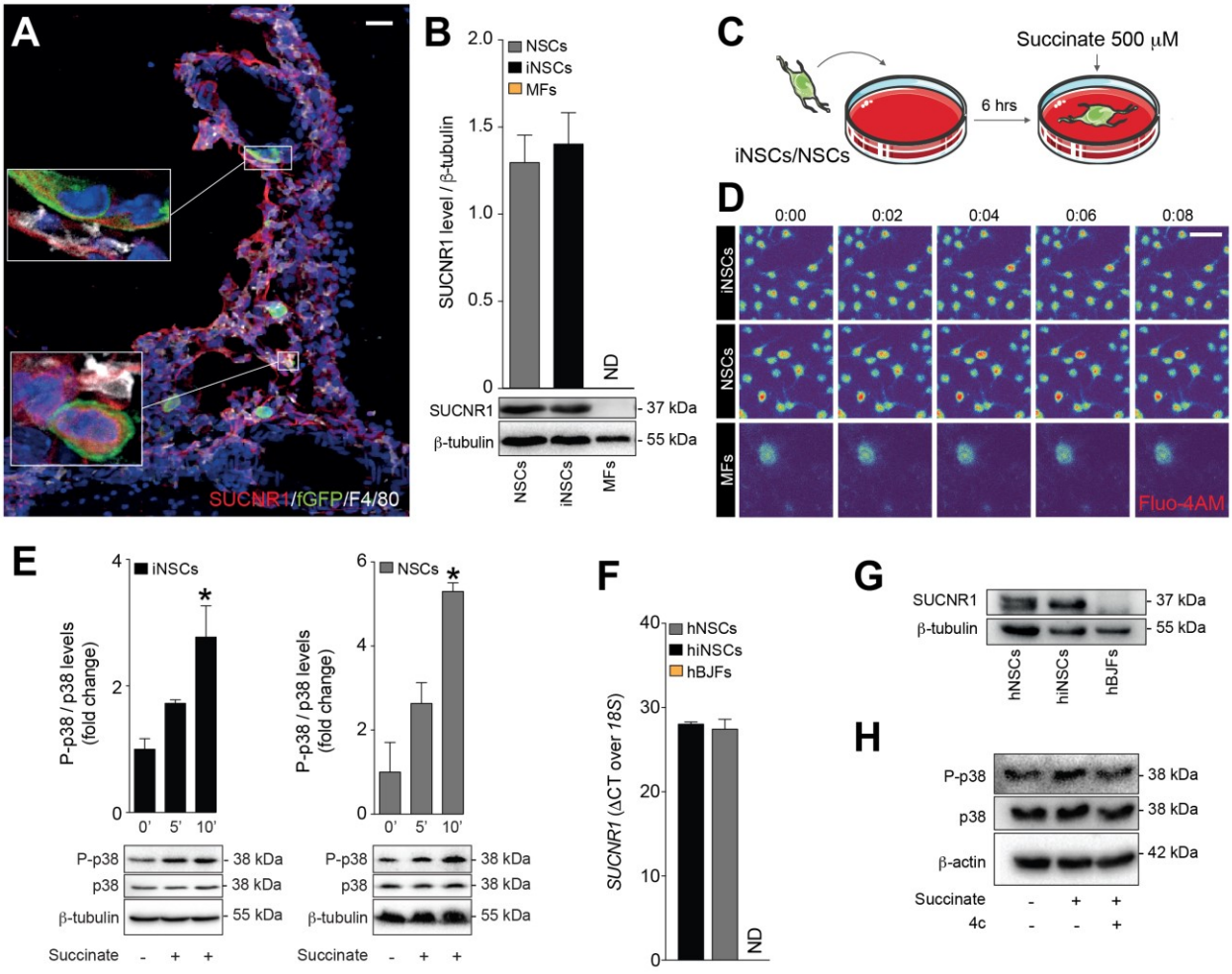

Peruzzotti-Jametti et al. Figure 3

Figure 3. Succinate signals via SUCNR1 in mouse and human NSCs

(A) Representative confocal microscopy image of a perivascular area with transplanted fGFP+ iNSCs expressing SUCNR1 in vicinity to SUCNR1+/F4/80+ MPs in the brain of a EAE mouse. Nuclei are stained with DAPI.

(B) SUCNR1 protein expression relative to β-tubulin *in vitro*. Data are shown as mean (± SEM) of n≥ 3 independent replicates per condition.

(C) Experimental setup for succinate treatment of iNSCs/NSCs *in vitro*.

(D) Intracellular Ca^{2+} response after treatment with succinate as in C (live staining with Fluo-4AM). Images are shown at 2 sec intervals after treatment and pseudocolored with red/blue according to high/low fluorescence intensity.

(E) Phospho-p38 MAPK (P-p38) and total p38 MAPK (p38) protein expression after succinate treatment. Data are P-p38/p38 expression relative to β-tubulin and expressed as mean fold change (± SEM) vs. untreated cells, over n≥ 3 independent experiments per condition.

(F) qRT-PCR of SUCNR1 basal expression in human cells. Data are relative abundance (ΔCT) over 18S from n≥ 2 independent experiments.

(G) Representative blot of SUNCR1 basal protein expression in human cells.

(H) P-p38 and p38 protein expression after stimulation with succinate ± pre-treatment with the irreversible inhibitor of the human SUCNR1 4c.

Scale bars: 50 μm.

*p≤ 0.05 vs. 0'. ND: not detected, hBJFs: human BJ fibroblasts.

Figure 4

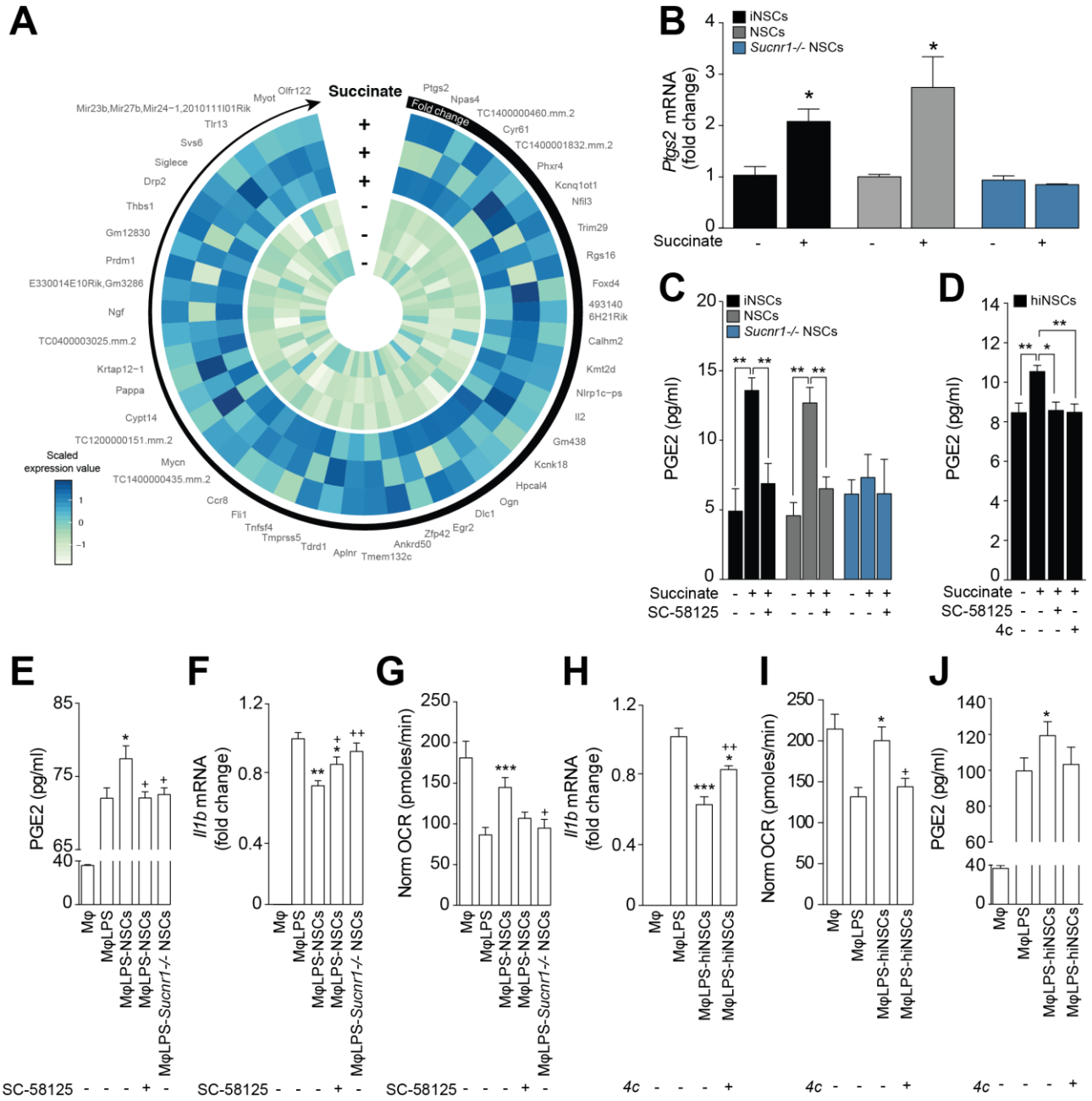

Peruzzotti-Jametti et al. Figure 4

Figure 4. SUCNR1 expression is necessary for the anti-inflammatory effect of NSCs on type-1 pro-inflammatory Mφ *in vitro*

(A) Heatmap showing the microarray expression profile of the 50 most up-regulated genes in NSCs after treatment with succinate. Data are shown as z-scores.

(B) qRT-PCR independent validation of Ptgs2 expression as in A. Data are calculated relative to Actb and shown as mean fold change (± SEM) vs. untreated cells, over n≥ 3 independent experiments per condition.
(C) PGE2 secretion following 1 hr treatment with succinate ± pre-treatment with the selective PTGS2 blocker SC-58125. Data are mean values (± SEM) over n≥ 3 independent experiments per condition.
(D) PGE2 secretion by hiNSCs treated with succinate ± pre-treatment with either SC-58125 or 4c. Data are mean values (± SEM) over n≥ 3 independent experiments per condition.
(E) PGE2 secretion in Mφ co-cultures. Data are mean values (± SEM) over n≥ 3 independent experiments per condition.
(F) Il1b expression relative to Actb in Mφ co-cultures. Data are mean fold change vs. $M\varphi^{LPS}$ (± SEM) from n≥ 3 independent experiments per condition.
(G) XF assay of the OCR of Mφ, as in E-F. Data are normalized on total protein content and expressed as mean values (± SEM) over n≥ 3 independent experiments per condition.
(H) Il1b expression relative to Actb of Mφ co-cultures with hiNSCs. Data are mean fold change vs. $M\varphi^{LPS}$ (± SEM) from n≥ 3 independent experiments per condition.
(I) XF assay showing the OCR of Mφ as in H. Data are normalized on total protein content and expressed as mean values (± SEM) over n≥ 2 independent experiments per condition.
(J) PGE2 secretion in Mφ co-cultures as in H-I. Data are mean values (± SEM) over n≥ 3 independent experiments per condition.
*p≤ 0.05 vs. untreated cells (B); *p≤ 0.05 and **p≤ 0.01 (C-D); *p≤ 0.05, **p≤ 0.01, *** p≤ 0.001 vs. $M\varphi^{LPS}$ (E-J); +p≤ 0.05, ++p≤ 0.01 vs. $M\varphi^{LPS}$-NSCs (E-G) or $M\varphi^{LPS}$-hiNSCs (H-I).
See also **Figure S5** and **Data S4**.

Figure 5

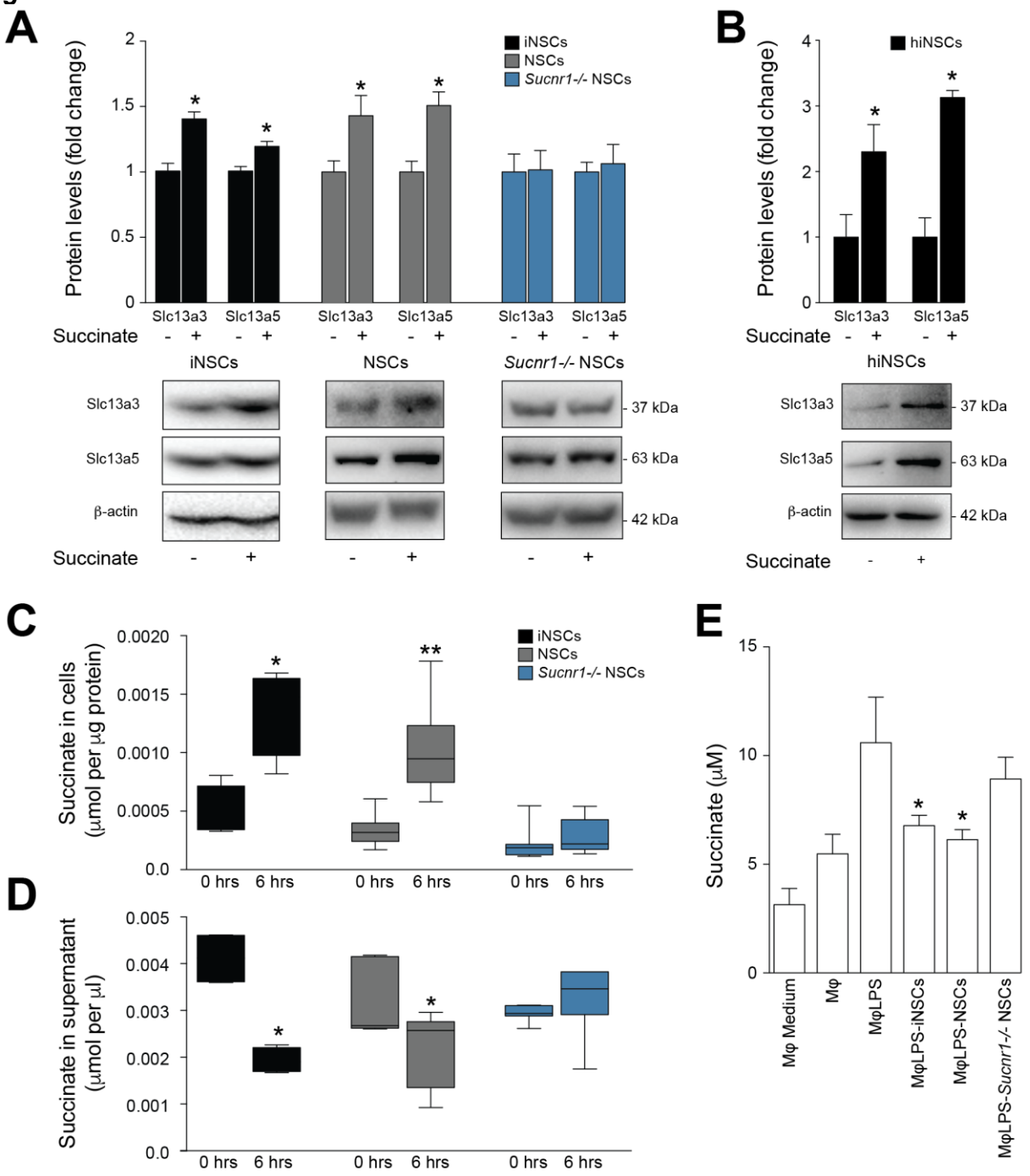

Peruzzotti-Jametti et al. Figure 5

Figure 5. SUCNR1 regulates the uptake of succinate by NSCs *in vitro.*
(A) SLC13A3 and SLC13A5 protein expression levels after 2 hrs of succinate treatment. (B) SLC13A3 and SLC13A5 protein expression levels after 6 hrs of succinate treatment in hiNSCs. Data in A and B are relative to β-actin and expressed as mean fold change (± SEM) vs. untreated cells, over n≥ 3 independent experiments per condition.
(C-D) Uptake assay of [14C] - labelled succinate at 0 and 6 hrs. (C) Intracellular [14C] - labelling and (D) extracellular [14C] - signal in tissue culture media. Box-whiskers plots ± min and max value from n≥ 4 technical replicates per group from n= 2 independent experiments.

(E) Succinate release in Mφ co-cultures. Data are mean fold change vs. Mφ (± SEM), from n≥ 2 independent experiments per condition.
*p≤ 0.05 vs. untreated cells (A-B), or $M\varphi^{LPS}$ (E). *p≤ 0.05 and **p≤ 0.01 vs. 0 hrs, Mann-Whitney test (C-D).
See also **Figure S6**.

Figure 6

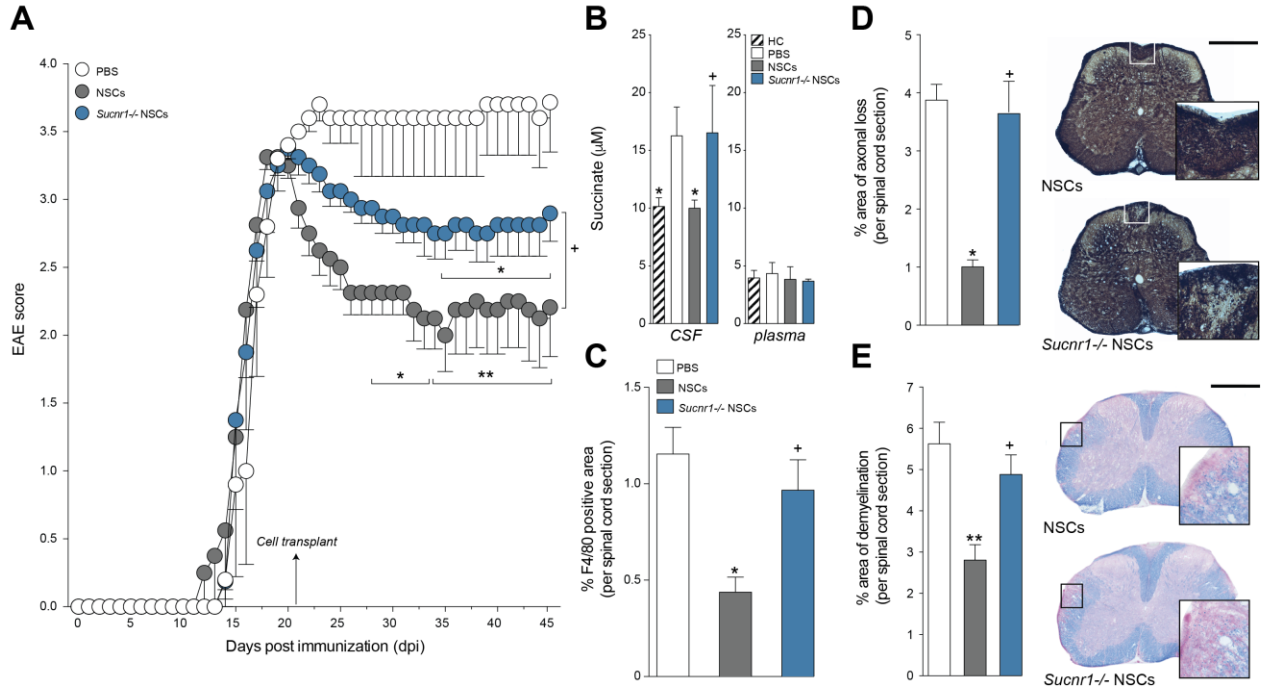

Peruzzotti-Jametti et al. Figure 6

Figure 6. Transplantation of Sucnr1 loss-of-function NSCs shows impaired ability to ameliorate chronic neuroinflammation *in vivo.*

(A) Behavioural outcome of EAE mice. Data are mean EAE score (± SEM) from n≥ 5 mice/group.

(B) Succinate levels in the CSF and plasma of EAE mice at 30 dpt. Data are mean values (± SEM) from n≥ 4 mice/group.

(C-E) Pathological outcomes of experiments as in A. Data are mean % of F4/80-positive (C), Bielschowsky negative-stained axonal loss (D) or LFB negative-stained demyelinated (E) areas/spinal cord section (± SEM) from n≥ 4 mice/group. Scale bars: 400 μm.

*p≤ 0.05 and **p≤ 0.01 vs. PBS; +p≤ 0.05 vs. NSCs (A-E); HC: healthy controls.

Figure S1

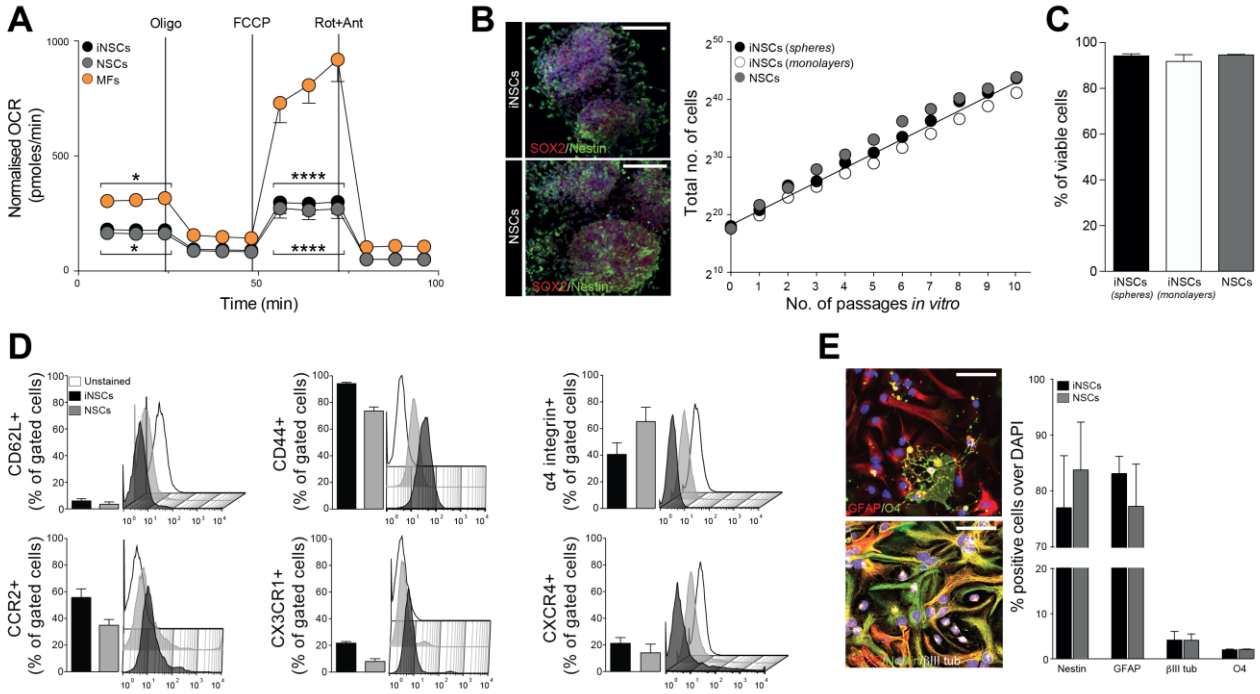

Peruzzotti-Jametti et al. Figure S1

Figure S1. Mouse iNSCs and NSCs *in vitro* features

(A) Extracellular Flux (XF) assay of the Oxygen Consumption Rate (OCR) during a mitochondrial stress protocol. Data are normalized on total protein content and expressed as mean values (± SEM) from n≥ 3 independent experiments.

(B) Representative confocal microscopy images of iNSCs and NSCs growing *in vitro* as SOX2+/Nestin+ neurospheres. Nuclei are stained with DAPI. Linear growth curves of iNSCs and NSCs over 10 passages *in vitro*. Data are mean numbers (± SEM) from n≥ 3 independent experiments per condition.

(C) Cell viability as in B. Data are mean percentages of viable cells (± SEM) from n≥ 3 independent experiments per condition.

(D) Fluorescence-activated cell sorting (FACS) analysis. Data are positive cells over gated cells (mean percentages ± SEM) from n≥ 3 independent experiments per condition.

(E) *In vitro* differentiation properties of iNSCs and NSCs. Representative confocal microscopy images of differentiated iNSCs stained for GFAP, O4, Nestin and βIII tubulin are shown. Nuclei were stained with DAPI. Data are mean percentages of positive cells (± SEM) from n≥ 3 independent experiments per condition.

Scale bars: 100 μm (B), 40 μm (E).

*p≤ 0.05, ****p≤ 0.0001 vs. Mouse Fibroblasts (MFs).

Figure S2

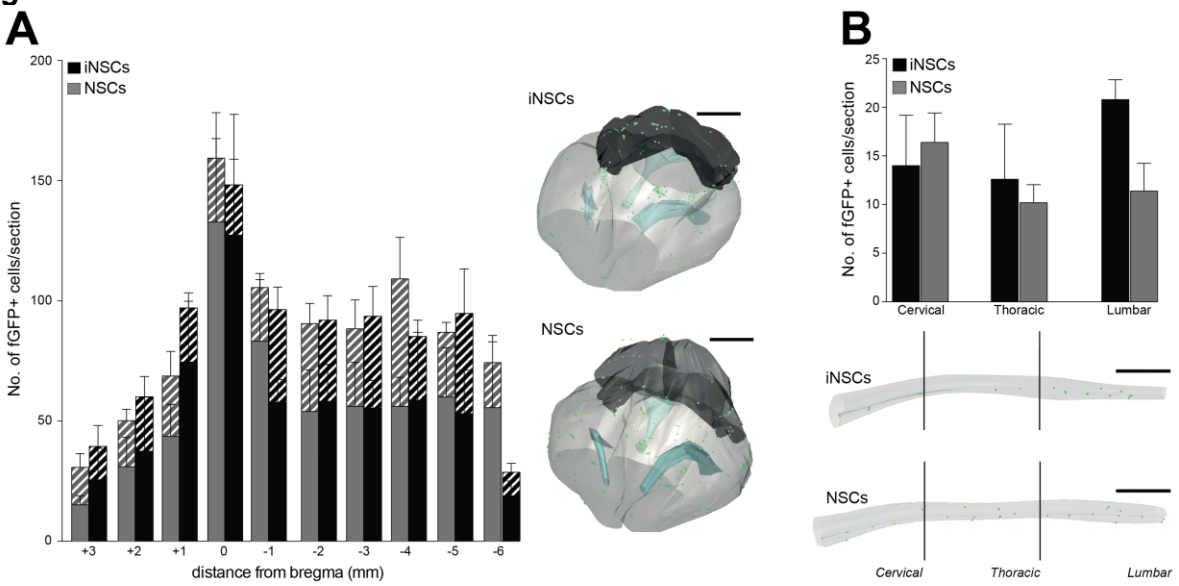

C

iNSCs			NSCs		
Mean ± SEM	**Brain**	**Spinal Cord**	**Mean ± SEM**	**Brain**	**Spinal Cord**
No. of fGFP+ cells	33344 ± 7505	1896 ± 338	**No. of fGFP+ cells**	29780 ± 4551	1520 ± 237
% Nestin+/fGFP+	1.03 ± 1.03	ND	**% Nestin+/fGFP+**	0.90 ± 0.90	1.54 ± 0.81
% Ki67+/fGFP+	2.11 ± 0.87	ND	**% Ki67+/fGFP+**	1.73 ± 0.11	ND
% NeuN+/fGFP+	2.28 ± 0.65	ND	**% NeuN+/fGFP+**	2.03 ± 0.32	ND
% GFAP+/fGFP+	15.04 ± 2.67	23.81 ± 12.40	**% GFAP+/fGFP+**	12.48 ± 2.40	31.34 ± 3.96
% Olig2+/fGFP+	5.12 ± 2.03	ND	**% Olig2+/fGFP+**	4.89 ± 0.71	ND
% DCX+/fGFP+	1.32 ± 0.30	ND	**% DCX+/fGFP+**	1.24 ± 0.20	ND

Peruzzotti-Jametti et al. Figure S2

Figure S2. Distribution and differentiation of icv-injected iNSCs and NSCs at 30 dpt
(A-B) Distribution in the brain and spinal cord of fGFP+ iNSCs or fGFP+ NSCs injected icv in EAE mice at peak of disease (PD). Stereology-based quantification of whole brain (A) and spinal cord (B) with representative 3D reconstructions (green dots indicate individual fGFP+ cells, contours of the ventricles are in light blue, those of the forebrain or spinal cord are in light grey, and those of the cerebellum are in dark grey). Solid bars in A are data from the left-brain hemisphere, while wide upward diagonal bars are from data of the right brain hemisphere. Data are mean numbers (± SEM) from n≥ 5 mice/group over n= 2 independent experiments.
(C) *In vivo* differentiation profile of transplanted fGFP+ iNSCs or NSCs as in A and B. Data are mean numbers (± SEM) from n≥ 5 mice/group over n= 2 independent experiments.
Scale bars: 2 mm.
ND: not detected.

Figure S3

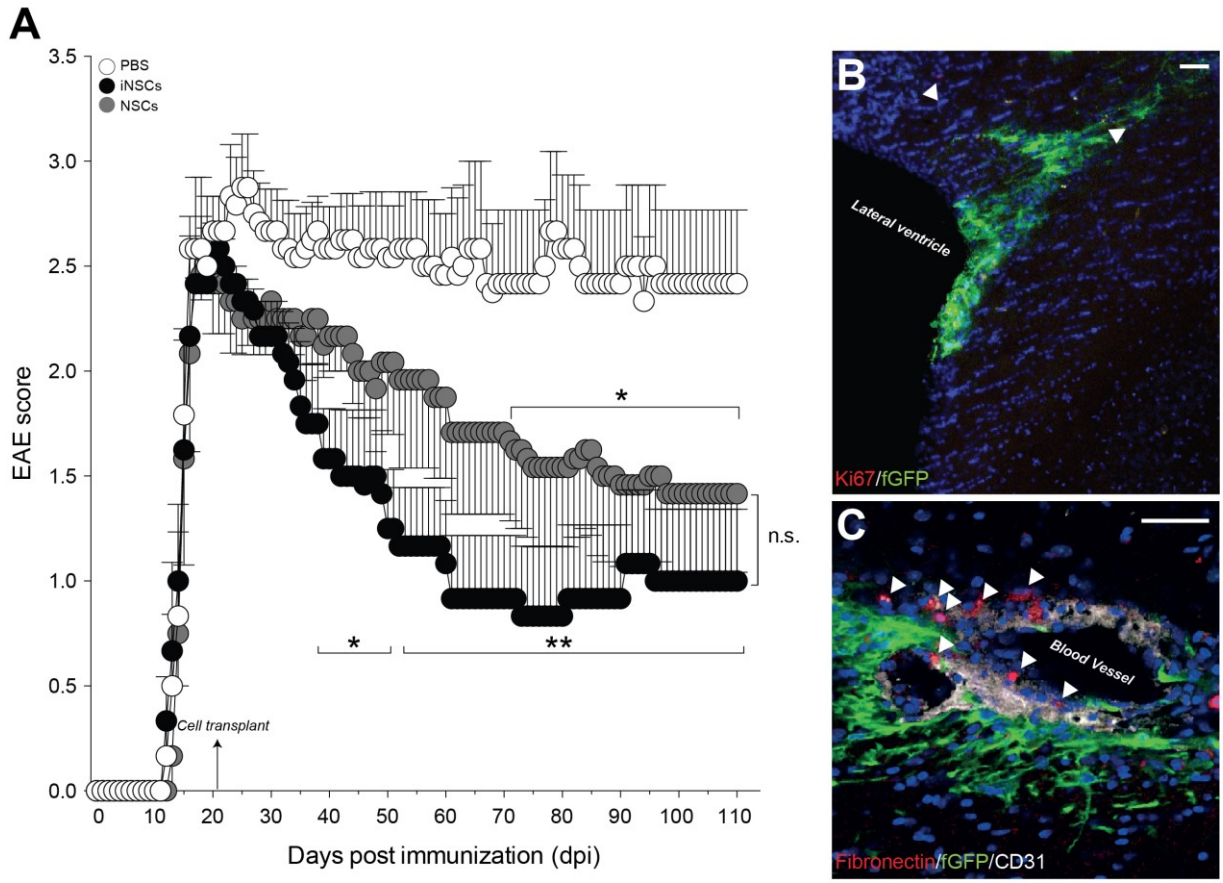

Peruzzotti-Jametti et al. Figure S3

Figure S3. Long-term outcome of iNSC-transplants in EAE mice
(A) Behavioural outcome of fGFP+ iNSC transplants up to 110 dpi. Data are mean EAE score (± SEM) from n= 6 mice/group.
(B-C) Representative confocal microscopy image of transplanted fGFP+ iNSCs in the brain of a EAE mouse at 110 dpi. Expression of Ki67 by fGFP+ iNSCs is indicated by arrowheads (B). Transplanted fGFP+ iNSCs are negative for fibronectin (arrowheads in C).
Scale bars: 50 µm.
*p≤ 0.05, **p≤ 0.01 vs. PBS; n.s.: not significant.

Figure S4

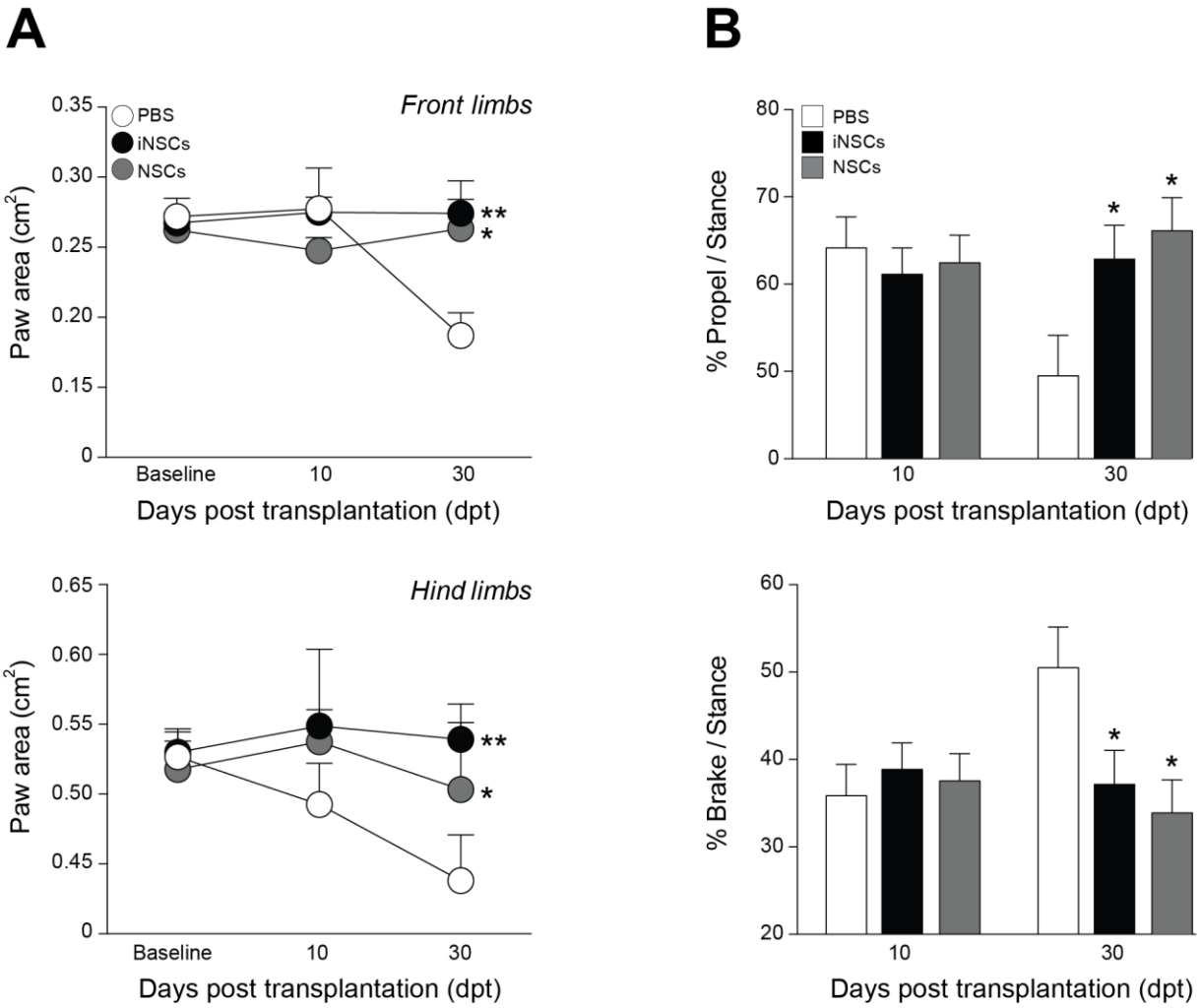

Peruzzotti-Jametti et al. Figure S4

Figure S4. DigiGaitTM ventral plane treadmill videography of EAE mice
(A) Changes in the areas of the paws (front limbs and hind limbs) in iNSC- and NSC-transplanted EAE mice. Data are mean areas (± SEM) from n≥ 5 mice/group. Baseline was assessed before EAE onset.
(B) Gait kinematics as in A. Data are percentages of time in which the paw is in the propulsion (propel) or breaking (brake) phase during the stance (± SEM) from n≥ 5 mice/group.
*p≤ 0.05, **p≤ 0.01 vs. PBS.

Figure S5

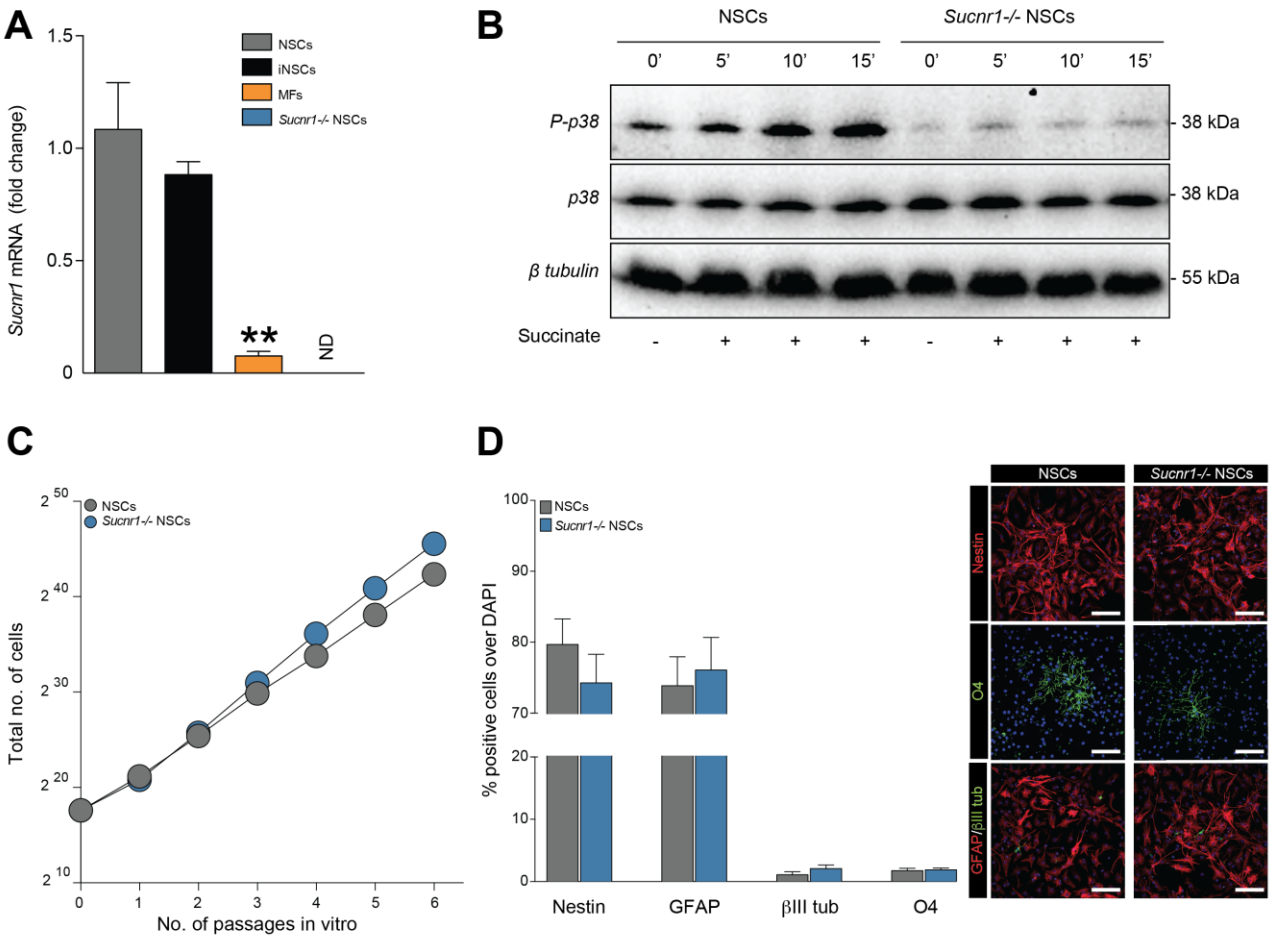

Peruzzotti-Jametti et al. Figure S5

Figure S5. Mouse Sucnr1$^{-/-}$ NSCs *in vitro* features

(A) Sucnr1 mRNA expression relative to Actb in mouse cells and Sucnr1$^{-/-}$ NSCs. Data are mean fold change (± SEM) vs. NSCs from n≥ 3 independent replicates per condition.

(B) Phospho-p38 MAPK (P-p38) and total p38 MAPK (p38) protein expression in mouse NSCs and Sucnr1$^{-/-}$ NSCs after succinate treatment.

(C) Linear growth curves of NSCs and Sucnr1$^{-/-}$ NSCs over 6 passages *in vitro*. Data are mean numbers (± SEM) from n≥ 3 independent experiments per condition.

(D) *In vitro* differentiation properties of NSCs and Sucnr1$^{-/-}$ NSCs. Representative confocal microscopy images of differentiated cells stained for Nestin, O4, GFAP and βIII tubulin are shown. Nuclei are stained with DAPI. Data are mean percentages of positive cells (± SEM) from n≥ 3 independent experiments per condition.

Scale bars: 200 μm.

**p < 0.01 vs. NSCs; ND: not detected.

Figure S6

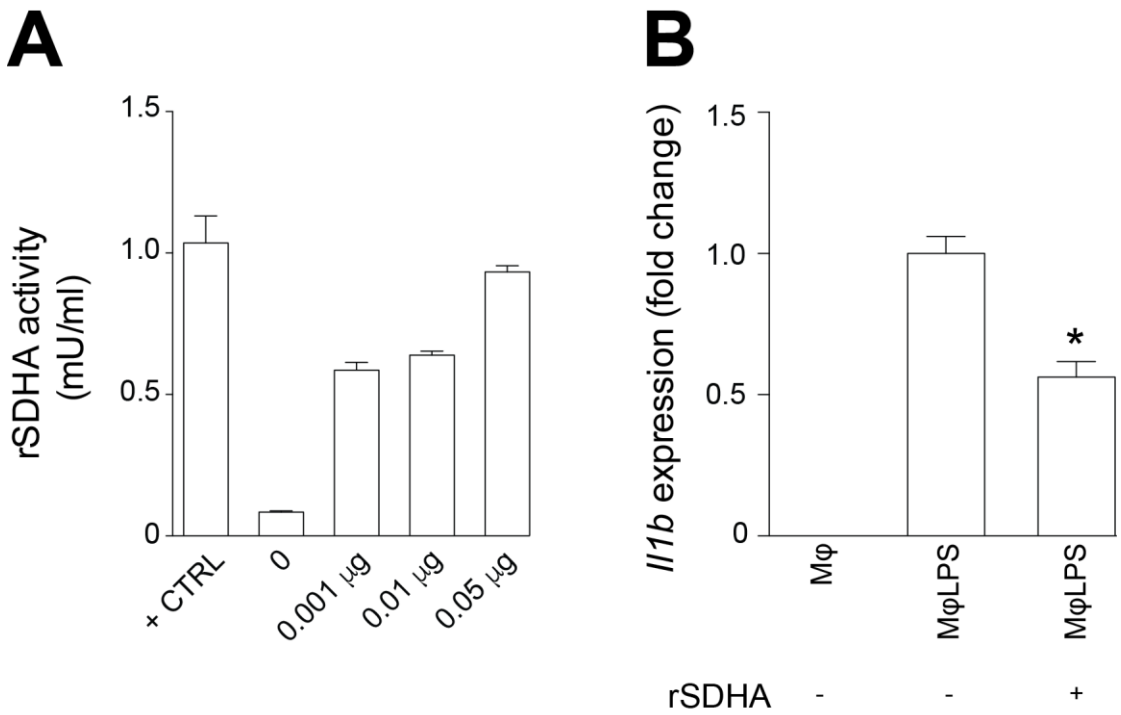

Peruzzotti-Jametti et al. Figure S6

Figure S6. Anti-inflammatory effect of recombinant SDHA on type 1 inflammatory Mφ *in vitro*

(A) Activity of increasing concentrations of mouse recombinant complex subunit A (rSDHA) compared to manufacturer's positive control (+ CTRL). Data are mean numbers (± SEM) from n= 3 independent replicates per condition.

(B) Il1b expression relative to Actb in $M\varphi^{LPS}$ treated with 0.05 µg/ml of mouse rSDHA. Data are mean fold change vs. $M\varphi^{LPS}$ (± SEM) from n≥ 3 independent experiments per condition.

*$p < 0.05$ vs. $M\varphi^{LPS}$.

STAR Methods

Contact for Reagent and Resource Sharing

Further queries and reagent requests may be directed and will be fulfilled by the lead contacts: Stefano Pluchino (spp24@cam.ac.uk) or Luca Peruzzotti-Jametti (lp429@cam.ac.uk).

EXPERIMENTAL MODEL AND SUBJECT DETAILS

All procedures involving animals were performed according to the guidelines of the Animal Ethical Committee of Cambridge University. Animal work was covered by the PPL 80/2457 (to S.P.) in line with the Association of Medical Research Charities (AMRC) recommendations. Details on mouse derived cell cultures and experimental procedures are here below. Wild type C57BL/6 mice were used to establish *in vivo* experimental models and to derive all mouse primary cell lines, except *Sucnr1*$^{-/-}$ Neural Stem Cells (NSCs). C57BL/6 *Sucnr1*$^{-/-}$ mice were provided by José M. Carballido (Novartis) (Rubic et al., 2008). RNA and protein extracts from human foetal NSCs (hNSCs) (Mazzini et al., 2015) were provided by Angelo Vescovi (Milano, Italy).

METHOD DETAILS

Human cell lines

All human cell lines were cultured at 37°C in a controlled humidified atmosphere of 5% CO_2. Human BJ fibroblasts (hBJFs) were purchased from ATCC (CRL-2522) and cultured as adherent cells in hBJF medium [DMEM high glucose (Gibco), 10% FBS, 1% GlutaMAX™ (Gibco), 1% pen/strep (Invitrogen)] until they reached confluency (80-90%). The day of passage, hBJFs were washed with PBS. Trypsin (0.05% in DMEM) was added at 37°C and inactivated after for 3 min with hBJF medium (2:1). Cells were collected and then split 1:3 for expansion.

Human induced Neural Stem Cells (hiNSCs) were obtained from direct reprogramming of hBJFs, as previously described (Meyer et al., 2015). Briefly, hBJFs were infected with Oct4-, Klf4-, Sox2- and c-myc-Sendai viruses and cultured in neuro-induction medium (NIM) [1:1 DMEM/F12 (Life Technologies): NeuroCult™ basal medium (Gibco), 1X B27 (Gibco), 1X N2 (ThermoFisher), 1% pen/strep (Invitrogen), 1% GlutaMAX™(Gibco), 10 ng/ml hLIF (Gibco), 3 μM ChiR (Axon MedChem), 2 μM SB (Invitrogen)]. 17 days after infection cultures showed morphological changes and neural stem cell colonies formation. hiNSCs were cultured as adherent monolayers in NIM and culture media was completely replaced every other day. When cells reached confluency of 50-60%, they were enzymatic dissociated with Accumax™ (Ebioscience) at 37°C for 5 min. Cells were then centrifuged at 300 g for 5 min and re-plated 1:6 on 6 well plates pre-coated with Matrigel™ (BD Bioscience). 10 mM ROCK inhibitor Y27632 (Calbiochem) was added upon seeding. Mycoplasma negative human cells at passage n≤ 20 were used in all experiments.

Mouse cell lines

All mouse cell lines were cultured at 37°C in a controlled humidified atmosphere of 5% CO_2. Mouse induced Neural Stem Cells (iNSCs) were obtained from direct reprogramming of Oct4-GiP Mouse Embryonic Fibroblasts (MEFs) from C57BL/6 mice. Briefly, Oct4-GiP MEFs were infected with retroviruses encoding for Sox2, Klf4, and c-Myc, as previously described (Their et al., 2012). iNSCs colonies were picked 19 days post infection and cultured as either small cellular aggregates (i.e. neurospheres) or adherent monolayers in iNSCs medium [DMEM/F12 (Life Technologies), 1% pen/strep (Invitrogen), 1X N2 (ThermoFisher), 10 ng/ml

purified human recombinant (EGF, Peprotech), 10 ng/ml human recombinant basic fibroblast growth factor (bFGF, Peprotech)]. For maintenance of adherent cells, laminin (1:100, Roche) was added to the iNSCs medium upon seeding. When neurospheres reached a diameter of 150-200 μm (or confluency of 70-80% for adherent cells), cells were collected and harvested in a 15 ml tube (Falcon) and centrifuged at 300 g for 8 min. The supernatant was removed, and the pellet was dissociated by enzymatic digestion with Accumax™ (Ebioscience) at 37°C for 10 min. In case of adherent cells, culture medium was instead removed, cells were washed in PBS, detachment was performed with Accumax™ (Ebioscience) at 37°C for 10 min. Then fresh iNSCs medium was added, and cells were centrifuged at 300 g for 8 min.

The number of viable cells was determined by trypan blue exclusion and viable cells were re-seeded at clonal density 9,700 cells/cm^2. New iNSCs medium was added to each flask every other day. Mycoplasma negative iNSCs at passage n≤ 25 were used in all experiments.

Somatic NSCs and *Sucnr1*$^{-/-}$ NSCs were obtained from the subventricular zone (SVZ) of 7-12 week old (18-20 g) C57BL/6 mice (Charles River, UK) and *Sucnr1*$^{-/-}$ C57BL/6 mice (Rubic et al., 2008) respectively, as previously described (Vescovi and Snyder, 1999). Briefly, mice were humanely culled by cervical dislocation followed by decapitation, the parietal bones were cut cranially to caudally using micro-surgery scissors, and the brains removed. A brain slice matrix was used to obtain 3 mm thick brain coronal sections starting from 2 mm after the anterior pole of the brain. The SVZ of the lateral ventricles was isolated from coronal sections using iridectomy scissors. Tissues derived from at least 2 mice were pooled to generate cultures. Dissected tissues were transferred to a 15 ml tube with digestion medium [early balance salt solution (EBSS, Gibco), papain (1 mg/ml, Worthington), ethylenediaminetetraacetic acid (EDTA) (0.2 mg/ml, Sigma-Aldrich) and L-cysteine (0.2 mg/ml, Sigma-Aldrich)] and incubated for 45 min at 37°C on a rocking platform. At the end of the incubation, the tube was centrifuged at 200 g for 12 min, the supernatant was removed and the pellet was mechanically disaggregated with 2 ml of EBSS. The pellet was centrifuged again at 200 g for 12 min and then dissociated with a 200 μl pipette and seeded in complete growth medium (CGM). CGM was constituted of mouse NeuroCult™ basal medium (Stem Cell Technologies) plus mouse NeuroCult™ proliferation supplements (Stem Cell Technologies) added with 2 μg/ml heparin (Sigma-Aldrich), 20 ng/ml EGF and 10 ng/ml bFGF. After approximately 4-7 days, a small percentage of the isolated cells begun to proliferate, giving rise to neurospheres. When neurospheres reached the necessary dimension (150-200 μm diameter), the cells were harvested in a 15 ml tube and centrifuged at 100 g for 8 min. The supernatant was then removed and the pellet dissociated by enzymatic digestion with Accumax™ at 37°C for 10 min. The number of viable cells was determined by trypan blue exclusion and viable cells were re-seeded at clonal density 8,000 cells/cm^2. Mycoplasma negative NSCs at passage n≤ 25 were used in all experiments.

Mouse Fibroblasts (MFs) were prepared from the kidneys of adult C57BL/6 mice, as previously described (Grupp and Muller, 1999). MFs were cultured as adherent cells in fibroblasts medium [DMEM high glucose (Gibco), 10% FBS, 1% GlutaMAX (Gibco), 1% pen/strep (Invitrogen)] until they reached confluency (80-90%). The day of passage, cells were washed with PBS. Trypsin (0.05% in DMEM) was added at 37°C and inactivated for 3 min with fibroblasts medium (2:1). Cells were collected and then split 1:3 for expansion.

Bone marrow derived macrophages (Mφ) were obtained from the bone marrow of C57BL/6 mice, as previously described (Masters et al., 2010). Briefly, 9-10 weeks-old C57BL/6 female mice were anesthetized with 2% isoflurane and killed by cervical dislocation. Bone marrow was flushed from femurs and tibiae and bone marrow progenitor cells were cultured for 6 days on Petri dishes (Thermo Scientific) in Mφ medium

[DMEM high glucose (Gibco), 10% FBS, 1% pen/strep (Invitrogen) and 10% of macrophage colony-stimulating factor (M-CSF) conditioned media from L-929 fibroblast cells].

L-929 fibroblast (NCTC clone 929) cells were purchased from ATCC and grown as adherent cells in L-929-medium [RPMI media, 10% Foetal Calf Serum (Gibco) and 1% pen/strep (invitrogen)] until they reached confluency (80%). The day of passage cells were washed with PBS. Trypsin (0.05% in DMEM) was added at 37°C and inactivated after for 10 min with, L-929-medium (2:1). Cells were collected and spun at 300 g for 5 min, and then re-seeded 1:10. Conditioned medium was collected from cultures and filtered through a membrane filter (0.22 μm pore diameter) to remove cells and debris and frozen (-80°C) until use.

The BV2 cell line was provided by Professor Maria Grazia Spillantini (Cambridge, UK). For normal expansion, cells were cultured in BV2 expansion medium [DMEM high glucose (Gibco), 2% FBS, 1% pen/strep (Invitrogen)] until they reached confluency (70%). The day of passage cells were washed with PBS. Trypsin (0.05% in DMEM) was added at 37°C and inactivated after for 3 min with BV2 expansion medium (2:1). Cells were collected and spun at 300 g for 5 min, and then re-seeded at 4,200 cells/cm^2 for expansion.

Mouse iNSC/NSC proliferation, viability and differentiation *in vitro*

Cellular viability of iNSCs/NSCs was assessed by vital stain exclusion (trypan blue staining) and a continuous growth curve was built up by seeding cells at clonal density. The linear growth curve was generated extimating the total number of cells by multiplying the growth rate (i.e. number of live cells divided by the number of seeded cells) for the total number of cells present at the previous time point. The mean number of cells per time point ± standard error of the mean (SEM) was reported to build the linear trend line. The daily growth rate was obtained dividing the growth rate by the number of days per passage. Viability was defined as the percentage of viable cells over dead cells ± SEM. For differentiation, cells were seeded on 13 mm glass coverslips pre-coated with Matrigel™ (8x10^4 cells/coverslips, BD Bioscience) and cultured in 400 μl differentiation medium [NeuroCult™ basal medium (Stem cells Technologies), 10% mouse differentiation supplement (Stem cells Technologies), 1% pen/strep (Invitrogen)], as previously described (Donegà et al. 2014). Half of the medium was replaced with fresh differentiation medium after 3 days. After 3 more days (6 days in total), coverslips were washed with PBS and fixed with 4% paraformaldehyde (PFA, Sigma-Aldrich) and 2% sucrose in PBS.

For immunofluorescence staining, cells were rinsed with PBS, and then blocked for 1 hr at room temperature (RT) in blocking buffer (0.1% Triton X100 and 10% secondary antibody species serum in PBS). The following primary antibodies diluted in blocking buffer were used: anti-nestin (1:200, Abcam), anti-SOX2 (1:100, Abcam), anti-glial fibrillary acidic protein (GFAP) (1:500, Abcam), anti-β-tubulin-III (1:500, Covance), anti-O4 (1:400, R&D). Primary antibodies were incubated at 4°C overnight. Cells were then washed in PBS with 0.1% Triton X100 and incubated with the appropriate fluorescent secondary antibodies (1:1,000 Alexa-fluor 405, 488, 555, 647, Invitrogen) 1 hr at RT. After washing in PBS, nuclei were counterstained with DAPI (1:10,000, Invitrogen) for 3 min and then mounted with Dako mounting kit (Fluka). Nonspecific staining was observed in control incubations in which the primary antibodies were omitted. For quantification, images were acquired on a CCD camera (DC 480, Leica) under a fluorescence microscope (Olympus, BX51) with a 40X objective on 6 regions of interest (ROI) of each coverslip. Images were analysed and prepared using ImageJ software. Data were represented as the percentage of positive cells over the total of 4',6-diamidino-2-phenylindole (DAPI) positive cells ± SEM, from a total of n≥ 3 independent experiments.

Fluorescence-activated cell sorting (FACS) analysis of surface molecules

For the analysis of the expression of surface molecules, cells were harvested and dissociated for counting, as previously described. A total of $5x10^5$ cells were kept in the blocking solution [2% FBS (Gibco) in PBS] for 15 min. Cells were then incubated for 30 min, at RT with fluorescence-conjugated antibodies: anti-CD44-fluorescein isothiocyanate (FITC) (1:100, BD Biosciences), anti-alpha-4-integrin-phycoerythrin (PE) (1:100, Abcam), anti-L-selectin-allophycocyanin (APC) (1:100, BD Biosciences), anti-CX3C chemokine receptor 1 (CX3CR1)-PE (10 μl, R&D), anti-CXC chemokine receptor type 4 (CXCR4)-PE (1:3, BD Biosciences), anti-C-C chemokine receptor type 2 (CCR2)-APC (10 μl, R&D). After incubation cells were rinsed with PBS and fixed in 0.5% PFA in PBS. All FACS analyses were carried out on a Cyan-ADP (Dako Cytomation) and data were analysed using FlowJo (Treestar).

Type-1 inflammatory Mφ or BV2 cells co-cultures with iNSCs/NSCs

After 6 days from bone marrow isolation, Mφ were re-seeded with fresh Mφ medium on 6 or 12 well plates ($5x10^5$ or $1x10^5$ cells/well respectively) for co-culture experiments. For gene microarrays and metabolomic studies, recombinant mouse M-CSF (50 ng/ml, Miltenyi Biotec) and dialyzed (d)FBS were used instead of M-CSF conditioned media from L-929 fibroblast cells and FBS. After 18 hrs from re-seeding, Mφ were stimulated by adding 50 ng/ml LPS (Enzo life sciences). To assess the metabolic profile of LPS-activated type-1 inflammatory Mφ ($M\varphi^{LPS}$), intracellular and extracellular metabolites were collected at given time points (see also section: *Metabolite extraction and LC-MS analysis*).

For co-culture experiments, treatment cells were dissociated, counted and re-suspended directly in Mφ medium. For co-culture experiments in which specific blockers were used, iNSCs/NSCs/*Sucnr*$^{-/-}$ NSCs/hiNSCs were kept in an Eppendorf tube at 37°C ± the irreversible blocker of COX2 *SC-58125* (10 μM*,* Sigma-Aldrich*),* the specific inhibitor of human SUCNR1 *4c* (1 μM, Advinus Therapeutics), or PBS (control) for 1 hr prior co-cultures. Cells were then spun at 400 g for 5 min, washed with PBS and re-suspended in Mφ medium. Co-cultures of Mφ and treatment cells were all started 1 hr after LPS stimulation using 0.4 μm-pore size trans-well inserts (Millipore) at a 1:1 ratio. 24 hrs after the start of the co-cultures, inserts were removed and Mφ/culture media were isolated for subsequent analysis.

After BV2 cell line reached ~ 70% confluence, cells were collected and re-seeded at a density of $1x10^5$ cells/3.7 cm^2 on 12 well plates in BV2 experiment medium [DMEM high glucose (Gibco), 1% pen/strep (Invitrogen)] to avoid excessive activation. After 12 hrs from re-seeding 50 ng/ml LPS (Enzo) was added to the medium for stimulation. For co-culture experiments, treatment cells were dissociated, counted and re-suspended in BV2 experiment medium. Co-cultures of BV2 and treatment cells were all started 1 hr after LPS stimulation using 0.4 μm-pore size trans-well inserts (Millipore) at a 1:1 ratio. 6 hrs after the start of the co-cultures, inserts were removed and BV2 were isolated for subsequent analysis.

Recombinant SDHA activity and treatment of type-1 inflammatory Mφ

Mouse recombinant succinate dehydrogenase complex subunit A (rSDHA) was purchased from Cloud-Clone Corp. (RPJ784Mu01), reconstituted on ddH_20 and kept at -80°C (stock solution 0.1 μg/μl). Activity measurements were performed using a SDH Activity Colorimetric Assay Kit (#K660-100, BioVision) following manufacturer's instructions. For mouse rSDHA treatment, $M\varphi^{LPS}$ were activated as described and rSDHA was added to the Mφ medium (0.05 μg/ml) 1 hr after LPS stimulation. After 24 hrs Mφ were isolated for subsequent gene expression analysis.

Lentiviral fGFP tagging

Cells used for transplantation studies were transduced *in vitro* using a third-generation lentiviral carrier (pRRLsinPPT-hCMV) coding for the enhanced farnesylated (f)GFP, which targets the fluorescent protein to the inner plasma membrane of transduced cells (Follenzi et al. 2000). The functional stability of these cells (in the absence or in the presence of the lentiviral transcript) has been confirmed with clonal and population studies (Pluchino et al. 2003). Briefly, neurospheres were harvested, dissociated to a single cell suspension and seeded at high density [$1.5x10^6$ in a T75 cm^2 flask (Sigma-Aldrich)] in 5 ml fresh medium. After 12 hrs, $3x10^6$ T.U./ml of lentiviral vectors were added and 6 hrs later additional 5 ml of fresh medium were added. 72 hrs after viral transduction, cells were harvested and re-seeded at normal concentration. Transgene expression was measured by FACS analysis before transplantation and 98.7 ± 0.2 (mean % ± SEM) of cells were found to be labelled.

EAE induction, transplantation and behavioural studies

4 independent *in vivo* transplantation studies were performed on a total n= 99 C57BL/6 female mice (weight 20 gr) with MOG-induced EAE, as previously described (Pluchino et al., 2003). Briefly, mice were anaesthetized with isoflurane (4% induction, 1.5% maintenance), and received n= 3 subcutaneous (s.c.) injections (2 flanks and 1 at the base of the tail) of 50 μl containing 200 μg/mouse MOG35-55 (Multiple Peptide System) (Espikem), incomplete Freund's Adjuvant (IFA) and 8 mg/ml Mycobacterium tuberculosis (Scientific Laboratories Supply). 100 μl of Pertussis Toxin (5 ng/μl) (List Biological Laboratories) was injected intravenously (i.v.) on the day of the immunization and again after 48 hrs.

Body weight and EAE clinical score (0 = healthy; 1 = limp tail; 2 = ataxia and/or paresis of hindlimbs; 3 = paralysis of hindlimbs and/or paresis of forelimbs; 4 = tetraparalysis; 5 = moribund or death) were recorded daily (Zargari et al. 2007).

After 11-19 days post immunisation (dpi), mice developed the first clinical signs of diseases (disease onset). At 3 days after disease onset, mice with similar scores were randomly assigned to the different treatment groups. After randomization, mice received a single intracerebroventricular (icv) injection (AP -0.15, ML +1.0 left, DV -2.4) of $fGFP^+$ NSCs, or $fGFP^+$ iNSCs or $fGFP^+$ *Sucnr1*$^{-/-}$ NSCs ($1x10^6$ in 5 μl PBS). EAE mice transplanted icv with $1x10^6$ MFs or injected icv with 5 μl PBS were used as controls.

Body weight and EAE clinical score were recorded daily up to 50 dpi or 110 dpi. Data were expressed as the mean of EAE score ± SEM from a total of n≥ 6 mice per group per time point**.**

Gait kinematics was assessed using a DigiGait™ (Mouse Specifics Inc., Boston, MA) ventral plane treadmill videography before EAE onset (baseline) and at 10-30 days post transplantation (dpt), as previously described (Dorman et al. 2014, Berryman et al. 2009, Eftaxiopoulou et al. 2014). Briefly, the treadmill speed was set at either 10 or 5 cm/sec (depending on each mouse fitness), and the gait of the mice was recorded. An analysable run was defined as a 5-sec video segment without wall or bumper contacts. The mouse was designated as noncompliant and the test was stopped if the mouse failed to accomplish an analysable run after 3 trials (a 30 sec rest was allowed between trials). Criteria for test failure where (i) at least 2 min of test without capturing an analysable run, and/or (ii) the mouse could not run without contacting the rear wall of the enclosure.

***Ex vivo* tissue pathology**

The day of sacrifice, mice were deeply anesthetized with an intraperitoneal (i.p.) injection of ketamine 10 mg/ml (Boehringer Ingelheim) and xylazine 1.17 mg/ml (Bayer) in sterile water and transcardially perfused

with 1ml EDTA 5M in 500ml saline 0.9% NaCl for 5 min, followed by a solution of 4% PFA in PBS for another 5 min.

Brains and spinal cords were isolated and post-fixed in 4% PFA in PBS at 4°C overnight. Tissues were then washed in PBS and left for at least 48-72 hrs in 30% sucrose in PBS at 4°C for cryo-protection. Brains and spinal cords were then embedded in optimum cutting temperature (OCT) medium, frozen with liquid nitrogen and cryo-sectioned (25 μm coronal section thickness for brains and 10 μm axial section thickness for spinal cords) using a cryostat (CM1850, Leica, Wetzlar, Germany) with a microtome blade (A35, Feather, Osaka, Japan). Sections were then stored at -80°C until use.

For quantification of graft survival and inflammatory infiltrates, sections were pre-treated with peroxidase 3% for 15 min, and then were incubated in the blocking solution [PBS + 10% normal goat serum (NGS, Sigma-Aldrich) ± 0.1% Triton X100] for 1 hr at RT. Primary antibodies were diluted in a solution of PBS + 1% NGS ± 0.1% Triton X100, and incubated at 4°C overnight. The following primary antibodies were used: anti-GFP (1:250, Invitrogen), anti-CD45 (1:100, Serotec), anti-F4/80 (1:100, Serotec), anti-CD3 (1:250, Abcam), anti-CD20 (1:100, Santa Cruz). The following day, tissues were washed with PBS and incubated for 1 hr with the appropriate secondary biotinilated antibody (1:500, Sigma-Aldrich) diluted in a solution of PBS + 1% NGS, ± 0.1% Triton X100. Components "A" and "B" of Vectastain Elite ABC kit were mixed for 45 min and the reaction developed by means of 3,3'-Diaminobenzidine (DAB) as per manufacturer's instructions. The reaction was blocked dipping the section into distilled water and sections were counterstained with haematoxylin. The tissues were then dehydrated (with increasing alcohol solutions), washed in xylene (Merck, Darnstadt, Germany) and mounted with a synthetic mounting medium (EUKITT, Hatfield, PA, USA). The numbers of transplanted $fGFP^+$ cells and the areas of $CD45^+/F4/80^+/CD3^+/CD20^+$ inflammatory infiltrates were calculated on n= 10 equally spaced sections axial brain sections and n= 15 equally spaced axial spinal cord sections. $fGFP^+$ cells and inflammatory contours were outlined using an Olympus BX53 microscope with motorized stage and Neurolucida software (11.07 64-bit, Microbrightfield) and descriptive 3D brain/spinal cord reconstructions were obtained.

For quantification of demyelination and axonal damage, cryostat 10 μm thick spinal cord sections were stained for Luxol fast blue (LFB)/periodic-acid Schiff and Bielschowsky silver impregnation respectively, as previously described (Pluchino et al. 2003). The LFB/Bielschowsky negative areas of n= 15 equally spaced axial spinal cord sections were outlined using an Olympus BX53 microscope with motorized stage and Neurolucida software (11.07 64-bit, Microbrightfield) and expressed as the percentage of damaged tissue per section ± SEM.

For the quantification of stem cell differentiation and of the % of MPs expressing pro/anti-inflammatory markers *in vivo*, sections were rinsed with PBS, and then blocked for 1 hr at RT in blocking buffer (0.1% Triton X100 and 10% secondary antibody species serum in PBS). A Fab fragment affinity purified IgG anti-mouse was applied if anti-mouse antibodies were used (1:10, Jackson ImmunoResearch). The following primary antibodies, diluted in blocking buffer, were used at 4°C overnight: anti-GFP (1:250, Invitrogen), anti-nestin (1:200, Abcam), anti-Ki67 (1:250, Abcam), anti-GFAP (1:500, Abcam), anti-NeuN (1:250, Chemicon), anti-MBP (1:100, AbD SeroTec), anti-Olig2 (1:500, Millipore), anti-von willebrand factor (vWF) (1:200 Abcam), anti-doublecortin (DCX) (1:250, Abcam), anti-fibronectin (1:400, Sigma-Aldrich), anti-CD31 (1:20, BD Pharmingen), anti-F4/80 (1:100 Serotec), anti-iNOS (1:100, BD Bioscience), anti-MRC1 (1:400, Abcam). Sections were then washed in PBS with 0.1% Triton X100 and incubated with the appropriate fluorescent

secondary antibodies (1:1,000 Alexa-fluor 405, 488, 555, 647, Invitrogen) for 1 hr at RT. After washing in PBS, nuclei were counterstained with DAPI (1:10,000, Invitrogen) for 3 min and then mounted with Dako mounting kit (Fluka). Nonspecific staining was observed in control incubations in which the primary antibodies were omitted.

Quantification of graft differentiation was obtained from randomized n≥ 3 brain ROIs and n≥ 5 brain spinal cord ROIs acquired using a confocal microscope (Leica TCS SP5 Microscope). Data are expressed as % of double positive cells over total $fGFP^+$ cells ± SEM (≥ 95 $fGFP^+$ cells for each marker of interest were counted). Quantification of MPs expressing pro/anti-inflammatory markers was obtained from the brain (n≥ 25 randomized ROIs) and the spinal cords (n= 6 equally spaced entire sections) of EAE mice using a fluorescence microscope (Leica DFC 3000G). Data are expressed as % of double positive area over total $F4/80^+$ area ± SEM.

Plasma and cerebrospinal fluid (CSF) sampling

For plasma sampling (at 10 and 30 dpt), the tail vein was punctured and whole blood was sucked by capillarity in EDTA filled Microvettes (Sarstedt) (10-30 μl/mouse). Samples were kept at 4°C until centrifugation (950 g for 5 min). Plasma was then collected from supernatant and stored at -80°C for subsequent analysis.

For CSF sampling (at 10 and 30 dpt), mice were deeply anesthetized with isoflurane (4% induction, 1.5% maintenance), and CSF (3-5 μl/mouse) was obtained as part of a terminal procedure from the cisterna magna, as previously described (Liu and Duff, 2008). CSF samples were initially put on dry ice and then stored at -80°C for subsequent analysis.

Calcium imaging

Cells were counted after dissociation and seeded in their own specific medium plus laminin (Roche) 1:100 (laminin was not added for MFs) on 35 mm glass bottom culture dishes (MatTek Corporation) ($1.5x10^5$ cells/dish). After 2 days in culture, media was changed with Tyrode's solution (isotonic solution resembling CSF composition and containing 129 mM NaCl, 5 mM KCl, 2 mM $CaCl_2$, 3 mM $MgCl_2$, 30 mM Glucose, 25 mM Hepes) with 5 μM Fluo-4AM (Life Technologies) for 30 min at 37°C. Cells were then washed twice (15 min) with fresh Tyrode's solution. The dish was then mounted in a home-made microfluidic chamber and put on the stage of a Leica DMI 6000B inverted live imaging microscope in a controlled humidified atmosphere of 5% CO_2 at 37°C. The chamber was connected to a perfusion system to allow a continuous/regular flow of solutions and stimulation with succinate dibasic hexa-hydrate (500 μM Sigma-Aldrich) when necessary. Cells were recorded for 90 sec: 15 sec of basal recording, 30 sec of stimulus and 45 sec of recovery. Images were acquired with a frequency of 2 frames per sec (fps).

ELISA

For measurements of PGE2 levels after succinate stimulation, cells were dissociated, counted, and $5x10^5$ cells/500 μl/well per condition were seeded in a 24 well plate. After 6 hrs, sodium succinate dibasic hexa-hydrate (500 μM, Sigma-Aldrich) in PBS (or PBS alone) was added to the wells. Cells pre-treated (1 hr before succinate stimulus) with ± *SC-58125* (10 μM, Sigma-Aldrich) or ± *4c* (1 μM, Advinus Therapeutics) were used as controls. After 30 min from succinate stimulation, media were collected, spun at 1,000 g for 5 min, and supernatants stored at -80°C for subsequent analysis.

For measurements of PGE2 levels after co-cultures, media were collected at 24 hrs of co-culture spun at 1,000 g for 5 min, and supernatants were stored at -80°C for subsequent analysis.

PGE2 levels were determined in both cases using PGE2 ELISA kit (Caymanchem) following the manufacturer's instructions. Briefly, 50 μl of samples were added to 96 wells pre-coated plates and incubated for 18 hrs at 4°C. Plates were then washed, developed for 60-90 min at RT, and read at 405-420 nm. PGE2 concentration was determined by comparison to the standard curve performing 4-parameter logistic fit.

Uptake experiments with [^{14}C] - labelled succinate

Cells were counted after dissociation and re-plated at high cell-density (2.4x10^5 cells/cm^2) the day before the experiment. The following day cells were collected and centrifuged at 300 g for 8 min. Pellet was re-suspended in CGM or iNSCs medium (previously adjusted at pH 6.8) and cells were seeded in a 6 well plate at a final concentration of 5x10^5 cells/ml/well. Each well was respectively stimulated with [^{14}C] - labelled succinate (American Radiolabelled Chemicals) at final concentration 500 μM (80 nCi [^{14}C] - succinate/mL) in PBS. PBS alone was used as controls. At the corresponding time points, culture media and cells were collected, and centrifuged at 400 g for 5 min. To isolate the extracellular fraction, 500 μl of supernatant from each sample was added to tubes containing 3 mL of Ultima Gold liquid scintillation cocktail (PerkinElmer). To isolate the cellular fraction, the remaining volume in the tube was removed first after a 1,000 g for 5 min spin. Another 1,000 g for 1 min spin was then performed to better separate the pellet from the residual supernatant. Finally, each pellet was dried with blotting paper (to further avoid any extracellular fraction's contamination) and 40 μl of Triton-X100 was added. Cellular fraction was then added to tubes containing 3 mL Ultima Gold liquid scintillation cocktail (PerkinElmer). Total radioactivity was then measured using a TriCarb LSC Counter (PerkinElmer). Radioactive counts were converted into decays per min and subsequently converted into amounts of succinate using a final specific activity of 0.15 mCi/mmol. Data were normalized on total proteins content evaluated by BCA Protein assay kit (Thermo Scientific).

Immunoblotting

Western blots for SUCNR1 were performed on freshly dissociated cells. Cells were collected and spun at 16,000g for 30 sec. Pellets were washed with PBS, and then re-suspended in 50 μl of 1X RIPA buffer (Abcam) with protease (Roche) and phosphatase inhibitors (Thermo Fisher Scientific). Samples were frozen at -80°C until further use.

Western blots after succinate stimulation were performed as it follows. Cells were dissociated, counted, and 1.5x10^6 cells/1ml/well per condition were seeded in a 6 well plate. After 6 hrs, either sodium succinate dibasic hexa-hydrate (Sigma-Aldrich) in PBS (final concentration 500 μM) or PBS alone (control) was added to each well. Cells pre-treated (1 hr before succinate stimulus) with ± *4c* (1 μM, Advinus Therapeutics) were used as controls for hiNSCs studies. After given time points (0min-5min-10min-2hr-6hrs) cells were collected and spun at 16,000g for 30 sec. Pellets were washed with PBS, and then re-suspended in 50 μl (or 25 μl for pP38/P38 WB) of 1X RIPA buffer (Abcam) (with protease/phosphatase inhibitors). Samples were frozen at -80°C and electrophoresis was performed the following day.

Western blots for IL-1β on Mφ were performed after 24 hrs of co-culture. Proteins were extracted by pooling 3 wells of a 12 well plate per condition (3x10^5 cells in total). First, cells were washed with PBS, and then 1X RIPA buffer (Abcam) with protease (Roche) and phosphatase inhibitors (Thermo Fisher Scientific) was added to each well (30 μl/well). Cells were frozen at -20°C for 1 hr, and then scraped before pooling. Samples were frozen at -80°C and electrophoresis was performed the following day.

Western blots for Hif-1α/PKM2 on Mφ were performed after 24 hrs of co-culture. Proteins were extracted by pooling 6 wells of a 12 well plate ($6x10^5$ cells in total) per condition. First, cells were washed with PBS, and then Laemmli buffer (Sigma-Aldrich) 1X final concentration with protease (Roche) and phosphatase inhibitors (Thermo Fisher Scientific) was added to each well (50 μl/well). Cells were scraped before pooling, samples were heated 95°C for 5 mins, and the same volume of extract (25 μl) was loaded for electrophoresis on the same day on a 10% Bis-Tris precasted gel (Life technologies).

For all the other samples (i.e. those stored at -80°C), extracts were instead defrosted, sonicated and proteins were quantified using Pierce™ BCA Protein Assay kit (Thermo scientific). These samples were then heated at 95°C for 5 mins, and the same amount of protein (50-60 μg of extract for p-P38/P38 or 10-20 μg of extract for all the other targets) per each condition was loaded with 1X NuPAGE LDS sample buffer and NuPAGE sample reducing agent 1X on a 10% SDS-PAGE gel.

After running at 120V, samples were then transferred on Immobilon™ PVDF filter paper sandwich at run completion (Millipore). The membrane was then blocked with 5% non-fat milk in 0.1% PBS-Tween 20 for 1 hr and then incubated with primary antibodies diluted in 5% non-fat milk in 0.1% PBS-Tween 20 [with phosphatase inhibitors (Thermo Fisher Scientific) in case of pP38/P38 WB] over night at 4°C.

The following primary antibodies were used for immunoblotting: anti-HiF1α (1:1,000, Novus Biologicals), anti-PKM2 (1:1,000 Cell Signaling), anti-IL-1β (1:1,000 R&D systems), anti-SUCNR1 (1:500 Novus Biologicals), anti-P-p38 MAPK (1:1,000 Cell Signaling), anti-p38 MAPK (1:1,000 Cell Signaling), anti-SLC13A5 (1:400 ThermoFisher), anti-SLC13A3 (1:1,000 Aviva Systems Biology), anti-β-actin (1:10,000 Sigma-Aldrich), anti-β-tubulin (1:1,000 Sigma-Aldrich). After 3 washes in 0.1% PBS-Tween 20, membranes were incubated for 1 hr at RT with the appropriate HRP-conjugated secondary antibodies: anti-rabbit HRP conjugated secondary (1:10,000 Thermo Scientific), anti-mouse HRP conjugated secondary (1:20,000 Thermo Scientific). Proteins bands were developed using Enhanced Chemiluminescence Substrate (Perkin Elmer) and acquired using a Biorad Chemidoc MP system. The density of each band was quantified using ImageJ software and normalized to housekeeping bands (β-actin or β-tubulin) measured in the same membranes.

Extracellular flux (XF) assays

A XF24^e Extracellular Flux Analyser (Seahorse Bioscience, Billerica, MA) was used for all XF assays.

For XF assay on Mφ co-cultures, Mφ were seeded 6 days after bone marrow isolation, with fresh Mφ medium on a 24 well XF24 cell culture microplate ($1x10^5$ cells/well) for co-culture experiments. After approximately 18 hrs from seeding, Mφ were stimulated by adding 50 ng/ml LPS (Enzo life sciences). Treatment (or control) cells were added at 1:1 ratio, 1 hr after LPS stimulation, using 0.4 μm-pore size trans-well inserts (24 well-size, Millipore). 24 hrs after the start of the co-culture the inserts were removed, Mφ medium was replaced with XF medium [Seahorse salt solution (Seahorse Bioscience), 1% glutamine 200 mM, 1% pyruvate 100 mM, 1% FBS, D-glucose (225 mg/50ml final volume)] pH 7.35-7.45, and baseline oxygen consumption rate (OCR) and extracellular acidification rate (ECAR) were measured for 10 reads.

For XF assay on all other cell types, cells were counted after dissociation and seeded in their own specific medium plus laminin (Roche) 1:100 (laminin was not added for MFs) on a 24 well XF24 cell culture microplate ($1x10^5$ cells/well). When cells reached >90% confluency, media were replaced with XF medium pH 7.35-7.45. Mitochondria stress protocol was performed using oligomycin, FCCP, rotenone and antimycin (1 μM final concentration).

After the completion of each XF assay, cells were washed with PBS and 25 μl of 1X RIPA buffer (with protease/phosphatase inhibitors) were added to each well. The total protein amount/well was estimated with a BCA Protein assay kit (Thermo Scientific) and used to normalize the OCR and ECAR values of the single well.

Gene expression analysis (microarrays and qRT-PCR)

Ex vivo samples were collected at 10 and 30 dpt. Mice were deeply anesthetized with isoflurane (4% induction) and decapitated. The entire brain and spinal cord were exposed, isolated and stored in RNAlater (QIAGEN) at 4°C until use. Samples were homogenated using a potter and total RNA was extracted using the RNeasy Midi Kit (QIAGEN) following manufacturer's instructions.

Total RNA from Mφ or BV2 microglial cell line in co-cultures was collected at given time points. Before collection, cells were washed with PBS, 350 μl of RLT buffer were added, and samples stored at -80°C until extraction.

Total RNA after succinate stimulation was collected as it follows. Cells were dissociated, counted, and $1.5x10^6$ cells/ml/well per condition were seeded in a 6 well plate. After 6 hrs, sodium succinate dibasic hexa-hydrate (500 μM, Sigma-Aldrich) in PBS or PBS alone (control) was added to each well. After 15 min cells were collected and spun at 16,000 g for 30 sec. Pellets were washed with PBS, resuspended in 350 μl of RLT buffer and stored at -80°C until extraction.

Total RNA from all *in vitro* samples was extracted using the RNeasy Micro Kit (QIAGEN) following manufacturer's instructions.

For microarrays, samples were prepared according to Affymetrix protocols (Affymetrix, Santa Clara, CA). RNA quality and quantity were ensured using the Bioanalyzer (Agilent, Santa Clara, CA) and NanoDrop (Thermo Scientific, Waltham, MA) respectively. For RNA labelling, 200 ng of total RNA was used in conjunction with the Affymetrix recommended protocol for the Clariom_S chips. The hybridization cocktail containing the fragmented and labelled cDNAs was hybridized to the Affymetrix Mouse Clariom_S GeneChip. The chips were washed and stained by the Affymetrix Fluidics Station using the standard format and protocols as described by Affymetrix. The probe arrays were stained with streptavidin phycoerythrin solution (Molecular Probes, Carlsbad, CA) and enhanced by using an antibody solution containing 0.5 mg/mL of biotinylated anti-streptavidin (Vector Laboratories, Burlingame, CA). An Affymetrix Gene Chip Scanner 3000 was used to scan the probe arrays. Gene expression intensities were calculated using Affymetrix AGCC software. Downstream analysis was conducted in R/Bioconductor.

The annotation package for the Clariom_S chips was generated with *pdInfoBuilder* (https://www.bioconductor.org/packages/release/bioc/html/pdInfoBuilder.html) using the platform files provided by Affymetrix. The CEL files were then loaded into R, RMA normalized with the *oligo* package, and filtered to only retain probes annotated as "main" (Carvalho and Irizarry, 2010). Differential expression testing was performed using *limma* (Ritchie et al. 2015) and the resulting p.values were corrected with the Benjamini-Hochberg method.

GO enrichment analyses were performed using the topGO package (https://bioconductor.org/packages/release/bioc/html/topGO.html) with the *classic* algorithm and *Fisher* statistic. Microarray heatmaps were generated with the *heatmap.2* function of the *gplots* package with the default clustering methods. The microarray raw data were deposited in ArrayExpress with the accession numbers E-MTAB-5579 and E-MTAB-5586.

For qRT-PCR analysis, equal amounts of RNA were reversed-transcribed using the High Capacity cDNA Reverse Transcription Kit (Applied Biosystems) according to the manufacturer's instructions. cDNA was then quantified with the NanoDrop 2000c instrument (Thermo Scientific) and qRT-PCR was performed with the TaqMan® Universal PCR Master Mix (Applied Biosystems) and TaqMan® Gene Expression Assays for: *Il12b* (Mm01288989_m1, Life Technologies), *Il15* (Mm00434210_m1, Life Technologies), *Il15ra* (Mm04336046_m1, Life Technologies), *Cd69* (Mm01183378_m1, Life Technologies), *Nos2* (Mm00440502_m1, Life Technologies), *Tnf* (Mm00443258_m1, Life Technologies), *Il1b* (Mm00434228_m1, Life Technologies), *Bst1* (Mm00477672_m1, Life Technologies), *Ust* (Mm00616790_m1, Life Technologies) *Arg1* (Mm00475988_m1, Life Technologies), *Mrc1* (Mm00485148_m1, Life Technologies), *Sucnr1* (Mm00519024_m1, Life Technologies), *SUCNR1* (Hs00908230_m1, Life Technologies), *Ptgs2* (Mm00478374_m1, Life Technologies), and *Actb*/18S (Life Technologies) were used as internal calibrators. All samples were tested in triplicate on a 7500 Fast Real-Time PCR System (Applied Biosystems) and analysed with the 2-ΔΔCT method.

Metabolite extraction and LC-MS analysis

Ex vivo CSF/plasma samples (stored at -80°C) were thawed on ice for metabolites extraction. Samples were diluted in cold methanol (1:10) and put in agitation for 15 min at 4°C (800 rpm). After a centrifugation (20,000 g for 10 min), the supernatants were transferred to a new pre-chilled Eppendorf tube. Samples were concentrated using a SpeedVac (ThermoScientific Savant DNA 120) for 15 min and the pellet was dissolved in cold acetonitrile/water (1:1) using 16X of the initial sample volume. Samples were transferred to pre-chilled autosampler vials (Thermo Fisher) and stored at -80°C for subsequent LC-MS analysis.

In vitro samples were collected from Mφ (*INTRA_Metab*) and cell culture media (*EXTRA_Metab*). *INTRA_Metab* were collected from Mφ at 1-2-4-6-8-12-25 hrs upon LPS stimulation and at 24 hrs after the start of co-cultures (for co-culture experiments). For *INTRA_Metab* extraction, Mφ (originally re-seeded as $1x10^5$ cells/well in a 12 well plate) were washed with PBS and kept on ice throughout the procedure. 200 μl of Metabolite Extraction Buffer (MEB) (50% Methanol, 30% Acetonitrile, 20% water, with 100 ng/mL HEPES) was added to each well, and after scraping, extracts from each single well were collected separately. Samples were kept in agitation at 4°C (800 rpm) for 15 min, and then spun at 13,000 g for 15 min at 4°C. 100 μl of the supernatant was transferred to a pre-chilled autosampler vial and stored at -80°C for subsequent LC-MS analysis. *EXTRA_Metab* were collected from Mφ media at 25 hrs from LPS stimulation and at 24 hrs after the start of co-cultures (for co-culture experiments). For *EXTRA_Metab* extraction, media were collected from Mφ, spun at 1,000 g for 5 min, and 50 μl of the supernatant transferred to a pre-chilled Eppendorf containing 750 μl of MEB. Samples were kept in agitation at 4°C (800 rpm) for 15 min, and then spun at 1,000 g for 10 min at 4°C. 600 μl of the supernatant was transferred to a pre-chilled autosampler vial and stored at -80°C for subsequent LC-MS analysis.

LC-MS analysis was performed on a QExactive Orbitrap mass spectrometer coupled to a Dionex U3000 UHPLC system (Thermo). The liquid chromatography system was fitted with a Sequant ZIC-HILIC column (150 mm x 2.1 mm, 5 μm) and guard column (20 mm × 2.1 mm, 5 μm) from HiChrom, Reading, UK. The mobile phase was composed of 0.1% formic acid (v/v) in water (solvent A), and 0.1% formic acid (v/v) in acetonitrile (solvent B). The flow rate was set at 300 μL/min with the following gradient: 0 min 80% B, 5 min 30% B, 15 min 10% B, 20 min 10% B, 21 min 80% B, 30 min 80% B. The mass spectrometer was operated in full MS and polarity switching mode. Samples were randomised in order to avoid bias due to machine drift.

The acquired spectra were analysed using XCalibur Qual Browser and XCalibur Quan Browser software (Thermo Scientific) by referencing to an internal library of compounds.

Statistical analysis

Statistical analyses of all data were performed with GraphPad Prism (version 5.00 for Mac, GraphPad Software) unless otherwise stated. Differences among groups were analysed using one-way ANOVA analysis, followed by Bonferroni post-test, unless otherwise stated. Statistical analysis of EAE score was performed using a two-way ANOVA analysis, followed by Tukey post-test. Statistical analysis of DigiGait data was performed with SPSS (version 21 for mac, IBM Software) and outcomes were analysed using a multivariate general linear model. All values are given in the text as mean ± SEM and a p value < 0.05 was accepted as significant in all analyses, unless otherwise stated.

Data availability

The microarray data have been deposited in ArrayExpress with the accession numbers E-MTAB-5579 and E-MTAB-5586 (see also Data S2 and S4).

KEY RESOURCES TABLE

REAGENT or RESOURCE	SOURCE	IDENTIFIER
Antibodies		
AffiniPure Fab Fragment Goat Anti-Mouse IgG (H+L)	Jackson	115-007-003
Chicken anti-GFP (polyclonal)	abcam	ab13870
Chicken anti-Nestin (polyclonal)	abcam	ab134017
Donkey anti-goat AF488 conjugated secondary	abcam	AB150129
Donkey anti-goat Biotin conjugated secondary	adb serotech	642008
Goat anti mouse-HRP conjugated secondary	Thermo Scientific	31430
Goat anti-CD20 (polyclonal)	Santa Cruz	sc-7735
Goat anti-chicken AF488 conjugated secondary	Invitrogen	A11039
goat anti-chicken AF555 conjugated secondary	Invitrogen	A21237
Goat anti-chicken AF647 conjugated secondary	Lifetech	A21449
Goat anti-cicken IgG biotin conjugated secondary	vector laboratories	BA-9010
Goat anti-il1β (polyclonal)	R&D systems	AF-401-NA
Goat anti-mouse AF488 conjugated secondary	Invitrogen	A11001
Goat anti-mouse AF546 conjugated secondary	Invitrogen	A21045
Goat anti-mouse AF647 conjugated secondary	Invitrogen	A21235
Goat anti-rabbit AF488 conjugated secondary	Invitrogen	A11008
Goat anti-rabbit AF546 conjugated secondary	Invitrogen	A11010
Goat anti-rabbit AF647 conjugated secondary	Invitrogen	A21244
Goat anti-rabbit HRP conjugated secondary	Thermo Scientific	31460
Goat anti-Rat AF405 conjugated secondary	abcam	ab175671
Goat anti-Rat AF488 conjugated secondary	Invitrogen	A11006
Goat anti-Rat AF546 conjugated secondary	Invitrogen	A11081
Mouse anti-CD3 (clone: PS1)	abcam	ab699
Mouse anti-GFAP (clone: 52/GFAP)	BD Biosciences	610566
Mouse anti-NeuN (clone: A60)	Millipore	MAB377
Mouse anti-O4 (clone: O4)	R&D systems	MAB1326
Mouse anti-β-actin (clone: AC-15)	Sigma Aldrich	A1978
Mouse anti-β-tubulin (clone: TUB 2.1)	Sigma Aldrich	T4026
Rabbit anti-MRC1 (polyclonal)	abcam	ab64693
Rabbit anti-GFAP (polyclonal)	DAKO	Z0334
Rabbit anti-Sucnr1 (polyclonal)	Novus Biologicals	NBP1-00861
Rabbit anti-iNOS (polyclonal)	abcam	ab3523
Rabbit anti-Ki67 (polyclonal)	abcam	ab15580
Rabbit anti-Olig2 (polyclonal)	Chemicon	AB9610
Rabbit anti-p38 MAPK (polyclonal)	Cell Signaling	9212
Rabbit anti-Phospho-p38 MAPK (polyclonal)	Cell Signaling	9211
Rabbit anti-Pkm2 (polyclonal)	Cell Signaling	3198
Rabbit anti-SLC13A3 (polyclonal)	Aviva Systems biology	ARP41438_T100
Rabbit anti-SLC13A5 (polyclonal)	ThermoFisher	PA5-24675
Rabbit anti-SOX2 (polyclonal)	Abcam	ab15830
Rabbit anti-vWF (polyclonal)	Abcam	ab6994
Rabbit HIF1α (polyclonal)	Novus Biologicals	NB100-134

Rat anti-CD45 (clone: 30-F11)	BD Biosciences	550539
Rat anti-F4/80 (clone: Cl:A3-1)	Bio-Rad	MCA497R
Rat anti-MBP (aa82-87) (clone: 12)	Bio-Rad	MCA409S
Biological Samples		
Chemicals, Peptides, and Recombinant Proteins		
[^{14}C]-succinic acid	American Radiolabelled Chemicals	ARC 3593-50µCi
4'6-diamidino-2-phenylindole (DAPI)	Invitrogen	D1306
4C	Advinus Therapeutics	N/A
Accumax	Affymetrix	00-4666
B27 w/vitamin A (50x)	Gibco	17504-044
Basal Fibroblast Growth Factor	Peprotech	100-18B-1000
Basement Membrane Matrix Growth Factor Reduced	Corning	354230
CHIR 99021	Axon MedChem	1386
Dialyzed Foetal Bovine Serum (dFBS)	Gibco	26400036
Dimethyl malonate	Sigma Aldrich	136441
DMEM high glucose	Gibco	41966029
DMEM/F12	Gibco	11320-033
Fluo-4AM	Life Technologies	F-14217
Foetal bovine serum (FBS)	Gibco	10500-064
freund adiuvant incomplete	Sigma Aldrich	f5506
Glutamax	Gibco	35050-038
Heparin	Sigma Aldrich	H3393
hLIF	Gibco	PHC9484
Insulin from bovine pancreas	Sigma Aldrich	I1882
Laemmli	Sigma	S3401-L
Laminin	Roche	11243217001
Lipopolysaccharide (LPS)	Enzo life sciences	ALX-581-013-L002
Basement Membrane Matrix Growth Factor Reduced	Cornig	354230
Mersalyl acid	Sigma Aldrich	M9784
Minimum Essential Medium Eagle	Sigma Aldrich	M7278
Mouse differentiation supplement	Stem cells Technologies	05703
Mycobacterium Tuberculosis H37Ra	Difco	231141
N2 supplement	ThermoFisher	17502-048
Neurobasal medium	Gibco	21103-049
NeuroCult proliferation supplements	Stem cells Technologies	05701
Normal goat serum	Invitrogen	10000C
Pen/strep	Invitrogen	151401
Pertussis Toxin from Bordetella pertussis	List Biological Laboratories	181
r(MOG 35-55)	Espikem	EPK 1
Recombinant human EGF	Peprotech	AF-100-15
Recombinant Human FEF-basic	Peprotech	100-18B
Recombinant Human Leukemia Inhibitory Factor	Gibco	PHC9484

Recombinant murine M-CSF	Miltenyi Biotec	130-101-706
Recombinant SDH subunit A	Cloud-clone corp	RPJ784Mu01
RNAlater	QIAGEN	76104
ROCK inhibitor Y27632	Calbiochem	688000
SB 431542	Invivogen	inh-sb43
SC-58125	Sigma Aldrich	PZ0139
Sodium succinate dibasic hexa-hydrate	Sigma Aldrich	S2378
Trypsin-EDTA (0.05%), phenol red	Gibco	25300-054
Ultima Gold liquid scintillation cocktail	PerkinElmer	6013329
Critical Commercial Assays		
High Capacity cDNA Reverse Transcription kit	applied biosystems	4368813
LDH-Cytotoxicity Assay kit	abcam	ab102526
NeuroCult NS-A proliferation kit (Human)	Stemcell	5750
Nitrite/Nitrate Assay Kit	Sigma-Aldrich	23479-1KT-F
Prostaglandin E2 ELISA Kit	Caymanchem	514010
RNeasy Micro Kit	QIAGEN	74006
RNeasy Midi kit	QIAGEN	73442
Succinate Dehydrogenase Activity Colorimetric Assay Kit	BioVision	K660-100
TaqMan Fast Universal PCR Master	applied biosystems	4352042
Deposited Data		
The microarray data have been deposited in ArrayExpress	Affymetrix	Accession numbers E-MTAB-5579 and E-MTAB-5586
Experimental Models: Cell Lines		
Human cell line: human BJ fibroblasts	Edenhofer lab	N/A
Human cell line: human fetal NSCs	Vescovi lab	N/A
Human cell line: human iNSCs	Edenhofer lab	N/A
Mouse cell line: 929	Pluchino lab	N/A
Mouse cell line: BMDM	Pluchino lab	N/A
Mouse cell line: BV2	Spillantini lab	N/A
Mouse cell line: MFs (mouse fibroblasts)	Pluchino lab	N/A
Mouse cell line: iNSCs	Edenhofer lab	N/A
Mouse cell line: NSCs	This paper	N/A
Mouse cell line: Sucnr1$^{-/-}$ NSCs	This paper	N/A
Experimental Models: Organisms/Strains		
C57BL/6 mice	Charles River	c57bl6
Sucnr1$^{-/-}$ mice	NOVARTIS AUSTRIA	N/A
Recombinant DNA		
pRRLsinPPT-hCMV		
pCT-f-GFP	System Bioscieces	CYTO120-PA-1
Sequence-Based Reagents		
Taqman Gene Expression assay: *18S* (4318839)	Life Technologies	# 4331182
Taqman Gene Expression assay: *ACTB*	Life Technologies	# 4331182
Taqman Gene Expression assay: *Arg1* (Mm00475988_m1)	Life Technologies	# 4331182
Taqman Gene Expression assay: *Bst1* (Mm00477672_m1)	Life Technologies	# 4331182

Taqman Gene Expression assay: *Cd69* (Mm01183378_m1)	Life Technologies	# 4331182
Taqman Gene Expression assay: *SUCNR1* (Hs00908230_m1)	Life Technologies	# 4331182
Taqman Gene Expression assay: *Sucnr1* (Mm00519024_m1)	Life Technologies	# 4331182
Taqman Gene Expression assay: *Il1b* (Mm00434228_m1)	Life Technologies	# 4331182
Taqman Gene Expression assay: *Il12b* (Mm01288989_m1)	Life Technologies	# 4331182
Taqman Gene Expression assay: *Il15* (Mm00434210_m1)	Life Technologies	# 4331182
Taqman Gene Expression assay: *Il15ra* (Mm04336046_m1)	Life Technologies	# 4331182
Taqman Gene Expression assay: *Mrc1* (Mm01329362_m1)	Life Technologies	# 4331182
Taqman Gene Expression assay: *Nos2* (Mm00440502_m1)	Life Technologies	# 4331182
Taqman Gene Expression assay: *Ptgs2* (Mm00478374_m1)	Life Technologies	# 4331182
Taqman Gene Expression assay: *Tnf* (Mm00443258_m1)	Life Technologies	# 4331182
Taqman Gene Expression assay: *Ust* (Mm00616790_m1)	Life Technologies	# 4331182
Software and Algorithms		
R/Bioconductor	(Huber et al., 2015)	
Bioconductor pdInfoBuilder package	https://www.bioconductor.org/packages/release/bioc/html/pdInfoBuilder.html	
Bioconductor oligo package	(Carvalho and Irizarry, 2010)	
Bioconductor limma package	(Ritchie et al., 2015)	
Bioconductor TopGO package	https://bioconductor.org/packages/release/bioc/html/topGO.html	
Bioconductor Gage package	(Luo et al., 2009)	
GraphPad Prism version 6.00 for Mac, GraphPad Software, La Jolla California USA	https://www.graphpad.com	
Other		
Microvettes	Sarstedt	CB300Z

Methods' References

Carvalho, B.S., and Irizarry, R.A. (2010). A framework for oligonucleotide microarray preprocessing. Bioinformatics 26, 2363-2367.

Grupp, C., and Muller, G.A. (1999). Renal fibroblast culture. Exp Nephrol 7, 377-385.

Liu, L., and Duff, K. (2008). A technique for serial collection of cerebrospinal fluid from the cisterna magna in mouse. Journal of visualized experiments : JoVE.

Masters, S.L., Dunne, A., Subramanian, S.L., Hull, R.L., Tannahill, G.M., Sharp, F.A., Becker, C., Franchi, L., Yoshihara, E., Chen, Z., et al. (2010). Activation of the NLRP3 inflammasome by islet amyloid polypeptide provides a mechanism for enhanced IL-1beta in type 2 diabetes. Nat Immunol 11, 897-904.

Meyer, S., Worsdorfer, P., Gunther, K., Thier, M., and Edenhofer, F. (2015). Derivation of Adult Human Fibroblasts and their Direct Conversion into Expandable Neural Progenitor Cells. Journal of visualized experiments : JoVE, e52831.

Pluchino, S., Quattrini, A., Brambilla, E., Gritti, A., Salani, G., Dina, G., Galli, R., Del Carro, U., Amadio, S., Bergami, A., et al. (2003). Injection of adult neurospheres induces recovery in a chronic model of multiple sclerosis. Nature 422, 688-694.

Ritchie, M.E., Phipson, B., Wu, D., Hu, Y., Law, C.W., Shi, W., and Smyth, G.K. (2015). limma powers differential expression analyses for RNA-sequencing and microarray studies. Nucleic Acids Res 43, e47.

Rubic, T., Lametschwandtner, G., Jost, S., Hinteregger, S., Kund, J., Carballido-Perrig, N., Schwarzler, C., Junt, T., Voshol, H., Meingassner, J.G., et al. (2008). Triggering the succinate receptor GPR91 on dendritic cells enhances immunity. Nat Immunol 9, 1261-1269.

Thier, M., Worsdorfer, P., Lakes, Y.B., Gorris, R., Herms, S., Opitz, T., Seiferling, D., Quandel, T., Hoffmann, P., Nothen, M.M., et al. (2012). Direct conversion of fibroblasts into stably expandable neural stem cells. Cell stem cell 10, 473-479.

Vescovi, A.L., and Snyder, E.Y. (1999). Establishment and properties of neural stem cell clones: plasticity in vitro and in vivo. Brain Pathol 9, 569-598.

Directly induced neural stem cells remyelinate chronic demyelinated mouse brain

Nunzio Vicario[1,2,‡], Luca Peruzzotti-Jametti[1,‡], Alice Braga[1], Joshua D. Bernstock[1], Sandra Rizzi[3], Giulio Volpe[1], Beatrice Balzarotti[1], Rosalba Parenti[2], Chao Zhao[1], Frank Edenhofer[3], Robin J.M. Franklin[1], Stefano Pluchino[1]*

[1]Dept of Clinical Neurosciences - Division of Stem Cell Neurobiology, Wellcome Trust-Medical Research Council Stem Cell Institute and NIHR Biomedical Research Centre, University of Cambridge, UK;
[2]Dept of Biomedical and Biotechnological Sciences, Physiology Section, University of Catania, Italy;
[3]Institut für Molekularbiologie – Universität Innsbruck, Austria;
‡Equal contribution
*Correspondence: Stefano Pluchino, spp24@cam.ac.uk

Manuscript in preparation

Abstract

Remyelination is a spontaneous reparative process that occurs following demyelination of the peripheral and central nervous system (CNS). However, in chronic demyelinating diseases of the CNS such as progressive multiple sclerosis (PMS), this endogenous regenerative process is mostly inefficient or impaired.

Neural Stem Cell (NSC) transplantation has emerged as a promising therapeutic approach for several CNS disorders. We have shown that NSCs can foster endogenous remyelination by replacing damaged tissue and providing local trophic support to the injured CNS. However, major hurdles still limit the use of conventional stem cell therapies in clinical settings.

The recently described directly induced Neural Stem Cells (iNSCs) have partially overcome these limitations by providing a source of autologous tissue-specific stem cells, which has no histocompatibility barriers and can be easily obtained from accessible somatic cells.

Here we investigated the potential of mouse iNSCs to promote remyelination after transplantation in a mouse model of focal spinal cord demyelination. We found that a single injection of mouse iNSCs in the lesioned spinal cord of wild type mice led to a successful integration of the graft into the host spinal cord. Transplanted iNSCs were able to promote remyelination by increasing endogenous myelinating cells and directly differentiating into mature oligodendrocytes. When injected in Olig1$^{-/-}$ mice, which lack endogenous remyelinating response after lesion, we found that the direct differentiation of the iNSCs grafts into mature oligodendrocytes was able to re-establish the spontaneous remyelination of the spinal cord.

Our results suggest that iNSCs can be used to efficiently replace and/or support endogenous remyelinating responses in the demyelinated CNS. These data further support the use of directly reprogrammed iNSCs as an effective therapeutic tool to enhance remyelination in chronic demyelinating CNS diseases.

Introduction

Multiple sclerosis (MS) is an autoimmune demyelinating disorder of the central nervous system (CNS) and the most common cause of neurological disability in young adults (1). Demyelination in MS patients is the result of a complex interaction between the immune system and myelin forming cells (2). In the early stages of disease, when lymphocytes mediate most of the damage, the endogenous pool of oligodendrocyte precursors cells (OPCs) is normally able to spontaneously remyelinate lesions by migrating into demyelinated area and differentiating into mature oligodendrocytes (OLs). However, in the later and progressive stage of disease, when inflammation is mostly driven by activated mononuclear phagocytes (MPs), this endogenous process is mostly insufficient and can hardly sustain a complete remyelination (3, 4).

Recent findings in stem cell neurobiology have raised great expectations for transplantation approaches to replace or enhance the endogenous regenerative potential of the CNS (5). We have shown that Neural Stem Cells (NSCs) injected in mouse and non-human primate models of MS can efficiently ameliorate clinical deficits and foster recovery (6-8). In particular, NSCs can interact with the multitude of pathological processes of the inflamed CNS by exerting beneficial immunomodulatory and neurotrophic effects.

Despite these compelling evidences, the prospective clinical translation of NSCs transplantation for progressive MS remains inconsistent due to major ethical and safety issues. Fibroblasts-derived directly induced neural stem cells (iNSCs) represent an ideal candidate for tissue-specific stem cell-based approaches due to the lack of histocompatibility barriers and their ease of reprogramming (9). We have shown that iNSCs display superimposable *in vitro* properties as to somatic subventricular zone derived NSCs (10). Most importantly, recent data from our group show that iNSCs display remarkable immunomodulatory activities on MPs, both *in vivo* and *in vitro*, which could be key in treating progressive MS patients (11).

Nevertheless, major key points still need to be addressed for the successful clinical application of iNSCs, including their effects on endogenous remyelinating responses and their guaranteed/controllable differentiation profile in OLs *in vivo* (12, 13).

Herein we have decided to evaluate the potential of iNSCs transplantation in enhancing remyelination in a murine model of focal demyelination (9, 10, 14). We found that iNSCs injected in lysophosphatidylcholine (LPC) lesioned spinal cords of wild type mice induced a significant enhancement of endogenous OPCs differentiation in OLs. Of note, part of the

transplanted cells could also directly differentiate into mature OLs *in vivo*. To avoid the confounding factor of the endogenous regenerative response after damage, we next decided to inject iNSCs in LPC lesioned Olig1$^{-/-}$ mice. These mice develop normally, but lack a remyelinating response after CNS demyelination (15, 16). Interestingly, we found that iNSCs could efficiently generate mature oligodendrocytes and completely remyelinate the demyelinated spinal cord of Olig1$^{-/-}$ mice.

These data show that iNSCs are therapeutically and functionally equivalent with somatic NSCs and that, upon focal transplantation in chronically demyelinated lesions, they are able to successfully integrate and differentiate into mature myelinating OLs. Our findings are adding a novel piece of evidence supporting the use of directly induced autologous stem cells-based therapies for chronic demyelinating disorders.

Results

Transplanted iNSCs integrate into the demyelinated CNS of adult wild type mice*.*

To advance the therapeutic translation of iNSCs for acquired demyelinating conditions of the CNS, we decided to perform a transplantation experiment in adult wild type mice previously subjected to a LPC injection in the ventro-lateral white matter of the spinal cord (Figure 1A).

Mice were injected intralesionally with mouse fGFP^{+} iNSCs (iNSCs-treated) at 3 days post-lesion (dpl) and pathological outcomes compared to mice receiving equal numbers of fGFP^{+} somatic NSCs (NSCs-treated) or mice treated with the vehicle solution (PBS-treated).

We found that the lesion volume in PBS-treated mice was not statistically different from iNSCs-treated and NSCs-treated mice at 21 dpl (0.055±0.009 mm^3 PBS *vs.* 0.035±0.017 mm^3 iNSCs *vs.* 0.039±0.017 mm^3 NSCs) (Figure 1B-C). Both cellular types successfully integrated in the lesioned spinal cord with 24.3±9,5% and 34.2±5.4% of transplanted cells surviving in iNSCs-treated and in NSCs-treated mice respectively (ns) (Figure 1D-E). The total number of iNSCs and NSCs found intralesionally in treated mice was also similar (19,599±6,485% iNSCs *vs.* 27,509±5,487% NSCs, ns) with both cells localising preferentially to the site of injection following a Gaussian distribution (Figure 1F).

These data suggest that the local transplantation of mouse iNSCs into the demyelinated spinal cord is feasible and leads to an overall integration into the host CNS that is undistinguishable from that of somatic NSCs.

iNSCs differentiate into both astrocytes and oligodendrocytes when transplanted into the LPC-lesioned spinal cords of wild type mice*.*

To further evaluate the integration of stem cell grafts into the demyelinated CNS, we analysed their phenotype at 21 dpl. We found that the majority of retrieved cells expressed the stem cells marker Sox2 (71.4±4.8% iNSCs *vs.* 66.5±4.5% NSCs, n.s.), while only a minority of cells were found to be actively replicating using a Ki67 staining (1.3±0.7% iNSCs *vs.* 0.5±0.3% NSCs, n.s.) (Figure 2A-C).

When we analysed the expression of neural lineage markers, we found that 18.6±2.5% of iNSCs and 23.3±4.1% of NSCs expressed the astroglial protein GFAP (n.s.) (Figure 2D), while no cell was found to express the neuronal marker NeuN (data not shown). Interestingly, up to 0.7±0.1% of iNSCs and 1.1±0.1% of NSCs were found to be NG2 and OLIG2 double-positive, indicative of oligodendrocytes precursors cells (OPCs) state (n.s.) (Figure 2E), while 8.5±1.3% of iNSCs and 11.5±1.8% of NSCs were found to differentiate into mature OLIG2 and CC1 double-positive oligodendrocytes (n.s.) (Figure 2F).

Overall, iNSCs and NSCs displayed a similar proliferation index within LPC lesions, and could efficiently contribute to the replacement of lost tissue by differentiating into astrocytes, OPCs and mature oligodendrocytes.

iNSCs transplanted in LPC-lesioned wild type mice *promote the differentiation of endogenous OPCs in oligodendrocytes.*

We next analysed the endogenous remyelinating response after transplant. Previous literature has shown that remyelination after LPC lesion of the spinal cord is multifactorial and depends on the differentiation of OPCs into mature oligodendrocytes and/or Schwann cells (SCs) and on the migration of SCs from the adjacent dorsal root ganglia (DRGs) (17).

We first decided to investigate the differentiation of OPCs into mature oligodendrocytes via immunofluorescence staining of intra-lesional $OLIG2^{+}CC1^{+}$ cells. We found that iNSCs-treated and NSCs-treated mice displayed an increase in endogenous $fGFP^{-}$ mature oligodendrocytes (321.4±29.6 cells/mm^2, $p<0.05$ and 244.7±7.3 cells/mm^2, $p<0.05$ respectively) compared to control LPC-lesioned PBS-treated mice (160.8±17.8 cells/mm^2) (Figure 3A). This enhancement of the endogenous OPCs differentiation was concurrent

with the differentiation of transplanted stem cells into fGFP$^+$OLIG2$^+$CC1$^+$ mature oligodendrocytes (116.4±17.4 iNSCs/mm^2 *vs.* 137.1±52.5 NSCs/mm^2, n.s.).

We next investigated whether stem cell grafts influenced the SCs contribution to remyelination. We found that iNSCs-treated and NSCs-treated mice had a significant reduction of the SC marker Periaxin intralesional area (6.8±2.0%, $p<0.05$ iNSCs and 7.1±2.3%, $p<0.05$ NSCs) compared to PBS-treated mice (16.1±2.0%) (Figure 3B). Most importantly, none of the transplanted cells were found to differentiate into Periaxin$^+$ SCs.

Finally, when we compared the total remyelination of LPC-lesioned mice, we found that iNSCs-treated and NSCs-treated mice displayed a significant increase of the expression of intra-lesional *Plp*-mRNA$^+$ cells (883.4±56.3 cells/mm^2 iNSCs, $p<0.05$ and 976.5±87.3 cells/mm^2 NSCs, $p<0.05$), compared to PBS-treated mice (557.6±44.5 cells/mm^2).

Altogether our data suggest that iNSCs can increase remyelination by (i) directly differentiating into mature oligodendrocytes, (ii) favouring the endogenous differentiation of OPCs into oligodendrocytes and (iii) reducing the contribute of SCs.

Transplanted iNSCs survive and distribute into demyelinated lesions of Olig1$^{-/-}$ mice.

So far, iNSCs have shown superimposable effects compared with NSCs in wild type mice, exerting both direct and indirect remyelinating effects. As such, we next focused our attention on the effects of iNSCs-grafts in mice that do not express the *Olig1* gene (Figure 4A-C). These Olig1$^{-/-}$ mice are viable and fertile, showing only a subtle delay in oligodendrocyte maturation but with an overall healthy and fully myelinated CNS (Figure 4D). However, when this transgenic mouse is subjected to focal demyelination, OPCs are recruited into the lesion but they are not able to differentiate into mature myelinating oligodendrocytes (18).

We performed an LPC-mediated lesion into the ventro-lateral white matter of Olig1$^{-/-}$ mice (Figure 4E) and focally injected 1x10^5 fGFP$^+$ iNSCs as before. We found that iNSCs-treated and PBS-treated mice had comparable lesion volumes at 21 dpl (0.091±0.019 and 0.080±0.022 mm^3 respectively) (Figure 4F), with 15.0±5.7% of total iNSCs surviving (13,668±5,420 cells found intralesionally) (Figure 4G). Cells were found close to the injection site showing a Gaussian distribution, confirming that iNSCs are capable to survive in a potentially inhospitable and chronic demyelinated environment (Figure 4H-I).

Transplanted iNSCs generate mature oligodendrocytes and remyelinate the demyelinated adult spinal cord of Olig1$^{-/-}$ mice.

To investigate whether transplanted iNSCs were capable to overcome the impaired remyelination of Olig1$^{-/-}$ mice, we analysed the LPC-lesions of PBS-treated and iNSCs-treated mice.

We found that in Olig1$^{-/-}$ mice progenitor cells were recruited into LPC-induced lesions (28.12±13.72 OLIG2^{+} cells/mm^{2} in PBS-treated mice) but only a minority of OPCs differentiate into mature oligodendrocytes (CC1^{+}OLIG2^{+} cells) intralesionally at 21 dpl (2.79±2.28 cells/mm^{2}) (Figure 5A). Instead, in iNSCs-treated mice, we found that 70.2±14.3 cells/mm^{2} were fGFP^{+}CC1^{+}OLIG2^{+}, demonstrating a remarkable oligodendrogenic potential of iNSCs in chronic demyelinated CNS (Figure 5A-B).

To further confirm that iNSCs-derived mature oligodendrocytes could remyelinate the lesion in Olig1$^{-/-}$ mice, we moved to analyse semi-thin sections of LPC-induced lesions. As expected, PBS-treated Olig1$^{-/-}$ showed demyelination at 21 dpl with very few axons that appeared slightly remyelinated, lacking the intense remyelinating response that characterizes LPC lesions of wild type mice (Figure 5C). Instead, iNSCs-treated Olig1$^{-/-}$ mice showed a remarkable remyelination of LPC lesions, which suggests that differentiation of grafted iNSCs into OLs was able to produce structurally conserved myelin (Figure 5C).

Discussion

Stem cells transplantation represents one of the most promising approaches for the treatment of multifactorial neurological disorders (19).

Herein, we investigated the remyelinating potential of autologous, accessible and stably expandable iNSCs (10), and compared it with that of somatic subventricular zone derived NSCs. We found that transplanted iNSCs were able to survive and integrate into the demyelinated CNS, distributing across lesioned areas. Transplanted iNSCs displayed stable survival rates with a good proportion of cells differentiating into astroglial and oligodendroglial cells. This propensity towards *in vivo* differentiation is in apparent contrast to previous transplantation studies in the experimental autoimmune encephalomyelitis (EAE) model of MS, in which the great majority of the cells remained undifferentiated in perivascular atypical niches. These differences can be accounted on the route of cell administration (intraparenchymal *vs.* intracerebroventricular) and the local microenvironment. As a matter of fact, while in the EAE model the overt inflammatory reaction might limit the differentiation of transplanted cells, in LPC demyelinating lesions the microenvironment might prompt transplanted cells to differentiate toward a specific reparative phenotype based on the tissue necessities.

The differentiation of transplanted iNSCs towards the astroglial lineage could play an important role in the suppression of SCs migration or the differentiation of progenitor cells into myelinating SCs. Particularly, it has been demonstrated that intralesional astrocytes exert a key role in modulating the differentiation of OPCs into mature OLs instead of SCs-like lineage (17). While members of the bone morphogenetic protein (BMP) family increase the differentiation of precursor cells into SCs (20, 21), astrocytes are able to secrete Noggin, an inhibitor of BMP signalling, to inhibit the differentiation of progenitor cells into myelinating SCs (22). Similarly, we observed that grafted iNSCs differentiating into astrocytes reduced the remyelination mediated by SCs. These evidences suggest that grafted cells augment endogenous remyelination shifting the balance toward an oligodendrocyte-mediated remyelination.

In order to fully grasp the direct remyelinating potential of iNSCs, we have transplanted cells in a transgenic mouse model of chronic demyelination of the CNS, which allowed us to study the net contribution of grafted cells to the whole regenerative process. Interestingly, we found that the number of exogenous cells differentiating into mature OLs was comparable to the number of cells that remyelinate LPC lesions in wild type mice. This suggests that iNSCs grafts are able to generate mature OLs to actively remyelinate

the CNS of mice in which endogenous remyelination is impaired, filling the gap between self-repairing and chronic demyelinating lesions.

Overall these effects highlight the plasticity of iNSCs *in vivo*, which are able to differentiate toward specific lineages by adapting their intrinsic potential, but also to act as biological tools capable to execute complex behaviours in response to environmental signals and endogenous cells. Our findings, together with the increasing body of evidences supporting the bystander neuroprotective and immunomodulatory effects of iNSCs (23) (7, 11, 24) (9), are paving the way for the use of iNSCs-based approaches in regenerative medicine and for their future clinical applications in chronic demyelinating disorders.

Methods

Animal models and animal care

Wild type C57BL/6 mice and Olig1$^{-/-}$ used in this study were purchased from Jackson laboratory and all procedures were performed according to the guidelines of the Animal Ethical Committee of Cambridge University. Animal work was covered by the PPL 70/7715 (to Professor Robin J.M. Franklin) in line with the Association of Medical Research Charities (AMRC) recommendations. The disruption of *Olig1* function in Olig1$^{-/-}$ were generated by deleting the majority of the *Olig1* coding region, including the bHLH domain, and incorporating at the *Olig1* locus knockin of bacteriophage P1 *cre* recombinase (15). All efforts were made to use the fewest number of animals and to minimize suffering of mice utilized.

Cell lines

All cell lines were cultured at 37 °C in a controlled humidified atmosphere of 5% CO_2.

Mouse iNSCs were obtained from direct reprogramming of Oct4-GiP Mouse Embryonic Fibroblasts (MEFs) from C57BL/6 mice. Briefly, Oct4-GiP MEFs were infected with retroviruses encoding for Sox2, Klf4, and c-Myc, as previously described (10). iNSCs colonies were picked 19 days post infection and cultured as either small cellular aggregates (i.e. neurospheres) or adherent monolayers in iNSCs medium (DMEM/F12 (Life Technologies), 1% pen/strep (Invitrogen), 1X N2 (ThermoFisher), 10 ng/ml purified human recombinant (EGF, Peprotech), 10 ng/ml human recombinant basic fibroblast growth factor (bFGF, Peprotech)). When neurospheres reached a diameter of 150-200 µm, cells were collected and harvested in a 15 ml tube (Falcon) and centrifuged at 300 g for 8 min. The supernatant was removed, and the pellet was dissociated by enzymatic digestion with Accumax^{TM} (Ebioscience) at 37 °C for 10 min. Then fresh iNSCs medium was added, and cells were centrifuged at 300 g for 8 min.

The number of viable cells was determined by trypan blue exclusion and viable cells were re-seeded at clonal density 9,700 cells/cm^2. New iNSCs medium was added to each flask every other day. Mycoplasma negative iNSCs at passage n≤ 25 were used in all experiments.

Somatic NSCs were obtained from the subventricular zone (SVZ) of 7-12 week old (18-20 g) C57BL/6 mice (Charles River, UK), as previously described (25). Briefly, mice were humanely culled by cervical dislocation followed by decapitation, the parietal bones were cut cranially to caudally using micro-surgery scissors, and the brains removed. A brain slice matrix was used to obtain 3 mm thick brain coronal sections starting from 2 mm after the anterior pole of the brain. The SVZ of the lateral ventricles was isolated from coronal sections using iridectomy scissors. Tissues derived from at least 2 mice were pooled to generate cultures. Dissected tissues were transferred to a 15 ml tube with digestion medium (early balance salt solution (EBSS, Gibco), papain (1 mg/ml, Worthington), ethylenediaminetetraacetic acid (EDTA) (0.2 mg/ml, Sigma-Aldrich)

and L-cysteine (0.2 mg/ml, Sigma-Aldrich)) and incubated for 45 min at 37 °C on a rocking platform. At the end of the incubation, the tube was centrifuged at 200 g for 12 min, the supernatant was removed and the pellet was mechanically disaggregated with 2 ml of EBSS. The pellet was centrifuged again at 200 g for 12 min and then dissociated with a 200 µl pipette and seeded in complete growth medium (CGM, mouse NeuroCult™ basal medium (Stem Cell Technologies) plus 1x mouse NeuroCult™ proliferation supplements (Stem Cell Technologies) added with 2 µg/ml heparin (Sigma-Aldrich), 20 ng/ml EGF and 10 ng/ml bFGF). After approximately 4-7 days, a small percentage of the isolated cells begun to proliferate, giving rise to neurospheres. When neurospheres reached a diameter of 150-200 µm were harvested in a 15 ml tube and centrifuged at 100 g for 8 min. The supernatant was then removed and the pellet dissociated by enzymatic digestion with Accumax™ at 37 °C for 10 min. The number of viable cells was determined by trypan blue exclusion and viable cells were re-seeded at clonal density 8,000 cells/cm^2. Mycoplasma negative NSCs at passage n≤ 25 were used in all experiments.

Lentiviral fGFP tagging

Cells used for transplantation studies were transduced *in vitro* using a 3rd-generation lentiviral carrier (pRRLsinPPT-hCMV) coding for the enhanced farnesylated-green fluorescent protein (fGFP), which targets the fluorescent protein to the inner plasma membrane of transduced cells (26). The functional stability of these cells (in the absence or in the presence of the lentiviral transcript) has been confirmed with clonal and population studies (6). Briefly, neurospheres were harvested, dissociated to a single cells suspension and seeded at high density (1.5x10^6 in a T75 cm^2 flask (Sigma-Aldrich)) in 5 ml fresh medium. After 12 hrs, 3x10^6 T.U./ml of lentiviral vectors were added and 6 hrs later additional 5 ml of fresh medium were added. 72 hrs after viral transduction, cells were harvested and re-seeded at normal concentration. Trans-gene expression analysis and positive cells sorting were performed by using fluorescence-activated cell sorting (FACS) before transplantation and 98.7 ± 0.2 (mean % ± SEM) of cells were found to be fGFP-labelled.

Experimental focal demyelination

Demyelinating lesions were induced in the spinal cord (T12-T13) of 8/12-week-old C57BL/6 or Olig1$^{-/-}$ mice by stereotaxic injection of 1 µl of 1% LPC, using a Hamilton syringe. Treated mice received a single focal transplantation of 1x10^5 fGFP$^+$ iNSCs/NSCs 3 days post-lesion (dpl) and vehicle (PBS) was used as control. At 21 dpl mice were deeply anesthetized with an intraperitoneal (i.p.) injection of ketamine 10 mg/ml (Boehringer Ingelheim) and xylazine 1.17 mg/ml (Bayer) in sterile water and trans-cardially perfused with 1 ml EDTA 5 M in 500 ml saline 0.9% NaCl for 5 min, followed by a solution of 4% PFA in PBS for *ex vivo* tissue pathology or 4% glutaraldehyde in PBS containing $CaCl_2$ 0.4 mM for Transmission Electron Microscopy (TEM) analysis.

For conventional pathology spinal cords were cryo-protected in sucrose 30% in PBS and embedded in optimum cutting temperature (OCT) medium in liquid nitrogen and stored at -80 °C until use.

Ex vivo tissue pathology

The day of sacrifice, mice were deeply anesthetized with an i.p. injection of ketamine 10 mg/ml (Boehringer Ingelheim) and xylazine 1.17 mg/ml (Bayer) in sterile water and transcardially perfused with 1 ml EDTA 5 M in 500 ml saline 0.9% NaCl for 5 min, followed by a solution of 4% PFA in PBS for 5 min.

Spinal cords were isolated and post-fixed in 4% PFA in PBS at 4 °C overnight. Tissues were then washed in PBS and cryo-protected for at least 48-72 hrs in 30% sucrose in PBS at 4 °C. Spinal cords were then embedded in OCT medium, frozen with liquid nitrogen and cryo-sectioned (20 µm axial section thickness) using a cryostat (CM1850, Leica, Wetzlar, Germany) with a microtome blade (A35, Feather, Osaka, Japan). Sections were then stored at -80 °C until use.

For quantification of graft survival, sections were pre-treated with hydrogen peroxide 3% for 15 min, and then were incubated in the blocking solution (10% normal goat serum (NGS, Sigma-Aldrich), 0.1% Triton X100 in PBS) for 1 hr at room temperature. Primary antibody anti-GFP (1:250, Invitrogen) diluted in a solution of PBS, 1% NGS and 0.1% Triton X100, and incubated at 4 °C overnight. The following day, tissues were washed with PBS and incubated for 1 hr with the appropriate secondary biotinilated antibody (1:1,000, Sigma-Aldrich) diluted in a solution of PBS with 1% NGS, 0.1% Triton X100. Components "A" and "B" of Vectastain Elite ABC kit were mixed for 45 min and the reaction developed by means of 3,3'-Diaminobenzidine (DAB) as per manufacturer's instructions. The reaction was blocked dipping the section into distilled water and sections were counterstained with haematoxylin. The tissues were then dehydrated (with increasing alcohol solutions), washed in xylene (Merck, Darnstadt, Germany) and mounted with a synthetic mounting medium (EUKITT, Hatfield, PA, USA). The numbers of transplanted $fGFP^+$ cells were calculated on n≤ 10 equally spaced axial spinal cord sections. $fGFP^+$ cells were outlined using an Olympus BX53 microscope with motorized stage and Neurolucida software (11.07 64-bit, Microbrightfield) and descriptive 3D spinal cord reconstructions were obtained.

For quantification of demyelination, cryostat 20 µm thick spinal cord sections were stained for Luxol fast blue (LFB), as previously described (6). The LFB negative areas of n≤ 10 equally spaced axial spinal cord sections were outlined using an Olympus BX53 microscope with motorized stage and Neurolucida software (11.07 64-bit, Microbrightfield) and expressed as mm^3 volume of damaged tissue per spinal cord ± SEM.

For the quantification of stem cell differentiation, sections were rinsed with PBS, and then blocked for 1 hr at room temperature in blocking buffer (10% secondary antibody species serum and 0.1% Triton X100 in PBS). A Fab fragment affinity purified IgG anti-mouse was applied if anti-mouse

antibodies were used (1:10, Jackson ImmunoResearch). The following primary antibodies, diluted in blocking buffer, were used at 4 °C overnight in a humid chamber: anti-GFP (1:250, Invitrogen), anti-KI67 (1:250, Abcam), anti-SOX2 (1:500, Santa Cruz Biotechnology), anti-GFAP (1:500, Abcam), anti-NG2 (1:200, Millipore), anti-CC1 (1:500, Millipore), anti-NeuN (1:250, Chemicon), anti-OLIG2 (1:500, Millipore), periaxin (1:1,000; a gift from Professor Peter Brophy, University of Edinburgh). Sections were then washed in PBS with 0.1% Triton X100 and incubated with the appropriate fluorescent secondary antibodies (1:1,000, Alexa-fluor 405, 488, 555, 647, Invitrogen) for 1 hr at room temperature. After washing in PBS, nuclei were counterstained with DAPI (1:10,000, Invitrogen) for 3 min and then mounted with Dako mounting kit (Fluka). Nonspecific staining was observed in control incubations in which the primary antibodies were omitted.
Quantification of graft differentiation was obtained from randomized n≥ 5 spinal cord regions of interest acquired using a confocal microscope (Leica TCS SP5 Microscope). Data are expressed as % of double or triple positive cells over total $fGFP^+$ cells ± SEM (≥ 95 $fGFP^+$ cells for each marker were counted).

Transmission electron microscopy analysis

Isolated spinal cords were post-fixed at 4 °C for 48-72 hrs and then the lesion site was sliced at 1 mm thickness and treated with 2% OsO_4 overnight at 4 °C. The following day, tissues were washed with water and dehydrated using increasing concentration of ethanol (70%, 95%, 100%) for 10 min at room temperature. Slices were then incubated with propylene oxide (BDH – Merck LTD) for 20 min at room temperature. Then slices were treated 6 hrs with 50% resin (TAAB lab equipment LDT Aldermaston) in propylene oxide at room temperature. After 2 additional overnight incubations at room temperature with 100% resin, tissues were incubated in 100% resin at 60 °C until polymerization was completed. Solid resin blocks containing spinal cord samples were semi-thin (1 µm) sectioned and stained with toluidine blue to localize the lesion. Ultra-thin sections were cut onto copper grids and stained with uranyl acetate.
Toluidine blue pictures were acquired using an Olympus BX53 microscope with motorized stage and Neurolucida software (11.07 64-bit, Microbrightfield) and ultra-thin sections were acquired using a Hitachi H-600 Transmission Electron Microscope.

In situ hybridization

The expression of *Plp* mRNA in demyelinated lesions was examined by *in situ* hybridization with digoxigenin-labeled cRNA probes. *In situ* hybridization for *Plp* was performed using an established protocol (27, 28). Tissue samples were analysed using an Olympus BX53 microscope with motorized stage and Neurolucida software (11.07 64-bit, Microbrightfield) to establish the number of *Plp*-positive cells within the lesions.

Immunoblotting

Western blots were performed on tissue samples. Tissue samples were mechanically dissociated and incubated 1 hr at 37 °C in lysis buffer and frozen at -80 °C until further use.

Extracts were defrosted, sonicated and proteins were quantified using Pierce™ BCA Protein Assay kit (Thermo scientific). These samples were then heated at 95 °C for 5 min, and the same amount of proteins were electrophoresed on 12% SDS-PAGE gels and transferred to nitrocellulose membranes. After blocking with 5% non-fat milk in 0.1% PBS-Tween 20 for 1 hr at room temperature, membranes were incubated overnight at +4 °C with the following primary antibodies: mouse anti-olig1 (1:500, Millipore) and rabbit β-actin (1:10,000, Cell Signaling). After 3 washes in 0.1% PBS-Tween 20, membranes were incubated for 1 hr at room temperature with the appropriate HRP-conjugated secondary antibodies: anti-rabbit HRP conjugated secondary (1:10,000 Thermo Scientific), anti-mouse HRP conjugated secondary (1:20,000 Thermo Scientific). Proteins bands were developed using premixed ready-to-use chemiluminescent HRP detection reagent (Millipore) according to the manufacturer's instructions and acquired using an Uvitec Cambridge Imaging System. The density of each band was quantified using ImageJ analysis software and normalized to housekeeping bands measured in the same membranes.

Statistical analysis

Statistical differences among groups were analysed with GraphPad Prism (version 5.00 for Mac, GraphPad Software) using a Kruskal-Wallis test, followed by a Mann-Whitney post-test. All values are expressed as mean ± SEM and a p value < 0.05 was consider as significant in all analyses.

Author contributions

N.V., L.P.J. and SP designed the research project; N.V., L.P.J., A.B., S.R., G.V., B.B. and C.Z. conducted the experiments; N.V. and L.P.J. data curation; N.V., L.P.J., R.P., C.Z., F.E., R.J.M.F. and S.P. data analysis; C.Z., F.E. and R.J.M.F. provided key reagents; N.V., L.P.J. and SP project administration; R.P., C.Z., F.E., R.J.M.F., and S.P. supervised the project; N.V., L.P.J. and S.P. wrote the manuscript.

Acknowledgments

The authors thank D. Morrison (Franklin Lab) and G. Gonzalez (Franklin lab) for their technical assistance and critical insights and the past and present members of the Pluchinolab for the constructive discussions of this project.

This work was supported by the Italian Multiple Sclerosis Association (AISM), the Italian Ministry of Health, the European Research Council, the Medical Research Council, the Bascule Charitable Trust and the Wellcome Trust – MRC Cambridge Stem Cell Institute. N.V. was supported by the International PhD program in Neuroscience. L.P.J. was supported by a research training fellowship from the Wellcome Trust. Work in FE lab was supported by grants from the ERA-Net E-rare research programme and the Austrian Science Fund (FWF).

Conflict of interest statement

The authors have declared that no conflict of interest exists.

References

1. Compston A, and Coles A. Multiple sclerosis. *Lancet.* 2008;372(9648):1502-17.
2. Nave KA. Myelination and support of axonal integrity by glia. *Nature.* 2010;468(7321):244-52.
3. Ben-Hur T. Cell therapy for multiple sclerosis. *Neurotherapeutics : the journal of the American Society for Experimental NeuroTherapeutics.* 2011;8(4):625-42.
4. Franklin RJM. Why does remyelination fail in multiple sclerosis? *Nature Reviews Neuroscience.* 2002;3(9):705-14.
5. Martino G, and Pluchino S. The therapeutic potential of neural stem cells. *Nature Reviews Neuroscience.* 2006;7(5):395-406.
6. Pluchino S, Quattrini A, Brambilla E, Gritti A, Salani G, Dina G, et al. Injection of adult neurospheres induces recovery in a chronic model of multiple sclerosis. *Nature.* 2003;422(6933):688-94.
7. Pluchino S, Zanotti L, Rossi B, Brambilla E, Ottoboni L, Salani G, et al. Neurosphere-derived multipotent precursors promote neuroprotection by an immunomodulatory mechanism. *Nature.* 2005;436(7048):266-71.
8. Bacigaluppi M, Pluchino S, Peruzzotti-Jametti L, Kilic E, Kilic U, Salani G, et al. Delayed post-ischaemic neuroprotection following systemic neural stem cell transplantation involves multiple mechanisms. (vol 132, pg 2239, 2009). *Brain.* 2010;133:3483-.
9. Meyer S, Worsdorfer P, Gunther K, Thier M, and Edenhofer F. Derivation of Adult Human Fibroblasts and their Direct Conversion into Expandable Neural Progenitor Cells. *J Vis Exp.* 2015(101):e52831.
10. Thier M, Worsdorfer P, Lakes YB, Gorris R, Herms S, Opitz T, et al. Direct Conversion of Fibroblasts into Stably Expandable Neural Stem Cells. *Cell Stem Cell.* 2012;10(4):473-9.
11. Peruzzotti-Jametti L, Bernstock J, Vicario N, Costa ASH, Kwok CK, Leonardi T, et al. Transplanted induced neural stem cells ameliorate experimental autoimmune encephalomyelitis by metabolic reprogramming of mononuclear phagocytes. *Glia.* 2017;65:E401-E2.
12. Wright LS, Prowse KR, Wallace K, Linskens MHK, and Svendsen CN. Human progenitor cells isolated from the developing cortex undergo decreased neurogenesis and eventual senescence following expansion in vitro. *Experimental Cell Research.* 2006;312(11):2107-20.
13. Anderson AJ, Piltti KM, Hooshmand MJ, Nishi RA, and Cummings BJ. Preclinical Efficacy Failure of Human CNS-Derived Stem Cells for Use in the Pathway Study of Cervical Spinal Cord Injury. *Stem Cell Reports.* 2017;8(2):249-63.
14. Lu J, Liu H, Huang CT, Chen H, Du Z, Liu Y, et al. Generation of integration-free and region-specific neural progenitors from primate fibroblasts. *Cell Rep.* 2013;3(5):1580-91.
15. Lu QR, Sun T, Zhu ZM, Ma N, Garcia M, Stiles CD, et al. Common developmental requirement for Olig function indicates a motor neuron/oligodendrocyte connection. *Cell.* 2002;109(1):75-86.
16. Arnett HA, Fancy SPJ, Alberta JA, Zhao C, Plant SR, Kaing S, et al. bHLH transcription factor Olig1 is required to repair demyelinated lesions in the CNS. *Science.* 2004;306(5704):2111-5.
17. Zawadzka M, Rivers LE, Fancy SPJ, Zhao C, Tripathi R, Jamen F, et al. CNS-Resident Glial Progenitor/Stem Cells Produce Schwann Cells as well as Oligodendrocytes during Repair of CNS Demyelination. *Cell Stem Cell.* 2010;6(6):578-90.
18. Arnett HA, Fancy SP, Alberta JA, Zhao C, Plant SR, Kaing S, et al. bHLH transcription factor Olig1 is required to repair demyelinated lesions in the CNS. *Science.* 2004;306(5704):2111-5.
19. Fischbach MA, Bluestone JA, and Lim WA. Cell-Based Therapeutics: The Next Pillar of Medicine. *Science Translational Medicine.* 2013;5(179).
20. Talbott JF, Cao QL, Enzmann GU, Benton RL, Achim V, Cheng XX, et al. Schwann cell-like differentiation by adult oligodendrocyte precursor cells following engraftment into the demyelinated spinal cord is BMP-dependent. *Glia.* 2006;54(3):147-59.

21. Crang AJ, Gilson JM, Li WW, and Blakemore WF. The remyelinating potential and in vitro differentiation of MOG-expressing oligodendrocyte precursors isolated from the adult rat CNS. *European Journal of Neuroscience.* 2004;20(6):1445-60.
22. Kondo T, and Raff MC. A role for Noggin in the development of oligodendrocyte precursor cells. *Developmental Biology.* 2004;267(1):242-51.
23. Pluchino S, Zanotti L, Brambilla E, Rovere-Querini P, Capobianco A, Alfaro-Cervello C, et al. Immune Regulatory Neural Stem/Precursor Cells Protect from Central Nervous System Autoimmunity by Restraining Dendritic Cell Function. *Plos One.* 2009;4(6).
24. Iraci N, Gaude E, Leonardi T, Costa ASH, Cossetti C, Peruzzotti-Jametti L, et al. Extracellular vesicles are independent metabolic units with asparaginase activity. *Nat Chem Biol.* 2017.
25. Vescovi AL, and Snyder EY. Establishment and properties of neural stem cell clones: plasticity in vitro and in vivo. *Brain Pathol.* 1999;9(3):569-98.
26. Follenzi A, Ailles LE, Bakovic S, Geuna M, and Naldini L. Gene transfer by lentiviral vectors is limited by nuclear translocation and rescued by HIV-1 pol sequences. *Nat Genet.* 2000;25(2):217-22.
27. Kotter MR, Li WW, Zhao C, and Franklin RJ. Myelin impairs CNS remyelination by inhibiting oligodendrocyte precursor cell differentiation. *J Neurosci.* 2006;26(1):328-32.
28. Gonzalez GA, Hofer MP, Syed YA, Amaral AI, Rundle J, Rahman S, et al. Tamoxifen accelerates the repair of demyelinated lesions in the central nervous system. *Sci Rep.* 2016;6:31599.

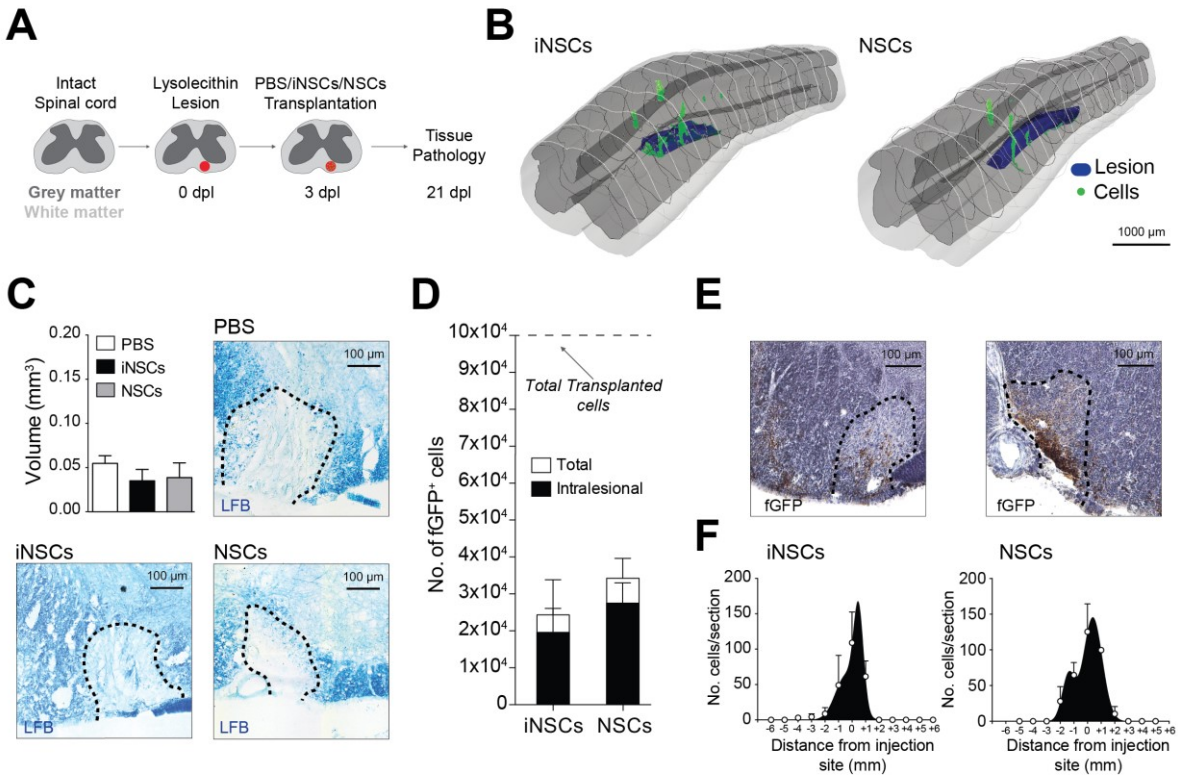

Figure 1. Transplanted iNSCs and NSCs survive and distribute in lysolecithin-induced lesions in wild type mice.

(A) Experimental setup for *in vivo* LPC-induced lesion and transplantation.

(B) Representative 3D reconstructions. Green dots indicate individual fGFP$^+$ cells, and blue area represent LPC-induced lesions in the ventral white matter.

(C) Quantification of Luxol fast blue (LFB) negative volume and representative pictures of lesions' area from n≥ 4 mice/group.

(D-F) Stereology-based cells survival quantification (D) with representative pictures of intralesional fGFP$^+$ iNSCs and fGFP$^+$ NSCs (E) and their distribution from the injection site (F).

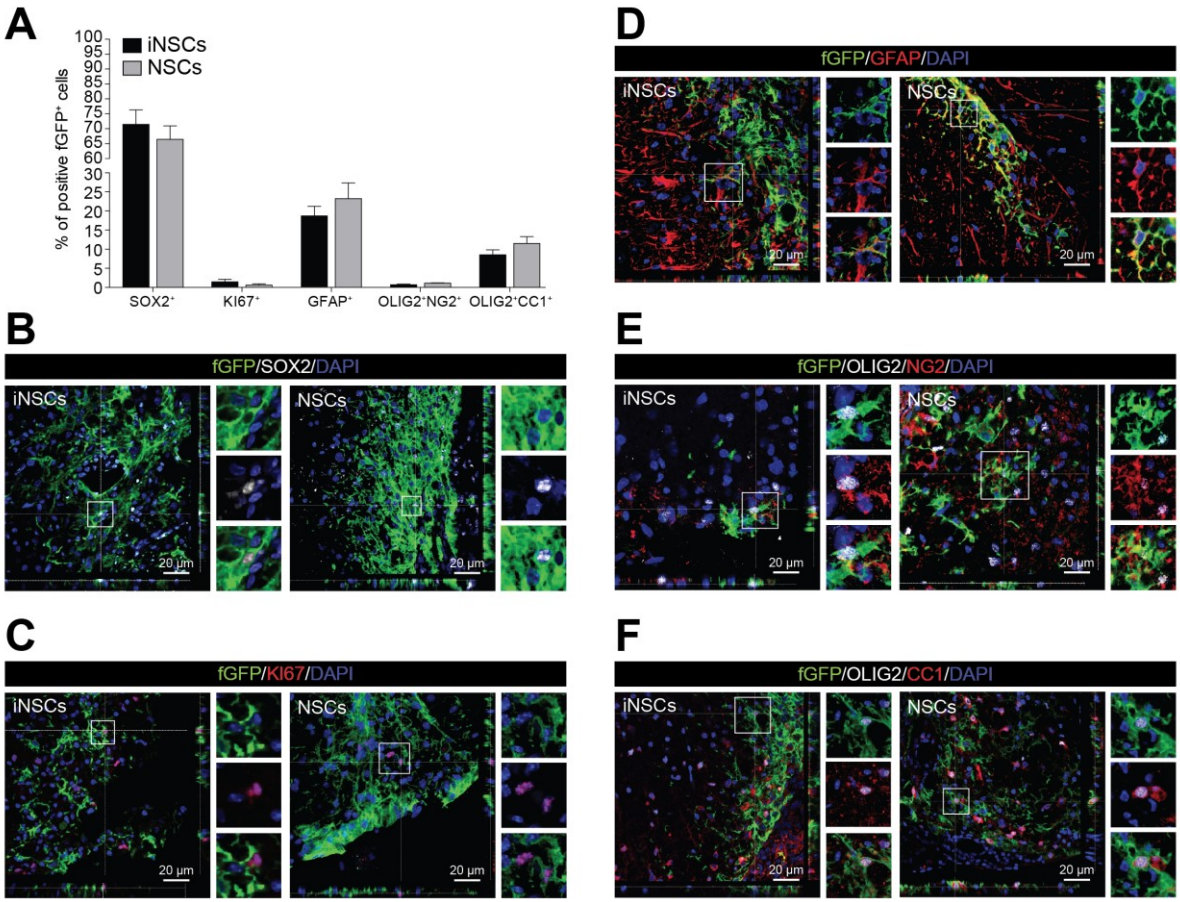

Figure 2. Transplanted iNSCs and NSCs differentiate intra-lesionally into astrocytes and oligodendroglial cells.

(A) Quantification of immunopositive cells for SOX2, KI67, GFAP, OLIG2 and NG2, and OLIG2 and CC1. Data are shown as percentage over total counted fGFP$^+$ cells.

(B-F) Representative imeges of fGFP$^+$ iNSCs and a fGFP$^+$ NSCs at 21 days post lesion (dpl) expressing SOX2 as a marker of undifferentiated iNSCs/NSCs (B), the proliferation marker KI67 (C), the astroglial lineage marker GFAP (D), the oligodendroglial progenitors markers NG2 and OLIG2 (E) or the mature oligodendrocytes markers CC1 and OLIG2 (F).

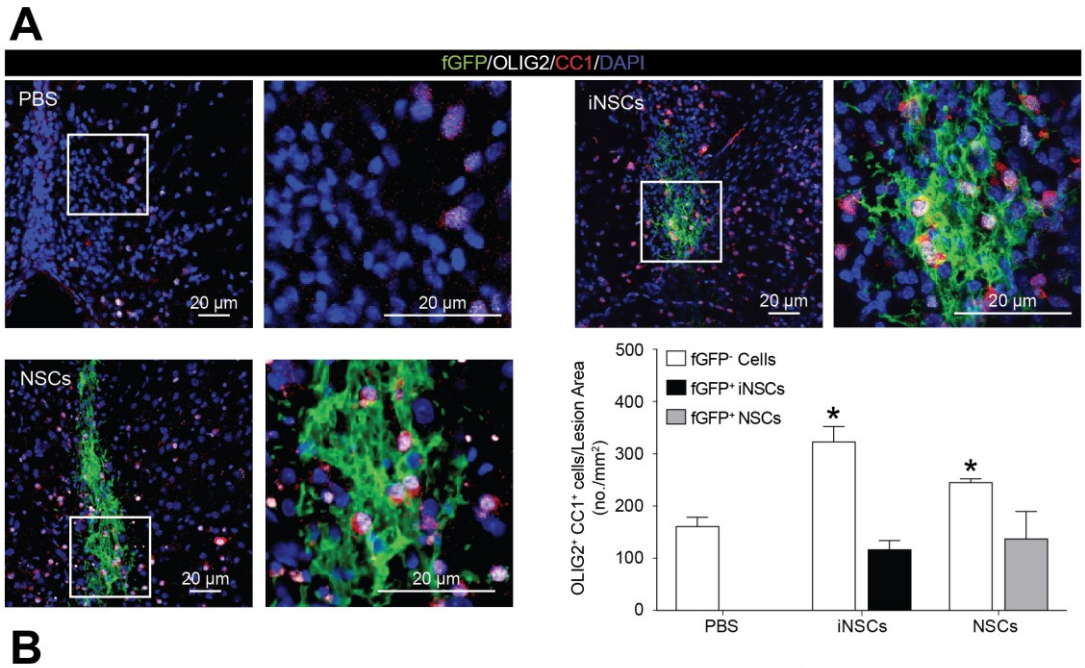
A
fGFP/OLIG2/CC1/DAPI
PBS
iNSCs
NSCs
20 μm
fGFP⁻ Cells
fGFP⁺ iNSCs
fGFP⁺ NSCs
OLIG2⁺ CC1⁺ cells/Lesion Area (no./mm²)
500
400
300
200
100
0
*
PBS
iNSCs
NSCs

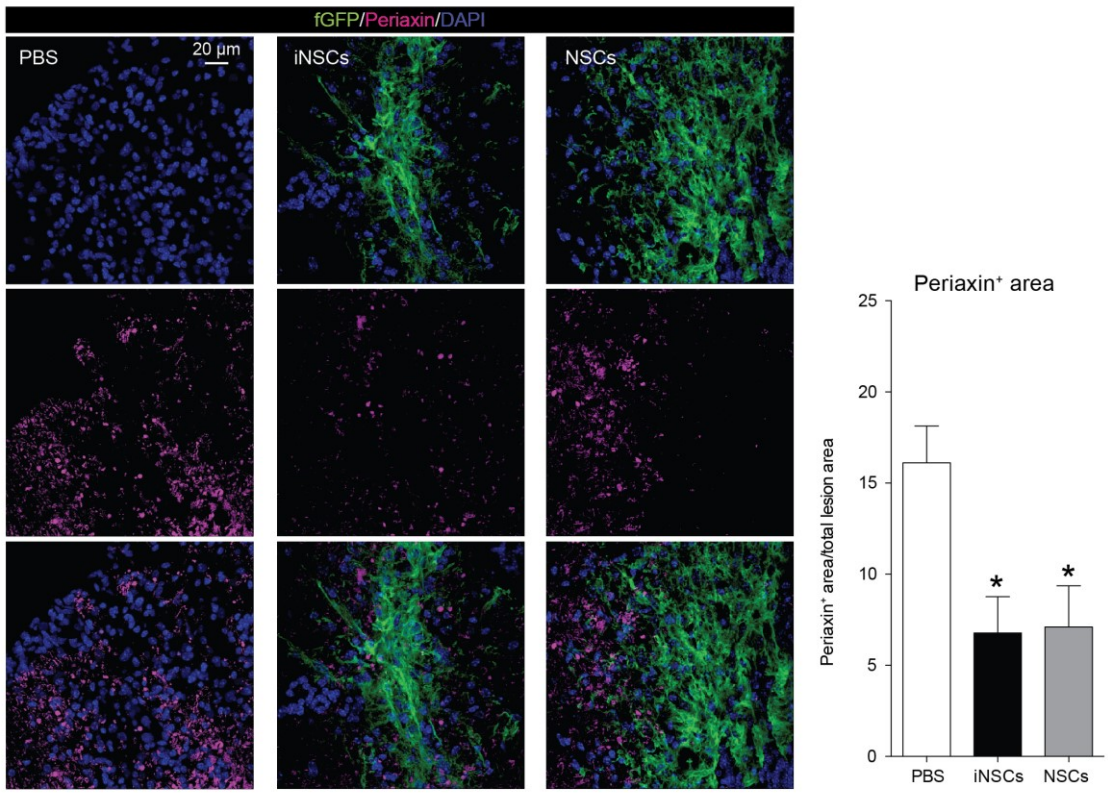
B
fGFP/Periaxin/DAPI
PBS
iNSCs
NSCs
20 μm
Periaxin⁺ area
Periaxin⁺ area/total lesion area
25
20
15
10
5
0
*
PBS
iNSCs
NSCs

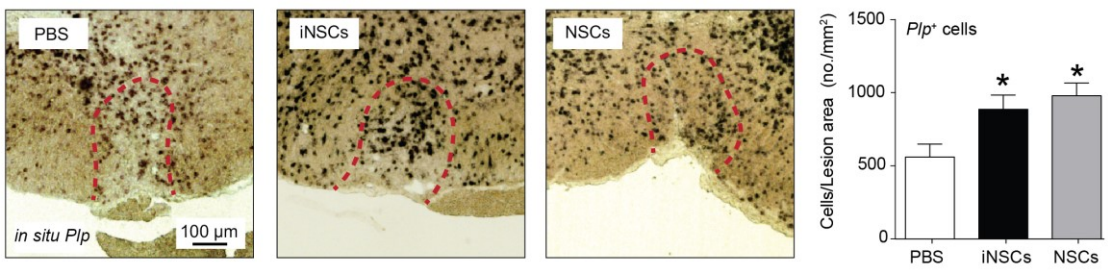
C
PBS
iNSCs
NSCs
in situ Plp
100 μm
Plp⁺ cells
Cells/Lesion area (no./mm²)
1500
1000
500
0
*
PBS
iNSCs
NSCs

Figure 3. Transplanted iNSCs and NSCs promote endogenous OPCs differentiation in demyelinated adult CNS.

(A) Representative images of OLIG2^{+} and CC1 positive cells in PBS, iNSCs and NSCs treated mice and quantification of endogenous (fGFP^{-}) and exogenous (fGFP^{+}) mature oligodendrocytes. Data are shown as OLIG2 and CC1 double positive cells per lesion area.

(B) Representative images of periaxin and quantification of periaxin positive area in lysolecithin-induced lesion and iNSCs/NSCs treated mice.

(C) Representative images of *in situ* hybridization for *Plp* on PBS, iNSCs and NSCs treated mice and quantification of *Plp*-mRNA^{+} cells per lesion area.

(B-C) *p< 0.05 vs. PBS.

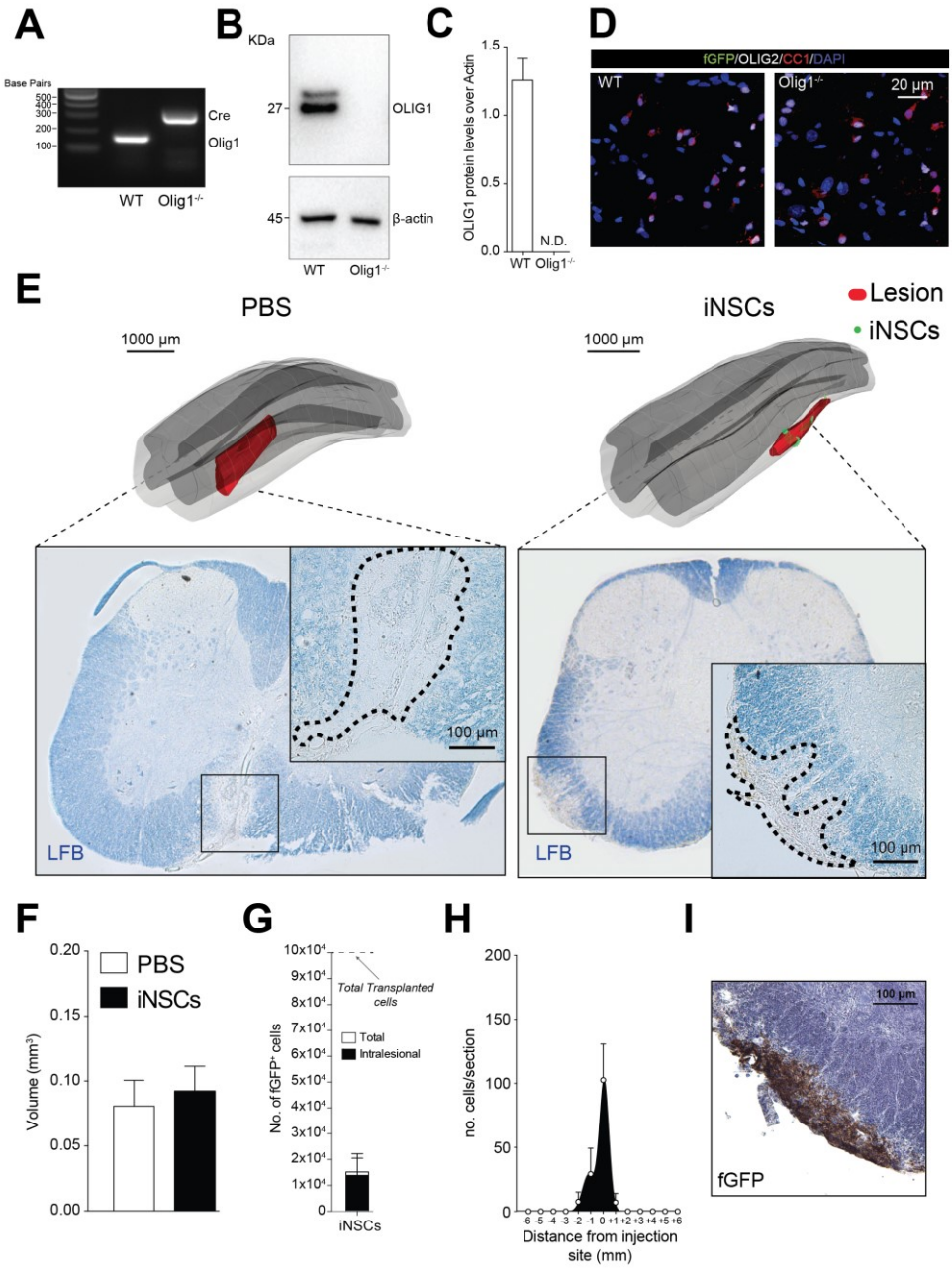

Figure 4. Transplanted iNSCs survive and distribute into demyelinated lesions of Olig1$^{-/-}$ mice.

(A) PCR analysis on wild type and Olig1$^{-/-}$ mice for Olig1 gene and Cre gene.

(B-C) Representative blot of OLIG1 protein expression levels in the spinal cord of wild type (WT) and Olig1$^{-/-}$ mice (B) and quantification over β-actin expression levels (C).

(D) Representative pictures of OLIG2^{+}CC1^{+} cells in the intact CNS white matter in wild type (WT) and Olig1$^{-/-}$ mice.

(E-F) Representative 3D reconstructions for PBS-treated and iNSCs treated Olig1$^{-/-}$ mice. Green dots indicate individual fGFP^{+} cells, and red area represents LPC-induced lesions in the ventro-lateral white matter. Luxol fast blue (LFB) representative pictures of

demyelinated lesions are shown. Quantification of volume of lesions' area in PBS and iNSCs treated Olig1$^{-/-}$ mice (F).

(G-I) Stereology-based survival quantification (G), distribution (H) and representative picture of intralesional fGFP+ iNSCs (I).

WT: wild type; N.D.: Not Detected.

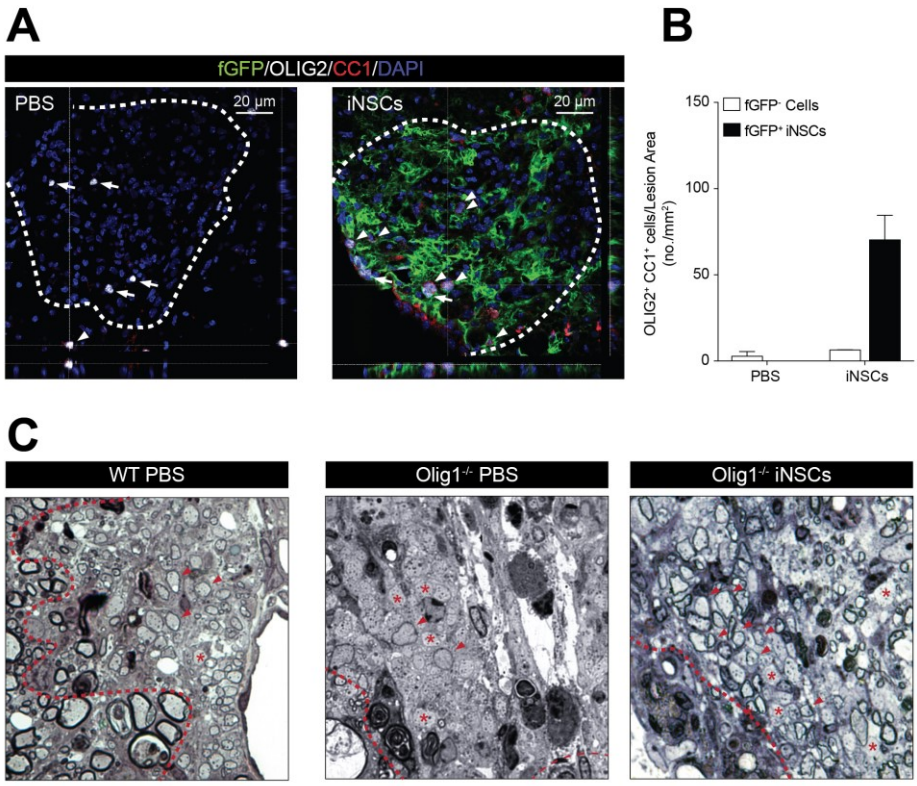

Figure 5. Transplanted iNSCs generate mature oligodendrocytes and remyelinate demyelinated lesions in Olig1$^{-/-}$ mice.

(A-B) Representative images of OLIG2^{+}CC1^{+} cells in PBS- and iNSCs-treated Olig1$^{-/-}$ mice (A) and quantification of endogenous (fGFP^{-}) and exogenous (fGFP^{+}) mature oligodendrocytes (B).

(C) Representative pictures of toluidine blue stained lesion on PBS-treated wild type mice and PBS- or iNSCs-treated Olig1$^{-/-}$ mice. Asterisks indicate demyelinated axons; arrowheads indicate remyelinated axons.

WT: wild type.

CONCLUDING REMARKS

Stem cells transplantation represents one of the most promising approaches to treat multifactorial neurological disorders (Fischbach et al., 2013; Martino and Pluchino, 2006). However, we still know little about the endogenous morphological and molecular changes that regenerate injured CNS and, the plethora of mechanisms that exogenous grafts introduce in this already complex scenario are still to be fully elucidated (Franklin, 2002).

OECs, have been considered as potential candidates for cell-replacement and have shown remarkable capabilities to exert neuroprotective mechanisms. I have developed an *in vitro* model of neuronal injury to demonstrate that OECs induce a reduction of cell-to-cell and cell-to-extracellular environment communication that favours neuroprotection. Despite their remarkable neuroprotective potential, little is known on their immunomodulatory effects and on their remyelination efficacy in the CNS (Franklin et al., 2000).

As such, the need to develop a cellular approach that conjugates neuroregenerative potential and clinical applicability prompted us to investigate a complementary stem cell-based approach.

Stem cells sense diverse signals, migrate to specific sites and execute complex response behaviours in the injured CNS. Herein I have used accessible, autologous and stably expandable iNSCs (Thier et al., 2012) to investigate the effects of stem cell transplantation in mouse models of chronic neuroinflammation and demyelination.

I found that the transplantation of iNSCs into the CSF circulation of EAE mice promotes equivalent outcomes to those previously observed in mice transplanted with somatic NSCs (Pluchino et al., 2003). Transplanted iNSCs induced significant clinical amelioration, reduced axonal and myelin damage, and lessen the infiltration of type-1 mononuclear phagocytes in the brain and spinal cord. I found that these effects were dependent on a novel anti-

inflammatory mechanism of somatic and directly-induced NSCs, which plays a crucial role in reducing the availability of key metabolic signal in chronic inflammatory contexts. I next evaluated the potential of iNSCs grafts in inducing self-repairing and remyelination in the chronically demyelinated brain. I revealed that iNSCs grafts can generate mature OLs and actively remyelinate demyelinated lesions in which endogenous remyelination was abolished or impaired. These data further support the use of directly reprogrammed iNSCs as an effective therapeutic tool to modulate inflammation and enhance remyelination in chronic demyelinating CNS diseases.

Nonetheless, before envisaging any clinical application of iNSCs, there are still some key points to address. Among those, the creation of clinical grade human iNSCs and establishing protocols/conditions for their manufacturing under Good Manufacturing Practice (GMP) standards is of particular importance. Future studies will need to address these issues and to optimize cell characteristics and dosages, administration route and patients' recruitment to maximize the success of stem cell-based therapies in the clinics. In conclusion, these data are paving the way for the future studies on the use of human iNSCs-based approach in preclinical regenerative medicine and for their forthcoming clinical application in chronic demyelinating disorders.

REFERENCES *(INTRODUCTION and CONCLUDING REMARKS)*

Ben-Hur, T. (2011). Cell therapy for multiple sclerosis. Neurotherapeutics : the journal of the American Society for Experimental NeuroTherapeutics *8*, 625-642.

Ben-Shaanan, T.L., Ben-Hur, T., and Yanai, J. (2008). Transplantation of neural progenitors enhances production of endogenous cells in the impaired brain. Mol Psychiatr *13*, 222-231.

Boruch, A.V., Conners, J.J., Pipitone, M., Deadwyler, G., Storer, P.D., Devries, G.H., and Jones, K.J. (2001). Neurotrophic and migratory properties of an olfactory ensheathing cell line. Glia *33*, 225-229.

Carvalho, B.S., and Irizarry, R.A. (2010). A framework for oligonucleotide microarray preprocessing. Bioinformatics *26*, 2363-2367.

Chandran, S., Hunt, D., Joannides, A., Zhao, C., Compston, A., and Franklin, R.J.M. (2008). Myelin repair: the role of stem and precursor cells in multiple sclerosis. Philos T R Soc B *363*, 171-183.

Compston, A., and Coles, A. (2008). Multiple sclerosis. Lancet *372*, 1502-1517.

Einstein, O., Friedman-Levi, Y., Grigoriadis, N., and Ben-Hur, T. (2009). Transplanted Neural Precursors Enhance Host Brain-Derived Myelin Regeneration. Journal of Neuroscience *29*, 15694-15702.

Ferguson, B., Matyszak, M.K., Esiri, M.M., and Perry, V.H. (1997). Axonal damage in acute multiple sclerosis lesions. Brain *120*, 393-399.

Fischbach, M.A., Bluestone, J.A., and Lim, W.A. (2013). Cell-Based Therapeutics: The Next Pillar of Medicine. Science Translational Medicine *5*.

Franklin, R.J.M. (2002). Why does remyelination fail in multiple sclerosis? Nature Reviews Neuroscience *3*, 705-714.

Franklin, R.J.M., and Barnett, S.C. (1997). Do olfactory glia have advantages over Schwann cells for CNS repair? Journal of Neuroscience Research *50*, 665-672.

Franklin, R.J.M., Smith, P.M., Iwashita, Y., Alexander, C.L., and Barnett, S.C. (2000). Remyelination of demyelinated CNS axons by olfactory ensheathing cell transplantation. European Journal of Neuroscience *12*, 317-317.

Hedstrom, A.K., Baarnhielm, M., Olsson, T., and Alfredsson, L. (2011). Exposure to environmental tobacco smoke is associated with increased risk for multiple sclerosis. Mult Scler J *17*, 788-793.

Huber, W., Carey, V.J., Gentleman, R., Anders, S., Carlson, M., Carvalho, B.S., Bravo, H.C., Davis, S., Gatto, L., Girke, T.*, et al.* (2015). Orchestrating high-throughput genomic analysis with Bioconductor. Nat Methods *12*, 115-121.

Keyoung, H.M., Roy, N.S., Benraiss, A., Louissaint, A., Suzuki, A., Hashimoto, M., Rashbaum, W.K., Okano, H., and Goldman, S.A. (2001). High-yield selection and extraction of two promoter-defined phenotypes of neural stem cells from the fetal human brain. Nature Biotechnology *19*, 843-850.

Kumagai, G., Okada, Y., Yamane, J., Nagoshi, N., Kitamura, K., Mukaino, M., Tsuji, O., Fujiyoshi, K., Katoh, H., Okada, S.*, et al.* (2009). Roles of ES Cell-Derived Gliogenic Neural Stem/Progenitor Cells in Functional Recovery after Spinal Cord Injury. Plos One *4*.

Li, Y., Field, P.M., and Raisman, G. (1997). Repair of adult rat corticospinal tract by transplants of olfactory ensheathing cells. Science *277*, 2000-2002.

Li, Y., Sauve, Y., Li, D.Q., Lund, R.D., and Raisman, G. (2003). Transplanted olfactory ensheathing cells promote regeneration of cut adult rat optic nerve axons. Journal of Neuroscience *23*, 7783-7788.

Lipson, A.C., Widenfalk, J., Lindqvist, E., Ebendal, T., and Olson, L. (2003). Neurotrophic properties of olfactory ensheathing glia. Experimental Neurology *180*, 167-171.

Lu, J., Feron, F., Mackay-Sim, A., and Waite, P.M.E. (2002). Olfactory ensheathing cells promote locomotor recovery after delayed transplantation into transected spinal cord. Brain *125*, 14-21.

Lu, P., Jones, L.L., Snyder, E.Y., and Tuszynski, M.H. (2003). Neural stem cells constitutively secrete neurotrophic factors and promote extensive host axonal growth after spinal cord injury. Experimental Neurology *181*, 115-129.

Lublin, F.D., and Reingold, S.C. (1996). Defining the clinical course of multiple sclerosis: Results of an international survey. Neurology *46*, 907-911.

Lublin, F.D., Reingold, S.C., Cohen, J.A., Cutter, G.R., Sorensen, P.S., Thompson, A.J., Wolinsky, J.S., Balcer, L.J., Banwell, B., Barkhof, F.*, et al.* (2014). Defining the clinical course of multiple sclerosis The 2013 revisions. Neurology *83*, 278-286.

Luo, W., Friedman, M.S., Shedden, K., Hankenson, K.D., and Woolf, P.J. (2009). GAGE: generally applicable gene set enrichment for pathway analysis. BMC Bioinformatics *10*, 161.

Mackay-Sim, A., and Chuah, M.I. (2000). Neurotrophic factors in the primary olfactory pathway. Progress in Neurobiology *62*, 527-559.

Martino, G., and Pluchino, S. (2006). The therapeutic potential of neural stem cells. Nature Reviews Neuroscience *7*, 395-406.

Martyn, C.N., Cruddas, M., and Compston, D.A.S. (1993). Symptomatic Epstein-Barr-Virus Infection and Multiple-Sclerosis. J Neurol Neurosur Ps *56*, 167-168.

Meyer, S., Worsdorfer, P., Gunther, K., Thier, M., and Edenhofer, F. (2015). Derivation of Adult Human Fibroblasts and their Direct Conversion into Expandable Neural Progenitor Cells. J Vis Exp, e52831.
Miller, D., Barkhof, F., Montalban, X., Thompson, A., and Filippi, M. (2005a). Clinically isolated syndromes suggestive of multiple sclerosis, part 1: natural history, pathogenesis, diagnosis, and prognosis. Lancet Neurology *4*, 281-288.
Miller, D., Barkhof, F., Montalban, X., Thompson, A., and Filippi, M. (2005b). Clinically isolated syndromes suggestive of multiple sclerosis, part 2: non-conventional MRI, recovery processes, and management. Lancet Neurology *4*, 341-348.
Nash, H.H., Borke, R.C., and Anders, J.J. (2002). Ensheathing cells and methylprednisolone promote axonal regeneration and functional recovery in the lesioned adult rat spinal cord. Journal of Neuroscience *22*, 7111-7120.
Nunes, M.C., Roy, N.S., Keyoung, H.M., Goodman, R.R., McKhann, G., Jiang, L., Kang, J., Nedergaard, M., and Goldman, S.A. (2003). Identification and isolation of multipotential neural progenitor cells from the subcortical white matter of the adult human brain. Nature Medicine *9*, 439-447.
Orton, S.M., Herrera, B.M., Yee, I.M., Valdar, W., Ramagopalan, S.V., Sadovnick, A.D., and Ebers, G.C. (2006). Sex ratio of multiple sclerosis in Canada: a longitudinal study. Lancet Neurology *5*, 932-936.
Penna, G., Roncari, A., Amuchastegui, S., Daniel, K.C., Berti, E., Colonna, M., and Adorini, L. (2005). Expression of the inhibitory receptor ILT3 on dendritic cells is dispensable for induction of CD4(+)Foxp3(+) regulatory T cells by 1,25-dihydroxyvitamin D-3. Blood *106*, 3490-3497.
Pluchino, S., Quattrini, A., Brambilla, E., Gritti, A., Salani, G., Dina, G., Galli, R., Del Carro, U., Amadio, S., Bergami, A.*, et al.* (2003). Injection of adult neurospheres induces recovery in a chronic model of multiple sclerosis. Nature *422*, 688-694.
Pluchino, S., Zanotti, L., Rossi, B., Brambilla, E., Ottoboni, L., Salani, G., Martinello, M., Cattalini, A., Bergami, A., Furlan, R.*, et al.* (2005). Neurosphere-derived multipotent precursors promote neuroprotection by an immunomodulatory mechanism. Nature *436*, 266-271.
Ritchie, M.E., Phipson, B., Wu, D., Hu, Y., Law, C.W., Shi, W., and Smyth, G.K. (2015). limma powers differential expression analyses for RNA-sequencing and microarray studies. Nucleic Acids Res *43*, e47.
Teng, Y.D., Lavik, E.B., Qu, X.L., Park, K.I., Ourednik, J., Zurakowski, D., Langer, R., and Snyder, E.Y. (2002). Functional recovery following traumatic spinal cord injury mediated by a unique polymer scaffold seeded with neural stem cells (vol 99, pg 3024, 2002). P Natl Acad Sci USA *99*, 9606-9606.
Thier, M., Worsdorfer, P., Lakes, Y.B., Gorris, R., Herms, S., Opitz, T., Seiferling, D., Quandel, T., Hoffmann, P., Nothen, M.M.*, et al.* (2012). Direct Conversion of Fibroblasts into Stably Expandable Neural Stem Cells. Cell Stem Cell *10*, 473-479.
Trapp, B.D., Peterson, J., Ransohoff, R.M., Rudick, R., Mork, S., and Bo, L. (1998). Axonal transection in the lesions of multiple sclerosis. New Engl J Med *338*, 278-285.
Wewetzer, K., Verdu, E., Angelov, D.N., and Navarro, X. (2002). Olfactory ensheathing glia and Schwann cells: two of a kind? Cell and Tissue Research *309*, 337-345.
Zhang, Y., Klassen, H.J., Tucker, B.A., Perez, M.T.R., and Young, M.J. (2007). CNS progenitor cells promote a permissive environment for neurite outgrowth via a matrix metalloproteinase-2-dependent mechanism. Journal of Neuroscience *27*, 4499-4506.

Papers:

• ***Vicario N**, Calabrese G, Zappalà A, Parenti C, Forte S, Graziano ACE, Vanella L, Pellitteri R, Cardile V, Parenti R. Inhibition of Cx43 mediates protective effects on hypoxic/reoxygenated human neuroblastoma cells. J Cell Mol Med, 2017 Feb 28. IF: 4.499.*

***Contribution**:* **N.V.** and R.Pa. designed the research study; **N.V.**, G.C. and R.Pe. performed experiments; **N.V.** and S.F. collected and analysed data; C.P. and L.V. provided some reagents and instruments; A.G., A.Z., C.P. and V.C. gave technical support and conceptual advice; **N.V.**, G.C. and R.Pa. wrote the manuscript.

• *Peruzzotti-Jametti L, Bernstock JD, **Vicario N**, Costa ASH, Kwok C, Leonardi T, Booty L, Bicci I, Balzarotti B, Volpe G, Mallucci G, Manferrari G, Iraci N, Braga A, Hallenbeck JM, Murphy MP, Edenhofer F, Frezza C and Pluchino S. Neural stem cell transplantation ameliorates chronic neuroinflammation via a succinate-SUCNR1 dependent mechanism. 1st Round revision, Cell Stem Cell. IF: 23.394.*

***Contribution**:* Conceptualization, L.P.J., C.F. and SP; Methodology, J.D.B., F.E. and S.P.; Formal Analysis, L.P.J., J.D.B., **N.V.**, A.S.H.C., T.L., C.F. and S.P.; Investigation, L.P.J., J.D.B., **N.V.**, I.B., A.S.H.C., B.B., G.Mal., G.Man., G.V., N.I. and L.M.B.; Resources, M.P.M., J.H., F.E., C.F. and S.P.; Data Curation, L.P.J., J.D.B. and **N.V.**; Writing – Original Draft, L.P.J., J.D.B., **N.V.**, C.F. and S.P.; Writing – Review & Editing, L.P.J., J.D.B., **N.V.**, M.P.M., J.H., F.E., C.F. and S.P.; Supervision, M.P.M., J.H., F.E., C.F. and S.P.; Project Administration, L.P.J., J.D.B., **N.V.**, C.F. and S.P.; Funding Acquisition, L.P.J. and S.P.

• ***Vicario N**‡, Peruzzotti-Jametti L‡, Braga A, Bernstock JD, Rizzi S, Volpe G, Balzarotti B, Parenti R, Zhao C, Edenhofer F, Franklin RJM, Pluchino S. Transplantation of directly induced Neural Stem Cell (iNSCs) in a mouse model of experimental focal demyelination. (Manuscript in preparation).*

‡Equal contribution

***Contribution**:* **N.V.**, L.P.J. and SP designed the research project; **N.V.**, L.P.J., A.B., S.R., G.V., B.B. and C.Z. conducted the experiments; **N.V.** and L.P.J. data curation; **N.V.**, L.P.J., R.P., C.Z., F.E., R.J.M.F. and S.P. data analysis; C.Z., F.E. and R.J.M.F. provided key reagents; **N.V.**, L.P.J. and SP project administration; R.P., C.Z., F.E., R.J.M.F., and S.P. supervised the project; **N.V.**, L.P.J. and S.P. wrote the manuscript.

Other papers

• ***Vicario N**, Parenti R, Arico' G, Turnaturi R, Scoto GM, Chiechio S, Parenti C. Repeated activation of delta opiod receptors counteracts nerve injury-induced TNF-α up-regulation in the sciatic nerve of rats with neuropathic pain: A possible correlation with delta opiod receptors-mediated antiallodinic effect. Mol Pain. 2016 Sep 2. IF: 3.070.*

• *Graziano AC, Cardile V, Avola R, **Vicario N**, Parenti C, Salvatorelli L, Magro G, Parenti R. Wilms' tumor gene 1 silencing inhibits proliferation of human osteosarcoma MG-63 cell line by cell cycle arrest and apoptosis activation. Oncotarget. 2017 Jan 18. IF: 5.008.*

• *Bernstock JD, Peruzzotti-Jametti L, Ye D, Gessler FA, **Vicario N**, Lee Y, Hallenbeck JM and Pluchino S. Neural Stem Cell transplantation in Ischemic Stroke: a Role for Preconditioning and Cellular Engineering. J Cereb Blood Flow Metab, 2017 Feb 24. IF: 5.081.*

# ***Vicario N**‡, Zappalà A‡, Calabrese G, Gulino R, Parenti C, Gulisano M, Parenti R. Connexins in the central nervous system: physiological traits and neuroprotective targets. Submitted. Frontiers in Physiology. I.F. 4.134. ‡equal contribution. I.F. 4.134*

*Bernstock JD, Peruzzotti-Jametti L, **Vicario N**, Ye D, Johnson KR, Maric D, Mou Y, Gessler FA, Balzarotti B, Leonardi T, Lee Y, Franklin RJM, Hallenbeck HM, Pluchino S. Overexpression of the SUMO E2-conjugase Ubc9 enhances neural stem cell survival in experimental models of ischemia. (Manuscript in preparation).*

# *Peruzzotti-Jametti L‡, **Vicario N**‡, Manferrari G, Bernstock JDB, Rogall R, Balzarotti B, Hernandez E, Viscomi C and Pluchino S. Neural stem cell-derived extracellular vesicles mediate the horizontal transfer of functional mitochondria to target cells. (Manuscript in preparation). ‡equal contribution.*

ACKNOWLEDGEMENT

I would like to thank everyone that has in some way contributed to this thesis.
First of all I would like to express my deepest gratitude to Stefano Pluchino and Rosalba Parenti for the opportunity to work with you, for all your help and for the guidance.
Thanks to all the scientists that help me during these years as PhD student: Frank Edenhofer, Christian Frezza, Aviva Tolkovsky and Robin JM Franklin, Rameen Shakur, Rosalia Pellitteri, Venera Cardile, Giovanni Li Volti, Lorella Pasquinucci, Carmela Parenti, Santina Chiechio, Agata Zappalà, Rosario Gulino, Massimo Gulisano and Salvatore Salomone for your time and your suggestions. A special thank to Chao Zhao for your critical insights, for having taught me a lot and for all your patience.
I would like to thank all the past and present members of the labs for all our productive discussions, and for the physical and mental support. Thanks to Marco, Elisa, Roberta, Ezio, Giuliana, Debora, Cristina, Adriana, Rosanna, Tiziana, Chiara, Stefano and Giovanna. Thanks to Jayden, Josh, Giulia, Iacopo, Giulio, Sara, Almu, Inma and Nunzio for welcoming me in Cambridge and for creating a friendly atmosphere in the Pluchinolab. Thanks to Alice for all your suggestions, to be a very empathic person and to make me laugh. Thanks to Bea, for your great organizational skills, for your advices and for singing with me during experiments. Luca, my friend, thank you for all your immeasurable help, for your time and for sharing science with me.
Thanks to Vera, Mario and Beppe for your affection, for your encouragement and for all your love.
I must thank mamma Carmela and Lio for your endless support and your comprehension.
Thank you Raissa, my sweetheart, for your love, for your tolerance towards my late working hours and for taking care of me. You enchant me, everyday.

University of Catania - Italy
Department of Biomedical and Biotechnological Sciences
International PhD Program in Neuroscience - XXX Cycle
Section of Physiology

UNIVERSITÀ
degli STUDI
di CATANIA

University of Cambridge - United Kingdom
Department of Clinical Neurosciences
Wellcome Trust-Medical Research Council Stem Cell Institute
Division of Stem Cell Neurobiology

UNIVERSITY OF
CAMBRIDGE

Ph.D. Candidate: Nunzio Vicario
Doctoral Dissertation
2017